Cell Death & Disease

https://doi.org/10.1038/s41419-026-09036-x

Article in Press

GDPPH1 induces cell cycle arrest by downregulation of CDK4/Cyclin D1 via the m^{6}A-METTL14-YTHDF2 axis, attenuating glioblastoma progression

Received: 9 November 2025

Revised: 4 June 2026

Accepted: 16 June 2026

Cite this article as: Li, S., Yuan, R., Su, J. *et al.* GDPPH1 induces cell cycle arrest by downregulation of CDK4/Cyclin D1 via the m^{6}A-METTL14-YTHDF2 axis, attenuating glioblastoma progression. *Cell Death Dis* (2026). https://doi.org/10.1038/s41419-026-09036-x

Sijia Li, Ruijie Yuan, Jinxuan Su, Ruxi Chen, Xinyi Qu, Lele Zhao, Xiaofeng Zhou, Qiuming Zou, Zhijing Zhang, Siyu Yang, Jianqin Lai, Xiaosong Zhuang, Zisheng Li, Kai Cui, Shengwei Hu, Yongqi Liu, Lili Liu, Zepeng Luo, Zhongping Luo, Wen Li, Yu Yan, Yubo Zhang, Zhiming Zheng & Qi Qi

We are providing an unedited version of this manuscript to give early access to its findings. Before final publication, the manuscript will undergo further editing. Please note there may be errors present which affect the content, and all legal disclaimers apply.

If this paper is publishing under a Transparent Peer Review model then Peer Review reports will publish with the final article.

ARTICLE IN PRESS

© The Author(s) 2026. **Open Access** This article is licensed under a Creative Commons Attribution 4.0 International License, which permits use, sharing, adaptation, distribution and reproduction in any medium or format, as long as you give appropriate credit to the original author(s) and the source, provide a link to the Creative Commons licence, and indicate if changes were made. The images or other third party material in this article are included in the article's Creative Commons licence, unless indicated otherwise in a credit line to the material. If material is not included in the article's Creative Commons licence and your intended use is not permitted by statutory regulation or exceeds the permitted use, you will need to obtain permission directly from the copyright holder. To view a copy of this licence, visit http://creativecommons.org/licenses/by/4.0/.

ARTICLE IN PRESS

GDPPH1 induces cell cycle arrest by downregulation of CDK4/Cyclin D1 via the m^{6}A-METTL14-YTHDF2 axis, attenuating glioblastoma progression

Sijia Li[1], Ruijie Yuan[1], Jinxuan Su[1, 2], Ruxi Chen[1], Xinyi Qu[1], Lele Zhao[3], Xiaofeng Zhou[1, 4], Qiuming Zou[1], Zhijing Zhang[1, 5], Siyu Yang[1], Jianqin Lai[6], Xiaosong Zhuang[1], Zisheng Li[1], Kai Cui[1], Shengwei Hu[7], Yongqi Liu[8], Lili Liu[1], Zepeng Luo[9], Zhongping Luo[9], Wen Li[10], Yu Yan[11, *], Yubo Zhang[1, *], Zhiming Zheng[12, *], Qi Qi[1, *]

[1] State Key Laboratory of Bioactive Molecules and Drug ability Assessment, MOE Key Laboratory of Tumor Molecular Biology, Guangdong Province Key Laboratory of Pharmacodynamic Constituents of TCM and New Drugs Research, Department of Pharmacology, School of Medicine, Jinan University, Guangzhou 510632, China

[2] Department of Dermatology, State Key Laboratory of Complex Severe and Rare Diseases, Peking Union Medical College Hospital, Chinese Academy of Medical Sciences and Peking Union Medical College, National Clinical Research Center for Dermatologic and Immunologic Diseases, Beijing 100730, China

[3] State Key Laboratory of Cellular Stress Biology, Innovation Center for Cell Signaling Network, School of Life Sciences, Xiamen University, Xiamen 361102, China

ARTICLE IN PRESS

ARTICLE IN PRESS

[4] Department of Physiology, Zunyi Medical University, Zunyi, 563000, Guizhou, China

[5] Department of General Surgery, The First Affiliated Hospital of Jinan University, Guangzhou 510632, China

[6] Department of Gastrointestinal Surgery, Guangzhou First People's Hospital, Guangzhou, 510180, China

[7] State Key Laboratory of Cellular Stress Biology, Fujian Provincial Key Laboratory of Innovative Drug Target Research, School of Pharmaceutical Sciences, Faculty of Medicine and Life Sciences, Xiamen University, Xiamen 361102, China

[8] Department of Respiratory and Critical Care, The First Hospital of China Medical University, Shenyang 110001, China

[9] Department of Neurosurgery, Affiliated Hospital of Xiangnan University, Chenzhou 423000, China

[10]Analytical and Testing Center, Jinan University, Guangzhou 510632, China

[11] Functional Experimental Teaching Center, School of Medicine, Jinan University, Guangzhou 510632, China

[11] Department of Neurosurgery, Shandong Provincial Hospital Affiliated to Shandong First Medical University, Jinan 250021, China

[*]Correspondence: Yu Yan (yanyu@jnu.edu.cn), Yubo Zhang (ybzhang99@126.com), Zhiming Zheng (zhiming0119@126.com) or Qi Qi (qiqikc@jnu.edu.cn)

ARTICLE IN PRESS

ARTICLE IN PRESS

ARTICLE IN PRESS

ARTICLE IN PRESS

Abstract

Glioblastoma (GBM) is the most prevalent and aggressive primary brain tumor in adults, with current therapies failing to achieve significant clinical advancements. GDPPH1, a natural compound derived from *Garcinia mangostana L.*, is known for its antioxidant properties; however, its anticancer effects and underlying mechanisms remain insufficiently understood. In this study, we demonstrate that GDPPH1 significantly inhibits GBM cell proliferation in a concentration-dependent manner by downregulating CDK4 and Cyclin D1 expression, inducing cell cycle arrest at G1/S checkpoint, and promoting apoptosis. Mechanistically, GDPPH1 reduces the m^6A methylation of *CDK4* and *CCND1* through METTL14-YTHDF2-mediated transcript decay, resulting in deceased *CDK4*/*CCND1* expression and subsequent decreased RB phosphorylation levels. Further studies revealed that m^6A-METTL14-YTHDF2 axis is responsible for GDPPH1-induced downregulation of CDK4 and Cyclin D1. Additionally, the *in vivo* anti-GBM efficacy of GDPPH1 was confirmed using both xenograft and orthotopic intracranial mouse models. Collectively, these findings provide robust evidence supporting GDPPH1 as a promising therapeutic candidate for GBM and offer novel insights into the role of m^6A RNA methylation in cell cycle regulation.

Keywords: GDPPH1; Glioblastoma; Cell cycle; m^6A; METTL14; YTHDF2

ARTICLE IN PRESS

ARTICLE IN PRESS

Introduction

Glioblastoma (GBM) is the most common malignant tumor of the central nervous system and is characterized by high aggressiveness, poor prognosis, and a low median survival rate[1]. Based on the differential expression of specific molecular markers, GBM is classified into proneural, proliferative, and mesenchymal subtype. Among them, the mesenchymal subtype is associated with the poorest prognosis[2]. Currently, the alkylating agent temozolomide (TMZ), serves as the standard chemotherapeutic treatment for GBM patients[3]. However, similar to many other anticancer agents, TMZ's clinical efficacy is hindered by low responsiveness and the development of drug resistance[4, 5]. Consequently, there is an urgent need to elucidate the molecular mechanisms underlying GBM progression, identify effective biomarkers, and develop novel therapeutic strategies to improve patient outcomes.

GDPPH1 is a natural compound extracted from *Garcinia mangostana L.* (mangosteen), a member of the *Clusiaceae* family[6]. The medical value of mangosteen is well-regarded; particularly due to xanthones-natural compounds isolated from its rind, such as α-Mangostin, γ-mangostin, guttiferones A[7]. These compounds have demonstrated significant antitumor efficacy, notably in inducing cell apoptosis[8], arresting the cell cycle[9], and suppressing metastasis[10, 11]. Given its biological activity, GDPPH1 represents a promising natural compound with substantial antitumor potential.

Post-transcriptional modifications of RNA play crucial role in the regulation of RNA stability, transport, processing, and gene expression[12]. Among these, N^6-methyladenosine (m^6A) is the most

ARTICLE IN PRESS

prevalent and widely studied RNA modification, involving the methylation of adenosine (A) at the N^6 position. This dynamic and reversible modification is mediated by RNA methyltransferases ("writers"), demethylases ("erasers"), and m^6A-binding proteins ("readers"), collectively regulating RNA stability, splicing, degradation, and translation[13]. Emerging evidence have highlighted the pivotal role of m^6A methylation in cancer development and progression[14, 15]. In GBM, several key components of the m^6A regulatory machinery, including METTL14 and YTHDF family members[16, 17], are significantly upregulated compared with normal brain tissue, with YTHDF2 particularly enriched in high-grade GBM[18]. Functionally, YTHDF2 has been reported to promote glioma stem cell maintenance and tumorigenesis by stabilization of oncogenic transcripts such as MYC and VEGF[18], whereas depletion of METTL3 or METTL14 impairs GBM stem cell growth, self-renewal, and tumor formation[19]. In addition, elevated m^6A levels are associated with increased invasiveness and chemotherapeutic resistance in GBM. GBM is also characterized by aggressive proliferation and profound dysregulation of the cell cycle, with 77% of GBM samples harboring RB pathway aberrations[20], representing a major barrier to effective therapy. Despite the growing recognition of m^6A as a hallmark of tumor progression[21, 22], its functional contribution to cell cycle regulation in GBM remains poorly understood, highlighting m^6A-mediated pathways as promising therapeutic targets in glioblastoma.

In the present study, we identified the anti-GBM effect and underlying mechanism of GDPPH1 both *in vitro* and *in vivo*. Our findings demonstrated that GDPPH1 diminishes the m^6A methylation of *CDK4* and *CCND1* through METTL14-YTHDF2-mediated transcript decay, thereby

ARTICLE IN PRESS

downregulating the protein expression of CDK4 and Cyclin D1, blocking retinoblastoma protein (RB) signaling, suppressing GBM cell proliferation through inducing cell cycle arrest at G1/S phase and promoting apoptosis. Moreover, the anti-GBM efficacy of GDPPH1 was confirmed in xenograft and orthotopic intracranial models *in vivo*. Hence, our study elucidates a novel epigenetic regulatory mechanism through which GDPPH1 exerts its anti-GBM effects, positioning GDPPH1 as a potential therapeutic candidate for GBM treatment.

2. Materials and methods

2.1 Chemical and reagents

The molecular structures and details of the nine candidate compounds, including GDPPH1, are summarized in Supplementary Table 1. GDPPH1 powder was extracted and purified independently by our research group. The chemical structure of the compound was elucidated by nuclear magnetic resonance (NMR) spectroscopy, and its purity was confirmed by high-performance liquid chromatography (HPLC) (Supplementary Fig. 1A-C, Supplementary Table 2). Stock solutions were prepared with dimethyl sulfoxide (DMSO) (Sigma Aldrich, St. Louis. MO, USA) and freshly diluted before experiments. Antibodies against CDK4 (#12790), Cyclin D1 (#55506), Retinoblastoma (#9309), Phospho-RB (Ser780) (#8180), β-tubulin (#2146), ERK1/2 (#4695), Phospho-ERK1/2 (Thr202/Tyr204) (#4377), AMPKα (#2532), and Phospho-AMPKα (Thr172) (#2535), p27 (#3686), Cyclin E1 (#20808), and β-actin (#3700) were purchased from Cell Signaling Technology. YTHDF2 (24744-1-AP), CDK2 (10122-1-AP) and E2F1 (66515-1-Ig)

ARTICLE IN PRESS

were purchased from Proteintech. METTL14 (F1391), YTHDF1 (F2505), and YTHDF3 (F2793) were purchased from Selleck. β-actin (T0022), Ki67 (#AF0198), and Cleaved Capsase-3 (Asp175) (AF7022) were purchased from Affinity. METTL3 (ab195352), ALKBH5 (16837-1-AP), and FTO (27226-1-AP) were purchased from Abcam. WTAP (TP74614) was purchased from Abmart. METTL14 (508530) used for IHC staining was purchased from Zenbio. Actinomycin D (KM16333) was obtained from KKL Med Inc. Inhibitors including Z-VAD-FMK (A834991) and Ferrostatin-1 (A228648) were purchased from Ambeed. Chloroquine (HY-17589A) and Necrostatin-1 (HY-15760) were purchased from MCE.

ARTICLE IN PRESS

2.2 Cell culture

Human glioblastoma cell lines U251, U118MG, U87MG, U87MG-luc, LN229, and LN18, as well as mouse brain endothelial cell line bEnd.3 were obtained from the American Type Culture Collection (ATCC). All cells were cultured in DMEM (Gibco, Invitrogen, Carlsbad, CA, USA) supplemented with 10% fetal bovine serum (Gibco, Invitrogen, Carlsbad, CA, USA) and 1% penicillin-streptomycin (MCE, China) at 37 °C in a humidified incubator with 5% CO_2 (Thermo Fisher Scientific, USA).

2.3 Animal study

Female BALB/c nude mice (5 – 6 weeks, 18 – 21 g) were purchased from Zhuhai BesTest Bio-Tech Co.,Ltd., and were maintained in accordance with Jinan University's Policy on the Care and

ARTICLE IN PRESS

Use of Laboratory Animals. All animal experiments were performed following institutional ethics and safety guidelines approved by Jinan University Institutional Animal Care and Use Committee. For the GBM xenograft subcutaneous model, U251 cells (2.0×10^6) were suspended in serum-free substrate and engrafted into the right flank of nude mice. Once the tumor volumes reached 70 mm^3, the mice were randomly divided into three groups receiving 2 mg/kg, 4 mg/kg GDPPH1/mouse/day, or 0.9% NaCl containing 0.5% DMSO (control) via peritoneal injection for 3 weeks. Tumor volumes were measured every two days using a vernier caliper through the skin and calculated as length (mm) × width^2 (mm^2) × 1/2. Mice were euthanized using CO_2 at the end of study, and their hearts, livers, spleens, kidneys, and lungs were immediately fixed and paraffin-embedded for H&E staining.

For the GBM orthotopic model, mice were anesthetized and positioned on a stereotaxic frame. A Hamilton syringe with a 30-gauge needle was affixed to the frame, and 5 μl (2.5×10^5 cells) of U87MG-luc cells were injected into the right brain (anteroposterior = 0.5 mm, middle = 2.0 mm, dorsoventral = 3.0 mm from bregma). Seven days later, mice were injected intraperitoneally with GDPPH1 (4 mg/kg/day) or vehicle for the duration of the survival period. Intracranial tumor growth was monitored on days 7, 14, and 28 using the IVIS Spectrum Live Imaging System (PerkinElmer, Branford, USA). Luciferase activity was quantified using Live Imaging Software (Xenogen). Mice were sacrificed when exhibiting signs of impaired activity or convulsion, and their brains were harvested and embedded in paraffin.

ARTICLE IN PRESS

2.4 Cell viability assay

Equal amount of cells (3.0×10^3 cells/well) were seeded into 96-well plates and grown overnight. After treatment with GDPPH1 at various concentrations for 48 h, 3-(4, 5-Dimethylthiazol-2-yl)-2, 5-Diphenyltetrazolium Bromide (MTT) solution was added at a final concentration of 0.5 mg/mL, and the cells were incubated for an additional 4 h at 37 °C. The medium was carefully removed, and 150 μL of DMSO was added to dissolve the formazan crystals. Absorbance at 562 nm was measured using a continuous wavelength microplate reader (Varioskan LUX, Thermo Fisher Scientific). The absorbance values of each group were normalized to the control group, and cell proliferation and inhibition rate were calculated.

2.5 Ethynyl deoxyuridine (EdU) assay

The Cell-Light^{TM} EdU staining kit (Ribobio, Guangzhou, China) was used for *in vitro* labelling of the nucleus in dividing cells. Cells were treated with 2 μM GDPPH1 and then incubated with 10 μM EdU for 16 h. Cells were fixed, and images were acquired using a confocal microscope (Zeiss).

2.6 Calcein and propidium iodide (PI) staining

Cell density was adjusted to 1×10^5 cells/ml, and cells were seeded in 6-well plates (2 mL/well). Cells were then incubated with different concentrations of GDPPH1. Viable and non-viable cells were detected using the Calcein/PI Cell Viability/Cytotoxicity Assay Kit (C2015M, Beyotime, China) according to the manufacturer's instructions. Fluorescence images were captured using an

ARTICLE IN PRESS

inverted microscope for further analysis.

2.7 Colony formation assay

Cells were seeded at 1000 cells/well in 6-well plates, with three replicates per group. After the cells were allowed to adhere, they were treated with different concentrations of GDPPH1, and the culture was continued for 14 days at 37 °C in a 5% CO_2 incubator. Following treatment, the medium was aspirated, and the cells were washed twice with PBS. The cells were then fixed with methanol for 30 min and stained with 0.1 % crystal violet (Beytime Biotechnology, Shanghai, China) at room temperature for 10 min. Colony quantification was performed using ImageJ software.

ARTICLE IN PRESS

2.8 RNA isolation and quantitative RT-PCR

RNA was extracted from cells using an RNA extraction kit (OMEGA Bio-Tek, USA). RNA was then reverse transcribed into cDNA using the RT Master Mix for qPCR II (MCE, USA). Real-time quantitative PCR was performed using ChamQ SYBR qPCR Master Mix (Vazyme, China). The primers for RT-PCR were synthesized by the BGI (BGI, Beijing, China). Primer sequences are listed in Supplementary Table 3. Relative expression levels were quantified using the $2^{-\Delta\Delta Ct}$ method, with normalization to reference genes.

2.9 Western blotting

ARTICLE IN PRESS

Cells or tissues were lysed using RIPA lysis buffer (Thermo Fisher Scientific), supplemented with PMSF and phosphatase inhibitor. Protein concentrations were measured using the BCA Protein Assay Kit (Thermo Fisher Scientific). A total of 20-50 μg of protein was loaded onto SDS-PAGE for separation and then transferred to 0.22 μm PVDF membranes (Millipore, USA). The membranes were blocked with 5% skim milk for 2 h and incubated with the appropriate primary antibody at 4 °C overnight. After washing, the membranes were incubated with HRP-conjugated secondary antibody (1:5000) at room temperature for 1 h. Protein expression was detected using Electrochemiluminescence (ECL) substrate reagents. Quantification was performed by Image J software v.1.8.0 (National Institutes of Health).

ARTICLE IN PRESS

2.10 Cell cycle analysis

Cell cycle analysis was performed using flow cytometry. After treatment with GDPPH1, cells were collected, fixed in cold 70 % ethanol at 4 ℃ overnight, and stained with Propidium Iodide (Beyotime, China) at 37 ℃ for 30 min. The stained cells were analyzed using flow cytometer (ACEA, USA).

2.11 Analysis of mRNA m^6A methylation

mRNA samples were diluted to concentrations of 400, 200, or 100 ng/μL and denatured by incubation at 70 ℃ for 5 min. Nitrocellulose membrane were prepared, with one membrane served as an internal reference. Two microliters of each mRNA sample were applied to the membrane

ARTICLE IN PRESS

surface. After UV cross-linking, the membrane was incubated with 5% BSA to block non-specific binding. The membrane was then incubated with m^6A antibody, and the subsequent experimental steps followed standard western blotting procedures. The internal reference was stained with 0.02 % methylene blue and stained for 2 h. Signals were detected using an ECL kit.

2.12 MeRIP-qPCR

The total mRNA was immunoprecipitated with pre-mixed m^6A antibody magnetic beads, while a portion of the mRNA was retained as the input. The m^6A immune magnetic beads were enriched using a magnetic rack after brief centrifugation. The mRNA-antibody complex was digested with proteinase, and the remaining mRNA was washed, dried, and resuspended in DEPC-treated water. *CDK4* and *CCND1* primers (Supplementary Table 4) were used for qPCR amplification of both input and MeRIP samples to calculate m^6A modification.

ARTICLE IN PRESS

2.13 RNA immunoprecipitation (RIP) assay

RIP assays were performed using the Magna RIP RNA-Binding Protein Immunoprecipitation Kit (Millipore, 17-700) according to the manufacturer's instructions. Cells were lysed with IP lysis buffer, and the lysates were divided into anti-YTHDF2, anti-IgG (control), and input samples. The lysates were incubated overnight at 4 °C with magnetic beads coated with 5 μg of specific antibodies. Following washing, the lysates were digested with Proteinase K, and the RNA bound to immunoprecipitated proteins was purified. Target RNA levels were quantified using qPCR.

ARTICLE IN PRESS

2.14 Isothermal Titration Calorimetry (ITC) assay

ITC measurements were performed using a MicroCal PEAQ-ITC instrument (Malvern). All experiments were conducted at 25 °C in a buffer comprising 600 mM NaCl and 5% DMSO. GDPPH1, loaded into the titration syringe, was sequentially injected into the reaction chamber containing the METTL14 protein. Each injection was performed at 120 s intervals with a stirring speed of 500 rpm. The thermodynamic response was monitored using high-feedback mode, and the raw calorimetric data were analyzed using the MicroCal PEAQ-ITC analysis software.

2.15 Surface plasmon resonance (SPR) assay

Analysis of direct interactions between GDPPH1 and METTL14 was performed at 25 °C on a Biacore S200 SPR instrument (GE Healthcare). SPR running buffer contained PBS (pH7.4) supplemented with 5% DMSO and was prepared immediately before measurement. Recombinant human protein METTL14 was immobilized via amine coupling on a flow cell of the chip. The remaining binding sites on the chips were blocked by 1 M ethanolamine (pH 8.5) at a flow rate of 10 uL/min for 7 min. Responses from a reference flow cell were subtracted to correct for nonspecific binding and bulk refractive index effects. GDPPH1, diluted in running buffer, was injected at different concentrations over both the reference and protein-immobilized flow cells at a flow rate of 30 uL/min for 180 s, followed by a dissociation phase of 300 s. The bound analytes were removed by a 30-s wash with running buffer.

ARTICLE IN PRESS

2.16 Immunohistochemistry (IHC)

Immunohistochemical staining was performed on paraffin-embedded tissues sections (5 μm thick). Sections were dried at 60 °C for 1 h, deparaffinized with xylene, and hydrated with graded ethanol solution. The sections were incubated with primary antibodies followed by HRP-conjugated secondary antibodies. DAB reagents were used as the substrate, and tissues were counterstained with hematoxylin at room temperature for 1 min. A negative control was included by omitting the primary antibodies. Images were captured using digital microscope camera (E100) and analyzed with ImageJ software (version 2.0; National Institutes of Health).

2.17 *In vitro* BBB model and permeability assays

The bEnd.3 cells (5×10^4 cells/well) were seeded onto 24-well Transwell plates (Corning Life Sciences, Tewkesbury, MA, USA) with a pore size of 0.4 μm. The medium was refreshed every 1-2 days, and the cells were cultured for 5-7 days. Tight confluency was typically observed around day 7. Sodium fluorescein (NaF) transport was measured to evaluate whether the BBB model was successfully established. U251 cells were seeded in another 24-well plate at a density of 5×10^4 cells/well and cultured for 24 h. The bEnd.3 monolayer in the upper chamber was transferred into the 24-well plate containing U251 cells. Subsequently, 500 μL of complete DMEM containing GDPPH1 at a concentration of 12 μM was added to the upper chamber and incubated for 48 h. Cell viability was evaluated using an MTT assay as described before.

ARTICLE IN PRESS

2.18 Statistical analysis

All experiments were performed at least three times, and the data were expressed as mean ± SD. Statistical analyses were conducted using GraphPad Prism 8.4.0 software. Kaplan–Meier survival analysis with a two-sided log-rank test was used to compare the overall survival between groups. Group differences were analyzed using the *t*-test and one-way ANOVA, followed by Tukey's post hoc test for multiple comparisons. Statistical significance was defined as $P < 0.05$. Significant differences were indicated as $*P < 0.05$, $**P < 0.01$, or $***P < 0.001$.

3. Results

3.1 GDPPH1 suppresses GBM cell proliferation and induces apoptosis

Mangosteen has long been recognized for its therapeutic potential in treating various diseases, with its natural compounds garnering significant attention for their anti-tumor properties. In this study, nine candidate compounds isolated from mangosteen were screened, including symphonone I, WA76, garcinol (benzophenone), WA142-1-3, GDPPH1 (Garcim1), GDPPH2 (Garcim2), garmultin D, isoxanthochymol, and garcinialone (Supplementary Table 1). Among these, according to data from five GBM cell lines, GDPPH1 was identified as the most effective compound in suppressing GBM cell proliferation (Supplementary Fig. 2, Supplementary Table 5). Furthermore, the MTT assay demonstrated a concentration-dependent reduction in cell viability in U251 and U87MG cells treated with GDPPH1, with IC_{50} values of 6.73 μM and 6.37 μM,

ARTICLE IN PRESS

respectively (Fig. 1A). Colony formation assays also showed concentration-dependent inhibition of cell proliferation in U251 and U87MG cells (Fig. 1B). Similarly, EdU assay revealed a decrease of EdU-positive cells following GDPPH1 treatment (Fig. 1C, E). Moreover, calcein and propidium iodide (PI) staining showed reduced cell viability in GBM cells, as evidenced by an increase in red punctuate staining in the PI group (Fig. 1D, F). Flow cytometric analysis confirmed that GDPPH1 induced concentration-dependent increases in both early and late phase apoptotic cell (Fig. 1G). In contrast, no significant effects were observed on the migration, invasion, or stemness of GBM cells following GDPPH1 treatment (Supplementary Fig. 3). Collectively, these results demonstrate that GDPPH1 effectively suppresses GBM cell proliferation and induces apoptosis.

ARTICLE IN PRESS

3.2 GDPPH1 arrests the cell cycle at the G1/S phase by downregulation of CDK4 and Cyclin D1 in GBM cells

To explore the mechanism through which GDPPH1 inhibits the proliferation of GBM cells, we next investigated its effect on cell cycle progression, a critical determinant of cancer cell apoptosis and proliferation. Flow cytometry following propidium iodide (PI) staining revealed a significant concentration-dependent increase in the proportion of cells arrested at the G1/S phase upon GDPPH1 treatment (Fig. 2A). Since the CDK4/Cyclin D1-RB pathway, a key regulator of the G1-to-S phase transition, are frequently observed in GBM[23], we then examined the effect of GDPPH1 on CDK4/Cyclin D1/RB axis in GBM cells. Notably, CDK4 and Cyclin D1, as well as the phosphorylated RB protein levels, were downregulated in U251 (Fig. 2B), U87MG (Fig. 2C),

ARTICLE IN PRESS

LN229, and U118MG (Supplementary Fig. 4A, B), while the levels of other G1/S phase regulators, including p21, p27, CDK2, Cyclin E1, and E2F1 remained unchanged (Supplementary Fig. 4C). Further analysis revealed that GDPPH1 downregulated *CDK4* and *CCND1* mRNA expression in a concentration-dependent manner (Fig. 2D, Supplementary Fig. 4D), while their protein stability was unaffected (Supplementary Fig. 5A, B). These data demonstrate that GDPPH1 induces cell cycle arrest in GBM cells through downregulation of CDK4 and Cyclin D1 at the mRNA level.

To determine the primary mode of cell death induced by GDPPPH1 in GBM cells, we employed specific inhibitors of apoptosis (Z-VAD-FKM, Z-VAD), ferroptosis (Ferrostatin-1, Fer-1), necrosis (Necrostatin-1, Nec-1), and autophagy (Chloroquine, CQ). Among these, only Z-VAD significantly rescued GDPPH1-induced cell death (Fig. 3A), suggesting that apoptosis is the predominant form of cell death induced by GDPPH1. Consistent with this, Western blot analysis revealed a concentration-dependent decrease in the anti-apoptotic protein Bcl-2 and increased cleavage of caspase-3, caspase-9, and PARP into their active forms (Fig. 3B, Supplementary Fig. 6). TUNEL staining further showed a marked increase in DNA fragmentation in GDPPH1-treated cells (Fig. 3C). Furthermore, Annexin/PI flow cytometry confirmed that Z-VAD treatment significantly reduced apoptosis in GDPPH1-treated GBM cells (Fig. 3D).

Collectively, these results demonstrate that GDPPH1 induces cell cycle arrest through downregulation of CDK4 and Cyclin D1, which subsequently leads to apoptosis in GBM cells.

3.3 GDPPH1 suppresses *CDK4* and *CCND1* mRNA levels in an m^{6}A-dependent manner

ARTICLE IN PRESS

To elucidate the regulatory mechanism through which GDPPH1 affects the mRNA levels of *CDK4* and *CCND1*, we first evaluated their mRNA stability. GDPPH1 treatment significantly reduced the stability of *CDK4* and *CCND1* mRNA in U251 cells (Fig. 4A). Given the established role of N^6-methyladenosine (m^6A) in regulating RNA stability, we hypothesized that GDPPH1 might exert its effects through m^6A-dependent mechanisms. Dot blot assays confirmed that GDPPH1 treatment reduced the global m^6A level in U251 and U87MG cells compared to controls (Fig. 4B). Using the SRAMP database, we identified high-confidence m^6A modification sites in *CDK4* and *CCND1* mRNAs (Supplementary Fig. 7A). Based on this information, we designed targeted primers for MeRIP-qPCR assays, which revealed that the RNA m^6A levels of specific positions within *CDK4* and *CCND1* were significantly enriched (Supplementary Fig. 7B).

To further validate the involvement of m^6A modifications, we utilized methyl piperidine-3-carboxylate (MP3C), an agonist of the METTL3-METTL14-WTAP complex[24, 25]. Co-treatment with MP3C could effectively rescue the inhibition of proliferation induced by GDPPH1 in GBM cells (Fig. 4C). Co-treatment with MP3C also rescued the GDPPH1-induced reductions in mRNA levels of *CDK4* and *CCND1* (Fig. 4D), and their protein levels were similarly reversed (Fig. 4E, F). Additionally, MP3C treatment reversed the G1/S phase arrest induced by GDPPH1 in both U251 and U87MG cells (Fig. 4G). These findings indicate that GDPPH1 downregulates CDK4 and Cyclin D1 expression through m^6A-dependent mechanisms.

3.4 GDPPH1-regulated CDK4 and Cyclin D1 expression is associated with downregulation

ARTICLE IN PRESS

of METTL14

The degradation of mRNA regulated by m^6A modification is largely influenced by m^6A methyltransferases such as METTL3 and METTL14, and demethylases like ALKBH5 and FTO[26]. We hypothesized that GDPPH1-induced dysregulation of the m^6A modification might stem from alterations in the expression of these key m^6A enzymes. RT-qPCR and Western blot analyses revealed that the levels of METTL14 were significantly reduced following GDPPH1 treatment in GBM cells (Fig. 5A, B, Supplementary Fig. 8A, B). To investigate whether METTL14 plays a functional role in GDPPH1's effects, RNA immunoprecipitation (RIP) assays were performed, and the results demonstrated that both *CDK4* and *CCND1* mRNAs were significantly enriched in METTL14 immunoprecipitates, indicating a direct association between METTL14 and these transcripts (Supplementary Fig. 8C, D). Overexpressed METTL14 in U251 and U87MG cells and subsequently treated the cells with GDPPH1. At the mRNA levels, overexpression of METTL14 rescued the GDPPH1-induced decrease of *CDK4* and *CCND1* (Fig. 5C). Similarly, METTL14 overexpression largely counteracted GDPPH1-mediated suppression of CDK4, Cyclin D1, and phospho-RB (Ser780) expression (Fig. 5D, Supplementary Fig. 8E, F). Importantly, METTL14 overexpression also increased the mRNA stability of *CDK4* and *CCND1* upon GDPPH1 treatment (Fig. 5E). Furthermore, GDPPH1-induced cell cycle arrest and proliferation was notably reversed in METTL14-overexpression group (Fig. 5F, G). These findings indicate that METTL14 plays a crucial role in the suppression of GBM progression induced by GDPPH1.

ARTICLE IN PRESS

ARTICLE IN PRESS

3.5 The m^{6}A-dependent downregulation of CDK4 and Cyclin D1 by GDPPH1 is mediated by YTHDF2

m^{6}A modifications, added by m^{6}A methyltransferases, are recognized by m^{6}A "reader" proteins, which influence gene expression by promoting or inhibiting mRNA degradation, such as YTHDF1, YTHDF2, and YTHDF3[27, 28]. To identify which "reader" directly binds to *CDK4* and *CCND1* mRNA, we performed RNA immunoprecipitation (RIP) assays. The RIP results demonstrated that anti-YTHDF2 antibodies co-immunoprecipitated significantly more *CDK4* mRNA compared to anti-YTHDF1 or anti-YTHDF3 antibodies (Fig. 6A). *CCND1* mRNA was also significantly enriched in anti-YTHDF2 immunoprecipitation (Supplementary Fig. 9A). YTHDF2 has been reported to be recruited by METTL14 to mediate mRNA decay[29]. Indeed, the binding between YTHDF2 and *CDK4* or *CCND1* were enhanced when METTL14 was overexpressed (Fig. 6B). However, the binding between YTHDF2 and these mRNAs was diminished upon GDPPH1 treatment (Fig. 6C). Further investigation revealed that overexpression of YTHDF2 in GBM cells elevated the protein levels of CDK4, Cyclin D1, and phospho-RB (Fig. 6D, Supplementary Fig. 9B, C), while also increasing the mRNA stability of *CDK4* and *CCND1* (Fig. 6E). Flow cytometry and cell proliferation assay confirmed that overexpression YTHDF2 rescued GDPPH1-induced cell cycle arrest, reversing the inhibitory effects of GDPPH1 on GBM cell proliferation (Fig. 6F, G). These findings demonstrate that GDPPH1 modulates CDK4 and Cyclin D1 expression through METTL14-mediated, YTHDF2-dependent m^{6}A modification.

ARTICLE IN PRESS

3.6 METTL14 is the direct target of GDPPH1

To fully clarify the mechanism of the anti-GBM effects of GDPPH1, we first examined whether GDPPH1 exerts broad effects on canonical proliferation-related signaling pathways, including ERK, Akt, AMPK, β-catenin, and Hippo signaling. The results showed that GDPPH1 treatment did not induce significant changes in the activation or expression of the core components of these pathways (Supplementary Fig. 10). Based on these observations, we next sought to identify a more specific molecular target underlying the effects of GDPPH1. To gain mechanistic insight, we performed molecular docking analysis focusing on METTL14. The results revealed a strong interaction between GDPPH1 and METTL14, with a binding energy of -7.5 kcal/mol (Fig. 7A). To further validate this interaction in a cellular context, a Cellular Thermal Shift Assay (CETSA) was conducted. GDPPH1 treatment markedly increased the thermal stability of METTL14, as evidenced by a higher proportion of METTL14 protein remaining at elevated temperatures compared with the control group (Fig. 7B). Consistently, a drug affinity responsive target stability (DARTS) assay showed that GDPPH1 protected METTL14 from protease-induced degradation in a concentration-dependent manner, further supporting a direct interaction between GDPPH1 and METTL14 (Fig. 7C).

To further characterize the binding, isothermal titration calorimetry (ITC) and surface plasmon resonance (SPR) analyses were performed. ITC revealed a dissociation constant (Kd) of 2.90 μM for the GDPPH1-METTL14 interaction (Fig. 7D). Consistently, SPR analysis further supported this interaction with a comparable micromolar-range affinity and a concentration-dependent

ARTICLE IN PRESS

binding response (Fig. 7E, F), indicating a direct interaction between GDPPH1 and METTL14. Collectively, these results identify METTL14 as a direct target of GDPPH1.

3.7 GDPPH1 suppresses GBM growth *in vivo*

To evaluate the potential anti-GBM effect of GDPPH1 *in vivo*, we established both subcutaneous and intracranial tumor mouse models. Mice with subcutaneous xenograft tumors, generated using U251 cells, were randomly divided into three groups and administered GDPPH1 (2 mg/kg and 4 mg/kg) or vehicle via intraperitoneal injection every other day. Tumor size and weight measurements showed that GDPPH1 treatment significantly reduced tumor growth compared to the vehicle control group (Fig. 8A-C). In the intracranial xenograft model constructed with U87MG-luc cells, the GDPPH1-treated group exhibited slower tumor growth (Fig. 8D) and significantly longer survival (Fig. 8E) compared to the vehicle-treated group, further supporting the *in vivo* efficacy of GDPPH1 in GBM treatment.

Western blot analysis of tumor tissues showed that the expression of CDK4, Cyclin D1, phospho-RB (Ser780), and METTL14 were downregulated in the GDPPH1-treated group (Fig. 8F, G). Immunohistochemical staining of the tumor tissues revealed decreased expression of Ki67, CDK4, Cyclin D1, and METTL14, alongside an increase in cleaved-caspase 3 in GDPPH1-treated groups (Fig. 8H, I). In addition, we evaluated the potential systemic toxicity of GDPPH1 by monitoring body weight and performing blood biochemical, hematological, and histological analyses of major organs. Mice treated with GDPPH1 showed no significant loss in body weight

ARTICLE IN PRESS

compared with controls (Supplementary Fig. 11A). Furthermore, blood biochemical (Supplementary Fig. 11B-E) and hematological (Supplementary Fig. 11F-H), as well as histological examination of major organs (Supplementary Fig. 11I), revealed no significant pathological abnormalities. Together, these results suggest that GDPPH1 inhibits GBM tumors *in vivo* without significant toxicity.

Discussion

Recent studies have highlighted the significant antitumor potential of natural compounds due to their relatively low systemic toxicity and their ability to modulate key oncogenic pathways. Recent studies have demonstrated that several phytochemicals[30, 31], including saponins, curcumin, and resveratrol, exert anti-glioma effects primarily by inducing cell cycle arrest and apoptosis[32, 33, 34]. However, the role of GDPPH1, a novel compound derived from mangosteen, in GBM remains unclear. In addition, most existing studies have focused on downstream signaling events, while the upstream regulatory mechanisms governing these effects remain incompletely understood. In this context, our study introduces an additional layer of regulation by demonstrating that GDPPH1 modulates GBM progression through the METTL14-m^{6}A-YTHDF2 axis, which in turn influences the expression of key cell cycle regulators, CDK4 and Cyclin D1. These findings suggest that epitranscriptomic regulation may represent a previously underappreciated mechanism underlying the anti-tumor effects of natural compounds in glioblastoma.

Targeting cell cycle regulators has emerged as an effective strategy for cancer therapy. CDK4

ARTICLE IN PRESS

and Cyclin D1 are critical regulators of the cell cycle. Analysis of TCGA and GTEx datasets showed that *CDK4* and *CCND1* are significantly upregulated in GBM tissues compared with normal brain tissues (Supplementary Fig. 12A, B). Aberrant CDK4 activation—often due to gene amplification or overexpression—has been implicated in various cancers, including GBM[35]. Furthermore, CDK4 expression showed a significant positive correlation with increasing WHO grade. CDK4/6 inhibitors, including palbociclib, ribociclib, and abemaciclib, have been investigated in GBM. However, their clinical translation remains challenging, and early studies of palbociclib in recurrent GBM have shown limited therapeutic benefit. In contrast, ribociclib and abemaciclib have demonstrated more promising preclinical activity, with ribociclib being evaluated in diffuse hemispheric glioma and in ongoing early-phase clinical trials in recurrent GBM[36].

Beyond the classical CDK4/Cyclin D1 cell cycle axis, our findings further implicate m^{6}A RNA modification as an additional regulatory layer in GBM progression. Key m^{6}A regulators, including METTL14 and YTHDF2, were associated with the expression pattern of the identified target genes, which were significantly enriched in recurrent GBM (Supplementary Fig. 12C-I). Elevated YTHDF2 expression has been linked to chemoresistance, malignant progression, and adverse clinical outcomes in GBM[37]. This suggests that epitranscriptomic regulation may contribute to the activation of cell cycle-related signaling in tumor recurrence. Therefore, our results expand the current understanding of CDK4/Cyclin D1-associated tumor biology by incorporating an m^{6}A-mediated regulatory dimension and may provide a theoretical basis for exploring epitranscriptome-

ARTICLE IN PRESS

targeted strategies in combination with cell cycle inhibition in GBM.

METTL14, a core component of the m^{6}A "writer" complex, and YTHDF2, a major m^{6}A reader protein, are critical regulators of post-transcriptional gene expression and have been implicated in cancer progression through the modulation of mRNA stability. Previous studies have shown that METTL14 can regulate the expression of cell cycle-related genes, including CDK4, via m^{6}A-dependent mechanisms. For example, in prostate cancer, METTL14 overexpression has been reported to increase m^{6}A modification on *CDK4* mRNA, leading to accelerated transcript degradation and reduced *CDK4* expression, thereby inducing G1 phase arrest[38]. In parallel, YTHDF2, although classically known to mediate mRNA decay, has been reported to exhibit context-dependent regulatory functions in tumor cells, including the modulation of cell cycle-related genes expression[18, 39, 40]. Despite these findings, the roles of METTL14 and YTHDF2 in regulating CDK4 and Cyclin D1 expression in GBM remain poorly defined. In the present study, we demonstrated that overexpression of either METTL14 or YTHDF2 partially reversed GDPPH1-induced G1/S phase arrest, indicating that the m^{6}A regulatory machinery is functionally involved in mediating the anti-proliferative effects of GDPPH1.

Building upon these observations, we further sought to determine whether GDPPH1 directly targets components of the m^{6}A regulatory machinery. Molecular docking analysis predicted a favorable interaction between GDPPH1 and METTL14. This interaction was subsequently supported by multiple orthogonal approaches, including CETSA and DARTS assays, which demonstrated enhanced thermal stability and protease resistance of METTL14 upon GDPPH1

ARTICLE IN PRESS

treatment. Furthermore, biophysical analyses using ITC and SPR confirmed a direct interaction between GDPPH1 and METTL14 with micromolar-range binding affinity. Taken together with the rescue experiments described above, these findings indicate that METTL14 is not only functionally involved but also serves as a direct molecular target of GDPPH1 in GBM cells.

Interestingly, in addition to its direct interaction with METTL14, GDPPH1 treatment also resulted in altered METTL14 expression levels. While small molecule-protein interactions are typically associated with modulation of protein activity, the observed changes in METTL14 abundance may reflect additional regulatory mechanisms at the transcriptional or post-translational level [41, 42]. Further investigation is required to determine whether this effect is mediated directly or indirectly.

The clinical application of many candidate drugs for GBM is hindered by their insufficient penetration across the blood–brain barrier (BBB). In this study, both theoretical considerations and experimental evidence were used to evaluate the potential BBB permeability of GDPPH1. From a physicochemical perspective, GDPPH1 possesses a relatively low molecular weight, a limited number of hydrogen bond donors, and high lipophilicity, features generally favorable for passive diffusion across the lipid-rich BBB. Experimentally, the anti-GBM efficacy observed in the bEnd.3 *in vitro* BBB model (Supplementary Fig. 13) and the orthotopic GBM animal model (Fig. 8D) provides additional evidence supporting the potential BBB permeability of GDPPH1.

In summary, our study reveals a novel mechanism by which the natural product GDPPH1 targets m^6A methylation regulators to suppress GBM proliferation. Specifically, GDPPH1 downregulates

ARTICLE IN PRESS

CDK4 and Cyclin D1 expression via the METTL14 /YTHDF2 axis, leading to cell cycle arrest and subsequent apoptosis (Fig. 9). These findings offer new therapeutic insights into targeting the m^6A epitranscriptome in GBM and highlight the potential of GDPPH1 as a promising candidate for GBM treatment.

Abbreviations

Act D: Actinomycin D; ALKBH5: AlkB homolog 5; BBB: blood-brain barrier; CDK4: Cyclin-dependent kinase 4; CDK6: Cyclin-dependent kinase 6; CQ: Chloroquine; EdU: Ethynyl deoxyuridine; ER: endoplasmic reticulum; Fer-1: Ferrrostatin-1; FTO: Obesity-associated protein; GBM: Glioblastoma multiforme; HRD1: HMG-CoA Reductase Degradation Protein 1; IGF2BP2: insulin-like growth factor 2 mRNA-binding proteins; IHC: Immunohistochemistry; mRNA: Messenger RNA; m^6A: *N*6-methyladenosine; ITC: Isothermal Titration Calorimetry; MeRIP-qPCR: methylated RNA immunoprecipitation; METTL3: Methyltransferase-like 3; METTL14: Methyltransferase-like 14; MP3C: methyl piperidine-3-carboxylate; MTT: 3-(4,5)-dimethylthiahiazo (-z-y1)-3,5-diphenytetrazoliumromide; Nec-1: Necrostatin-1; OE: overexpression; PI: Propidium iodide; RB: Retinoblastoma protein; RIP: RNA immunoprecipitation; SPR: Surface plasmon resonance; SRAMP: Sequence-based RNA Adenosine Methylation site Predictor; TMZ: temozolomide; WTAP: Wilms' tumor 1-associated protein; YTHDF2: YTH *N*6-methyladenosine RNA binding protein; Z-VAD: Z-VAD-FMK.

Acknowledgements

The figures in this article were created using BioRender.com.

ARTICLE IN PRESS

Funding

This work was supported by the National Natural Science Foundation of China (82573391), the Guangdong Basic and Applied Basic Research Foundation (2024A1515013108), Qilu Sanitation and Health Leading Talent Cultivation Project (to Zhiming Zheng, 2020-2025), and the Natural Science Foundation of Hunan Province (2025JJ70536).

Author information

Authors and Affiliations

State Key Laboratory of Bioactive Molecules and Drug Ability Assessment, MOE Key Laboratory of Tumor Molecular Biology, Guangdong Province Key Laboratory of Pharmacodynamic Constituents of TCM and New Drugs Research, Department of Pharmacology, School of Medicine, Jinan University, Guangzhou 510632, China

Sijia Li, Ruijie Yuan, Jinxuan Su, Ruxi Chen, Xinyi Qu, Xiaofeng Zhou, Qiuming Zou, Zhijing Zhang, Siyu Yang, Xiaosong Zhuang, Zisheng Li, Kai Cui, Lili Liu, Yubo Zhang & Qi Qi

Department of Dermatology, State Key Laboratory of Complex Severe and Rare Diseases, Peking Union Medical College Hospital, Chinese Academy of Medical Sciences and Peking Union Medical College, National Clinical Research Center for Dermatologic and Immunologic Diseases, Beijing 100730, China

Jinxuan Su

ARTICLE IN PRESS

ARTICLE IN PRESS

State Key Laboratory of Cellular Stress Biology, Innovation Center for Cell Signaling Network, School of Life Sciences, Xiamen University, Xiamen 361102, China

Lele Zhao

Department of Physiology, Zunyi Medical University, Zunyi, 563000, Guizhou, China

Xiaofeng Zhou

Department of General Surgery, The First Affiliated Hospital of Jinan University, Guangzhou 510632, China

Zhijing Zhang

Department of Gastrointestinal Surgery, Guangzhou First People's Hospital, Guangzhou, 510180, China

Jianqin Lai

State Key Laboratory of Cellular Stress Biology, Fujian Provincial Key Laboratory of Innovative Drug Target Research, School of Pharmaceutical Sciences, Faculty of Medicine and Life Sciences, Xiamen University, Xiamen 361102, China.

Shengwei Hu

ARTICLE IN PRESS

ARTICLE IN PRESS

Department of Respiratory and Critical Care, The First Hospital of China Medical University, Shenyang 110001, China

Yongqi Liu

Department of Neurosurgery, Affiliated Hospital (Clinical College) of Xiangnan University, Chenzhou, 423000, China

Zepeng Luo, Zhongping Luo

Analytical and Testing Center, Jinan University

Wen Li

Functional Experimental Teaching Center, School of Medicine, Jinan University, Guangzhou, 510632, China

Yu Yan

Department of Neurosurgery, Shandong Provincial Hospital Affiliated to Shandong First Medical University, Jinan, 250021, China

Zhiming Zhen

ARTICLE IN PRESS

ARTICLE IN PRESS

Contributions

SL, RY, JS, RC, XQ, and LZ led data collection and interpretation, performed statistical analysis, and drafted the manuscript. XZ, QZ, ZZ, SY, and JL provided guidance on study design. XZ, ZL, KC, SH, YL, and LL acquired and analyzed the data. ZL, ZL, and WL improved visualization. YZ and QQ conceived and designed the study, supervised the overall study, and obtained funding. YY and ZZ provided project administration and critically revised the manuscript. All the authors revised the manuscript for important intellectual content and approved the final version.

Corresponding author

Correspondence to Yu Yan, Yubo Zhang, Zhiming Zheng & Qi Qi

ARTICLE IN PRESS

Ethics declarations

Competing interests

The authors declare no competing interests.

Ethics approval and consent to participate

All experiments involving mice were performed in accordance with the guidelines of the Jinan University Institutional Animal Care and Use Committee.

ARTICLE IN PRESS

References

1. Schaff LR, Mellinghoff IK. Glioblastoma and Other Primary Brain Malignancies in Adults: A Review. *JAMA* 2023, **329**(7)**:** 574-587.

2. Shen Y, Thng DKH, Wong ALA, Toh TB. Mechanistic insights and the clinical prospects of targeted therapies for glioblastoma: a comprehensive review. *Exp Hematol Oncol* 2024, **13**(1)**:** 40.

3. Yan Y, Zhou S, Chen X, Yi Q, Feng S, Zhao Z*, et al.* Suppression of ITPKB degradation by Trim25 confers TMZ resistance in glioblastoma through ROS homeostasis. *Signal Transduct Target Ther* 2024, **9**(1)**:** 58.

4. Yue Q, Wang Z, Shen Y, Lan Y, Zhong X, Luo X*, et al.* Histone H3K9 Lactylation Confers Temozolomide Resistance in Glioblastoma via LUC7L2-Mediated MLH1 Intron Retention. *Adv Sci (Weinh)* 2024, **11**(19)**:** e2309290.

5. Lassman AB, Polley MC, Iwamoto FM, Sloan AE, Wang TJC, Aldape KD*, et al.* Dual Immune Check Point Blockade in MGMT-Unmethylated Newly Diagnosed Glioblastoma: NRG Oncology BN007, a Randomized Phase II/III Clinical Trial. *J Clin Oncol* 2025, **43**(27)**:** 3032-3040.

6. Li J, Nie X, Panthakarn R, Wu X, Zheng C, Cheng Y*, et al.* Structure and activity relationship analysis of xanthones from mangosteen: Identifying garcinone E as a potent dual EGFR and VEGFR2 inhibitor. *Phytomedicine* 2024, **122:** 155140.

7. Nauman MC, Johnson JJ. The purple mangosteen (Garcinia mangostana): Defining the anticancer potential of selected xanthones. *Pharmacol Res* 2022, **175:** 106032.

8. Nittayananta W, Srichana T, Chuerduangphui J, Hitakomate E, Netsomboon K. Formulation of 1% α-mangostin in orabase gel induces apoptosis in oral squamous cell carcinoma. *BMC Complement Med Ther* 2024, **24**(1)**:** 276.

9. Fredimoses M, Li P, Zhang Y, Jia H, Liu S, Tian J*, et al.* Design, synthesis, and antiproliferative activity evaluation of novel α-mangostin derivatives by ROS/MAPK signaling pathway. *Bioorg Chem* 2024, **153:** 107968.

10. Hung SH, Shen KH, Wu CH, Liu CL, Shih YW. Alpha-mangostin suppresses PC-3 human prostate carcinoma cell metastasis by inhibiting matrix metalloproteinase-2/9 and urokinase-plasminogen expression through the JNK signaling pathway. *J Agric Food Chem* 2009, **57**(4)**:** 1291-1298.

11. Shibata MA, Iinuma M, Morimoto J, Kurose H, Akamatsu K, Okuno Y*, et al.* α-Mangostin extracted from the pericarp of the mangosteen (Garcinia mangostana Linn) reduces tumor growth and lymph node metastasis

ARTICLE IN PRESS

in an immunocompetent xenograft model of metastatic mammary cancer carrying a p53 mutation. *BMC Med* 2011, **9:** 69.

12. Barbieri I, Kouzarides T. Role of RNA modifications in cancer. *Nat Rev Cancer* 2020, **20**(6)**:** 303-322.

13. Chen XY, Zhang J, Zhu JS. The role of m(6)A RNA methylation in human cancer. *Mol Cancer* 2019, **18**(1)**:** 103.

14. Karachi A, Dastmalchi F, Mitchell DA, Rahman M. Temozolomide for immunomodulation in the treatment of glioblastoma. *Neuro-oncology* 2018, **20**(12)**:** 1566-1572.

15. An Y, Duan H. The role of m6A RNA methylation in cancer metabolism. *Mol Cancer* 2022, **21**(1)**:** 14.

16. Zhang Z, Guo X, Qi T, Wang C, Zhai X, Wang M. METTL14/IGF2BP2-mediated m6A modification of PD-L1 promotes proliferation, metastasis, and immune escape in high-grade gliomas. *J Neuropathol Exp Neurol* 2026, **85**(1)**:** 39-49.

17. Yu P, Xu T, Ma W, Fang X, Bao Y, Xu C*, et al.* PRMT6-mediated transcriptional activation of ythdf2 promotes glioblastoma migration, invasion, and emt via the wnt-β-catenin pathway. *J Exp Clin Cancer Res* 2024, **43**(1)**:** 116.

18. Dixit D, Prager BC, Gimple RC, Poh HX, Wang Y, Wu Q*, et al.* The RNA m6A Reader YTHDF2 Maintains Oncogene Expression and Is a Targetable Dependency in Glioblastoma Stem Cells. *Cancer Discov* 2021, **11**(2)**:** 480-499.

19. Cui Q, Shi H, Ye P, Li L, Qu Q, Sun G*, et al.* m(6)A RNA Methylation Regulates the Self-Renewal and Tumorigenesis of Glioblastoma Stem Cells. *Cell Rep* 2017, **18**(11)**:** 2622-2634.

20. Comprehensive genomic characterization defines human glioblastoma genes and core pathways. *Nature* 2008, **455**(7216)**:** 1061-1068.

21. Liu K, Zhou X, Li C, Shen C, He G, Chen T*, et al.* YTHDF2 as a Mediator in BDNF-Induced Proliferation of Porcine Follicular Granulosa Cells. *International Journal of Molecular Sciences* 2024, **25**(4).

22. Wang S, Sun C, Li J, Zhang E, Ma Z, Xu W*, et al.* Roles of RNA methylation by means of N(6)-methyladenosine (m(6)A) in human cancers. *Cancer Lett* 2017, **408:** 112-120.

23. Ueki K, Ono Y, Henson JW, Efird JT, von Deimling A, Louis DN. CDKN2/p16 or RB alterations occur in the majority of glioblastomas and are inversely correlated. *Cancer Res* 1996, **56**(1)**:** 150-153.

ARTICLE IN PRESS

24. Cui L, Wu Y, Chen Z, Li B, Cai J, Chang Z*, et al.* N6-methyladenosine modification-tuned lipid metabolism controls skin immune homeostasis via regulating neutrophil chemotaxis. *Sci Adv* 2024, **10**(40)**:** eadp5332.

25. Xie R, Yan S, Zhou X, Gao Y, Qian Y, Hou J*, et al.* Activation of METTL3 Promotes White Adipose Tissue Beiging and Combats Obesity. *Diabetes* 2023, **72**(8)**:** 1083-1094.

26. Jiang X, Liu B, Nie Z, Duan L, Xiong Q, Jin Z*, et al.* The role of m6A modification in the biological functions and diseases. *Signal Transduct Target Ther* 2021, **6**(1)**:** 74.

27. Fang Z, Mei W, Qu C, Lu J, Shang L, Cao F*, et al.* Role of m6A writers, erasers and readers in cancer. *Exp Hematol Oncol* 2022, **11**(1)**:** 45.

28. Chen L, Gao Y, Xu S, Yuan J, Wang M, Li T*, et al.* N6-methyladenosine reader YTHDF family in biological processes: Structures, roles, and mechanisms. *Front Immunol* 2023, **14:** 1162607.

29. Wang Y, Chen J, Gao WQ, Yang R. METTL14 promotes prostate tumorigenesis by inhibiting THBS1 via an m6A-YTHDF2-dependent mechanism. *Cell Death Discov* 2022, **8**(1)**:** 143.

30. Chen YJ, Iyer SV, Hsieh DC, Li B, Elias HK, Wang T*, et al.* Gliocidin is a nicotinamide-mimetic prodrug that targets glioblastoma. *Nature* 2024, **636**(8042)**:** 466-473.

31. Giammona A, Commisso M, Bonanomi M, Remedia S, Avesani L, Porro D*, et al.* A Novel Strategy for Glioblastoma Treatment by Natural Bioactive Molecules Showed a Highly Effective Anti-Cancer Potential. *Nutrients* 2024, **16**(15).

32. Nowacka A, Ziółkowska E, Smuczyński W, Bożiłow D, Śniegocki M. Potential of Curcumin and Its Analogs in Glioblastoma Therapy. *Antioxidants (Basel)* 2025, **14**(3).

33. Liu B, Peng D, Chen Y, Li Q, Hu Y, Liu S*, et al.* Multi-omics analysis identifies CCNB1 as a cell cycle factor driving glioblastoma progression and its inhibition by resveratrol. *PLoS One* 2026, **21**(3)**:** e0344872.

34. Elsori D, Alshabrmi FM, Alharbi AM, Saeed M, Singh A, Pandey P*, et al.* Anticancer potential of natural bioactive compounds saponins in glioblastoma multiforme. *Front Pharmacol* 2025, **16:** 1712599.

35. Huang C-S, Zhu Y-Q, Xu Q-C, Chen S, Huang Y, Zhao G*, et al.* YTHDF2 promotes intrahepatic cholangiocarcinoma progression and desensitises cisplatin treatment by increasing CDKN1B mRNA degradation. *Clin Transl Med* 2022, **12**(6)**:** e848.

36. Hsueh B, Steuart SJ, Odukoya AO, Prager BC, Kim YJ, Hill CM*, et al.* Immunotherapy and targeted therapy for high grade gliomas: current and future directions. *J Neurooncol* 2025, **176**(1)**:** 112.

ARTICLE IN PRESS

37. Chen Y, Wang YL, Qiu K, Cao YQ, Zhang FJ, Zhao HB*, et al.* YTHDF2 promotes temozolomide resistance in glioblastoma by activation of the Akt and NF-κB signalling pathways via inhibiting EPHB3 and TNFAIP3. *Clin Transl Immunology* 2022, **11**(5)**:** e1393.

38. Zhong X, Wang S, Yang X, Yang X, Zhou L. METTL14 inhibits the proliferation, migration and invasion of prostate cancer cells by increasing m6A methylation of CDK4. *Transl Androl Urol* 2024, **13**(7)**:** 1145-1163.

39. Liu K, Zhou X, Li C, Shen C, He G, Chen T*, et al.* YTHDF2 as a Mediator in BDNF-Induced Proliferation of Porcine Follicular Granulosa Cells. *Int J Mol Sci* 2024, **25**(4).

40. Zheng J, Liang Y, Xu X, Zhou J, Jiang S, Yu J. N6-methyladenosine binding protein YTHDF2 inhibits gastric cancer cell growth and predicts better prognosis in patients with gastric cancer. *Transl Oncol* 2025, **56:** 102395.

41. Hou Y, Zhang X, Yao H, Hou L, Zhang Q, Tao E*, et al.* METTL14 modulates glycolysis to inhibit colorectal tumorigenesis in p53-wild-type cells. *EMBO Rep* 2023, **24**(4)**:** e56325.

42. Wei J, Harada BT, Lu D, Ma R, Gao B, Xu Y*, et al.* HRD1-mediated METTL14 degradation regulates m(6)A mRNA modification to suppress ER proteotoxic liver disease. *Mol Cell* 2021, **81**(24)**:** 5052-5065.e5056.

ARTICLE IN PRESS

ARTICLE IN PRESS

Figure legends

Figure 1 GDPPH1 suppresses GBM cell proliferation and induces apoptosis

(A) Quantification of inhibitory activity of GDPPH1 on cell viability in U251 and U87MG cell lines. The cell viability was determined by MTT assay, after treatment with various concentrations of GDPPH1 (2, 4, 8, 16 μM) for 48 h. (B) Plate colony formation of U251 and U87MG cells after GDPPH1 treatment for 14 days and quantitation of colony numbers. (C) Effects of GDPPH1 (1 μM) on DNA synthesis in U251 and U87MG cells at 24 h measured by ethynyl deoxyuridine (EdU). Scale bar, 50 μm. (D) Live and dead cell staining in U251 and U87MG cells. Scale bar, 50 μm. (E) Quantitative analysis of EdU in U251 and U87MG cells. (F) Quantitative analysis of live and dead cell staining in U251 and U87MG cells. (G) Flow cytometry analysis of cell death for U251 and U87MG cells treated with GDPPH1 for 24 h and subsequently stained with Annexin V and propidium iodide (PI). The results of the representative experiments and quantitative analysis are shown. Data are presented as mean ± SD from at least three independent replicates. Statistical significance between two groups was determined using an unpaired two-tailed Student's t-test, while comparisons among multiple groups were performed using one-way ANOVA followed by Tukey's post hoc test. $P < 0.05$ was considered statistically significant. *$P < 0.05$, **$P < 0.01$, ***$P < 0.001$.

Figure 2 GDPPH1 arrests the cell cycle at the G1/S phase by downregulation of CDK4 and Cyclin D1 in GBM cells

(A) Effect of GDPPH1 on the cell cycle of U251 and U87MG cell lines assessed by PI staining-coupled flow cytometry. Quantitative analysis of concentration-dependent cell cycle arrest induced by GDPPH1 in U251 and

ARTICLE IN PRESS

U87MG cells. (B, C) GDPPH1 (3, 6, and 12 μM) treatment for 12 h decreased the protein expression of Cyclin D1, CDK4, CDK6, and p-RB (Ser780) in U251 and U87MG cell lines. β-tubulin was used as the loading control. (D) Relative mRNA expression of *CDK4* and *CCND1* in U251 and U87MG cell lines with 12 h GDPPH1 treatment at 3, 6, and 12 μM. Data are presented as mean ± SD from at least three independent replicates. Statistical significance among multiple groups was performed using one-way ANOVA followed by Tukey's post hoc test. $P < 0.05$ was considered statistically significant. *$P < 0.05$, **$P < 0.01$, ***$P < 0.001$.

Figure 3 GDPPH1 induces cell apoptosis in GBM cells

(A) U251 and U87MG cells treated with different cell death inhibitors, including Z-VAD-FMK (pan-caspase inhibitor, Z-VAD), Ferrrostatin-1 (ferroptosis inhibitor, Fer-1), Necrostatin-1 (necrosis inhibitor, Nec-1), and Chloroquine (autophagy inhibitor, CQ), in the presence of GDPPH1 (8 μM) treatment. (B) Western blot to detect the expression of apoptosis-related proteins in GBM cells after 18 h treatment with GDPPH1 (3, 6, 12 μM). (C) TUNEL staining reveals increased apoptosis in GDPPH1-treated tumors. Scale bars, 50 μm in merged images and 100 μm in individual channel images. (D) Flow cytometry analysis of cell apoptosis for U87MG cells treated with GDPPH1 (8 μM) with or without Z-VAD (10 μM) for 48 h and subsequently stained with Annexin V and PI. Data are presented as mean ± SD from at least three independent replicates. Statistical significance among multiple groups was performed using one-way ANOVA followed by Tukey's post hoc test. $P < 0.05$ was considered statistically significant. *$P < 0.05$, **$P < 0.01$, ***$P < 0.001$.

Figure 4 GDPPH1 suppresses CDK4 and *CCND1* mRNA levels in an m^{6}A-dependent manner

ARTICLE IN PRESS

(A) Stability of *CDK4* and *CCND1* mRNA upon GDPPH1 treatment on U251 cells examined by actinomycin D (Act D) chase assay. (B) The m^6A level of total RNA isolated from GDPPH1-treated U251 and U87MG cells was indicated by m^6A dot blot. (C) In U251 and U87MG cells treated with GDPPH1 and/or MP3C, cell viability was measured by MTT. (D) qPCR analysis of *CDK4* and *CCND1* in U251 and U87MG cells upon GDPPH1 and/or MP3C. (E) Western blot analysis of Cyclin D1, CDK4, and p-RB (Ser780) in U251 and U87MG cells upon GDPPH1 and/or MP3C. (F) Quantification of the expression of indicated protein levels in E. (G) Cell cycle analysis of U251 and U87MG cells upon GDPPH1 and/or MP3C. Data are presented as mean ± SD from at least three independent replicates. Statistical significance among multiple groups was performed using one-way ANOVA followed by Tukey's post hoc test. mRNA stability was analyzed using one-phase exponential decay analysis. $P < 0.05$ was considered statistically significant. $^*P < 0.05$, $^{**}P < 0.01$, $^{***}P < 0.001$.

ARTICLE IN PRESS

Figure 5 GDPPH1-regulated CDK4 and Cyclin D1 expression is primarily associated with METTL14

(A) qPCR analysis of key m^6A-related enzyme in U251 and U87MG cells followingGDPPH1 treatment. (B) Western blot analysis of METTL3, METTL14, WTAP, ALKBH5, and FTO in U251 and U87MG cells upon GDPPH1 treatment. (C) qPCR analysis of *METTL14*, *CDK4,* and *CCND1* in U251 and U87MG cells following GDPPH1 treatment with or METTL14 overexpression (OE) of METTL14. (D) Western blot analysis of Cyclin D1, CDK4, and p-RB (Ser780) in U251 and U87MG cells under GDPPH1 treatment with or without METTL14 OE. (E) Stability of *CDK4* and *CCND1* mRNA upon GDPPH1 treatment with or without METTL14 OE, assessed by Act D chase assay. (F) Cell cycle distribution of U251 and U87MG cells following GDPPH1 treatment with or without METTL14 OE. (G) Cell viability was measured by MTT assay in U251 and U87MG

ARTICLE IN PRESS

cells treated with GDPPH1 in the presence or absence of METTL14 OE. Data are presented as mean ± SD from at least three independent replicates. Statistical significance between two groups was determined using an unpaired two-tailed Student's t-test, while comparisons among multiple groups were performed using one-way ANOVA followed by Tukey's post hoc test. mRNA stability was analyzed using one-phase exponential decay analysis. $P < 0.05$ was considered statistically significant. *$P < 0.05$, **$P < 0.01$, ***$P < 0.001$.

Figure 6 The m^{6}A-dependent downregulation of CDK4 and Cyclin D1 by GDPPH1 is associated with YTHDF2

(A) Interaction between YTHDF1, YTHDF2, YTHDF3, and *CDK4* detected by RIP. (B) Interaction between YTHDF2 and *CDK4*, *CCND1*, with METTL14 OE detected by RIP. (C) The interaction between YTHDF2 and *CDK4*, *CCND1* were diminished by GDPPH1. (D) Western blot analysis of Cyclin D1, CDK4, and p-RB (Ser780) in U251 and U87MG cells upon GDPPH1 with or without YTHDF2 OE. (E) Stability of *CDK4* and *CCND1* mRNA upon GDPPH1 treatment with or without YTHDF2 OE examined by Act D chase assay. (F) Cell cycle analysis and cell viability of U251 and U87MG cells upon GDPPH1 with or without YTHDF2 OE. (G) U251 and U87MG cells treated with GDPPH1 and/or YTHDF2 OE, cell viability was measured by MTT. Data are presented as mean ± SD from at least three independent replicates. Statistical significance between two groups was determined using an unpaired two-tailed Student's t-test, while comparisons among multiple groups were performed using one-way ANOVA followed by Tukey's post hoc test. mRNA stability was analyzed using one-phase exponential decay analysis. $P < 0.05$ was considered statistically significant. *$P < 0.05$, **$P < 0.01$, ***$P < 0.001$.

ARTICLE IN PRESS

Figure 7 METTL14 is the direct target of GDPPH1

(A) Molecular docking analysis revealed that GDPPH1 forms a stable complex with METTL14, with a binding energy (ΔG) of −7.5 kcal/mol. (B, C) CETSA and DARTS assays confirm a direct and specific interaction between GDPPH1 and METTL14. (D) The binding affinity between GDPPH1 and METTL14 was determined using ITC. (E) The interaction between GDPPH1 and METTL14 protein was measured by SPR. (F) Steady-state affinity analysis based on equilibrium response units plotted against analyte concentration. Data are presented as mean ± SD from at least three independent replicates. Statistical significance among multiple groups was performed using one-way ANOVA followed by Tukey's post hoc test. $P < 0.05$ was considered statistically significant. *$P < 0.05$, **$P < 0.01$, ***$P < 0.001$.

Figure 8 GDPPH1 suppresses GBM growth *in vivo*

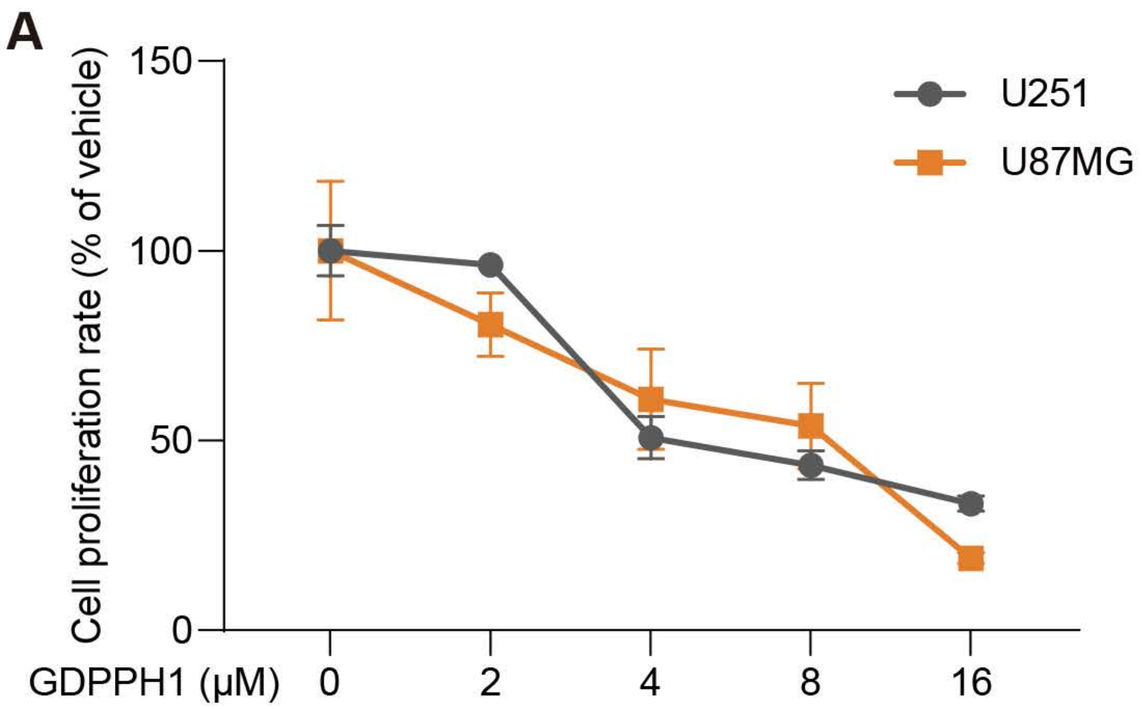
(A) Images of tumors from the vehicle and GDPPH1 (2 and 4 mg/kg) treatment groups (n = 6). (B) GDPPH1 (2 and 4 mg/kg) treatment reduced the tumor weight. (C) Measurement of tumor volume in each group. (D) Representative images of bioluminescence of mice on days 7, 14, and 21 after implantation and quantitative analysis of these bioluminescence images for the vehicle and GDPPH1 treatment groups. (E) The overall survival (OS) of mice in the vehicle and GDPPH1-treated groups in the orthotopic model. (F) Measurement of protein expression levels of METTL14, Cyclin D1, CDK4, and p-RB in tumor tissues in GDPPH1 (2 and 4 mg/kg). (G) Quantification of the expression of indicated protein levels in F. (H) Immunohistochemistry assay data showed that GDPPH1 (2 and 4 mg/kg) inhibited the protein expression of Ki67, METTL14, CDK4, Cyclin D1, and

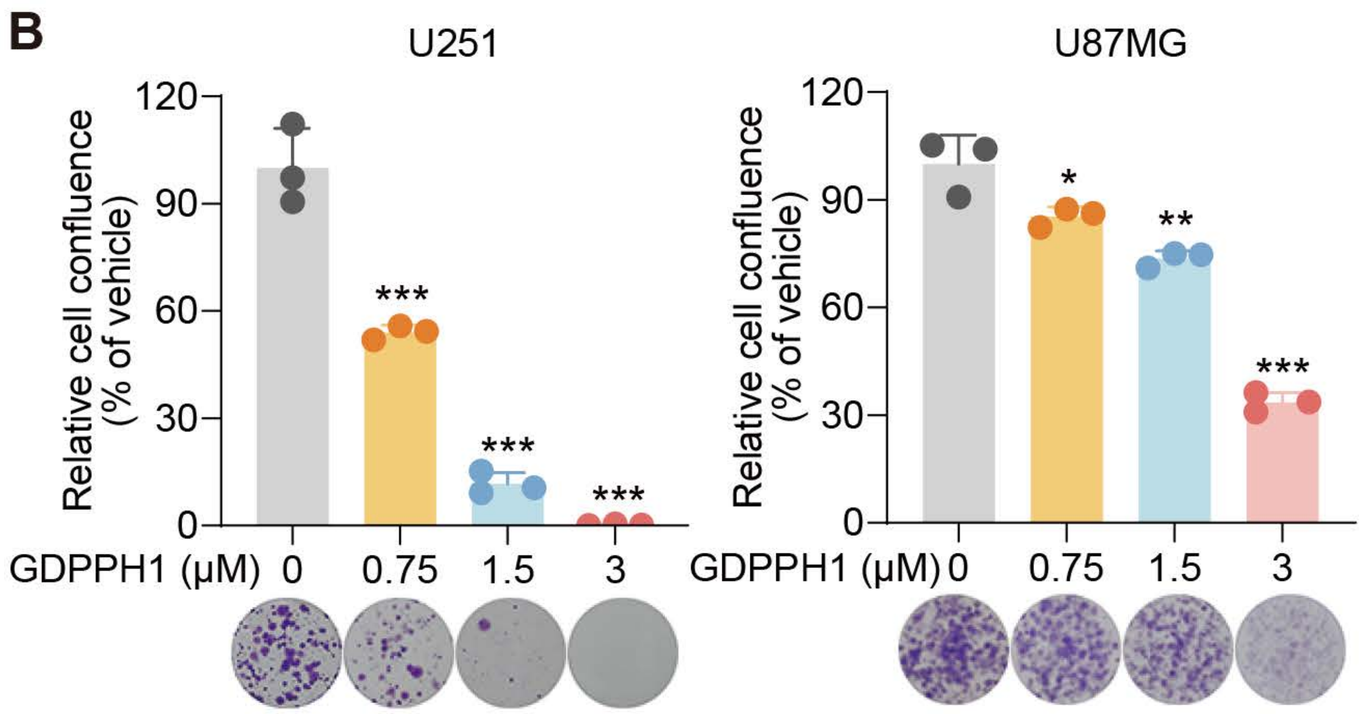
ARTICLE IN PRESS

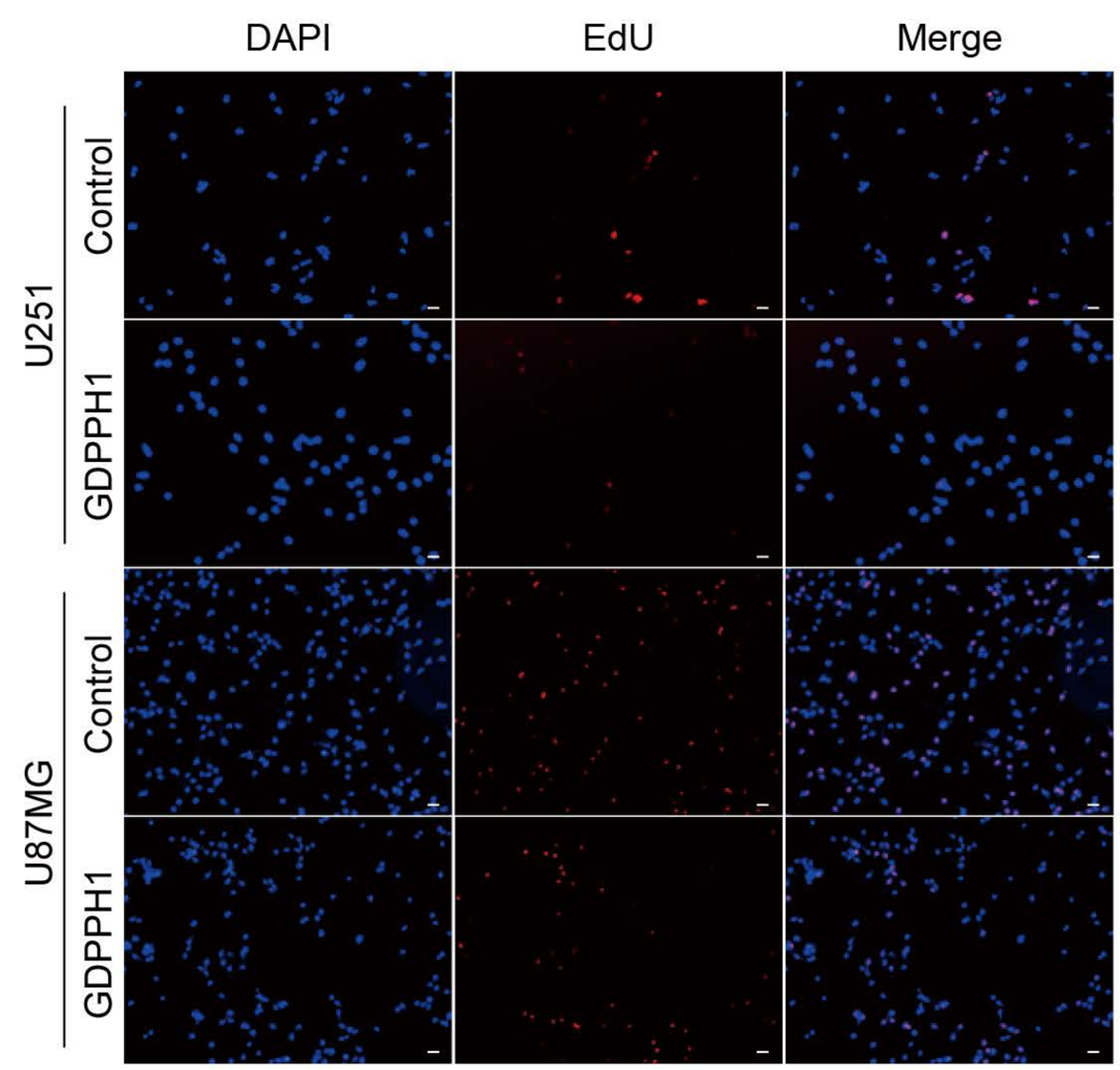
increased Cleaved Caspase-3 in tumor tissues. Scale bars, 100 μm in lower-magnification views; 25 μm in higher-magnification views. (I) Quantification of IHC staining in H. Data are presented as mean ± SD from at least three independent replicates. Statistical significance between two groups was determined using an unpaired two-tailed Student's t-test, while comparisons among multiple groups were performed using one-way ANOVA followed by Tukey's post hoc test. $P < 0.05$ was considered statistically significant. *$P < 0.05$, **$P < 0.01$, ***$P < 0.001$.

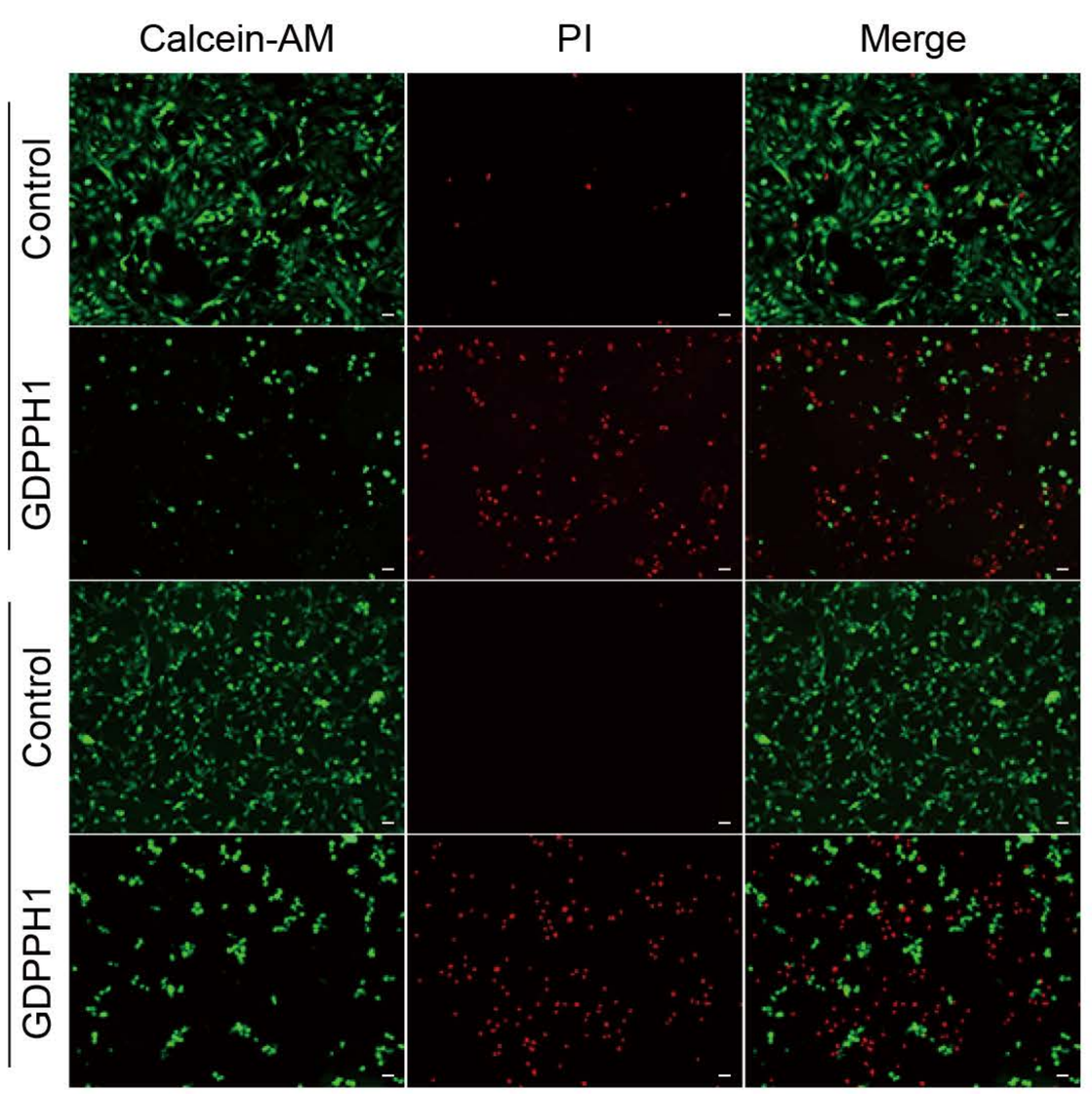
Figure 9 Schematic illustration of GDPPH1 induces cell cycle arrest at G1/S phase through regulation of YTHDF2-dependent *CDK4/CCND1* mRNA degradation in glioblastoma

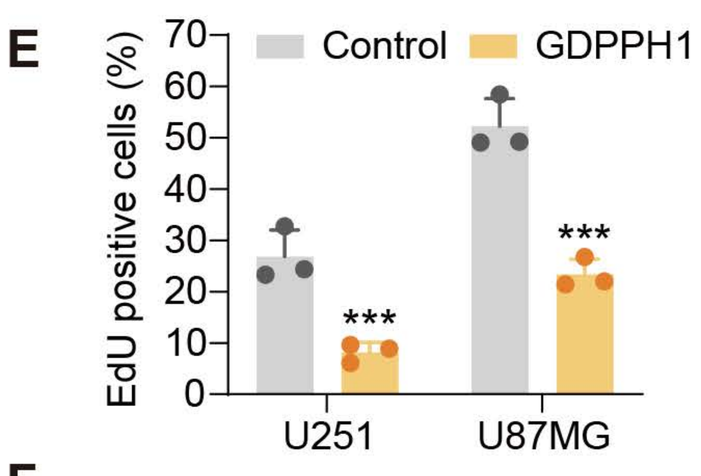
ARTICLE IN PRESS

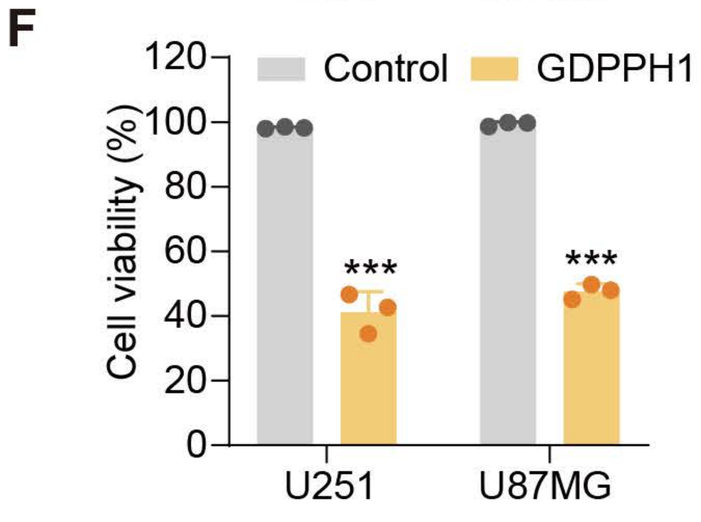

A
Cell proliferation rate (% of vehicle)
150
100
50
0
U251
U87MG
GDPPH1 (μM) 0 2 4 8 16

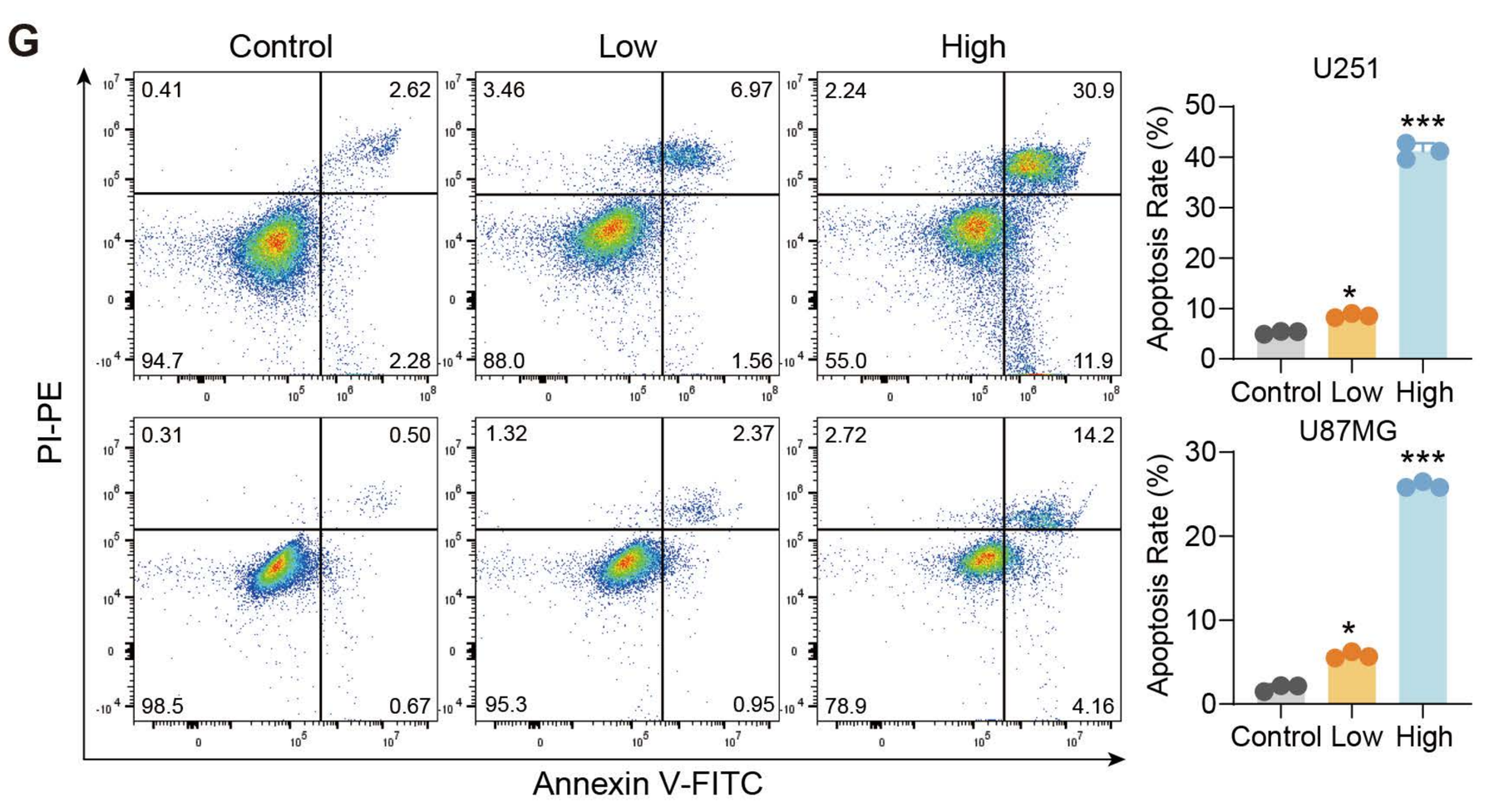

B
U251
U87MG
Relative cell confluence (% of vehicle)
120
90
60
30
0
*
**
***
GDPPH1 (μM) 0 0.75 1.5 3


C
DAPI
EdU
Merge
U251
U87MG
GDPPH1
Control

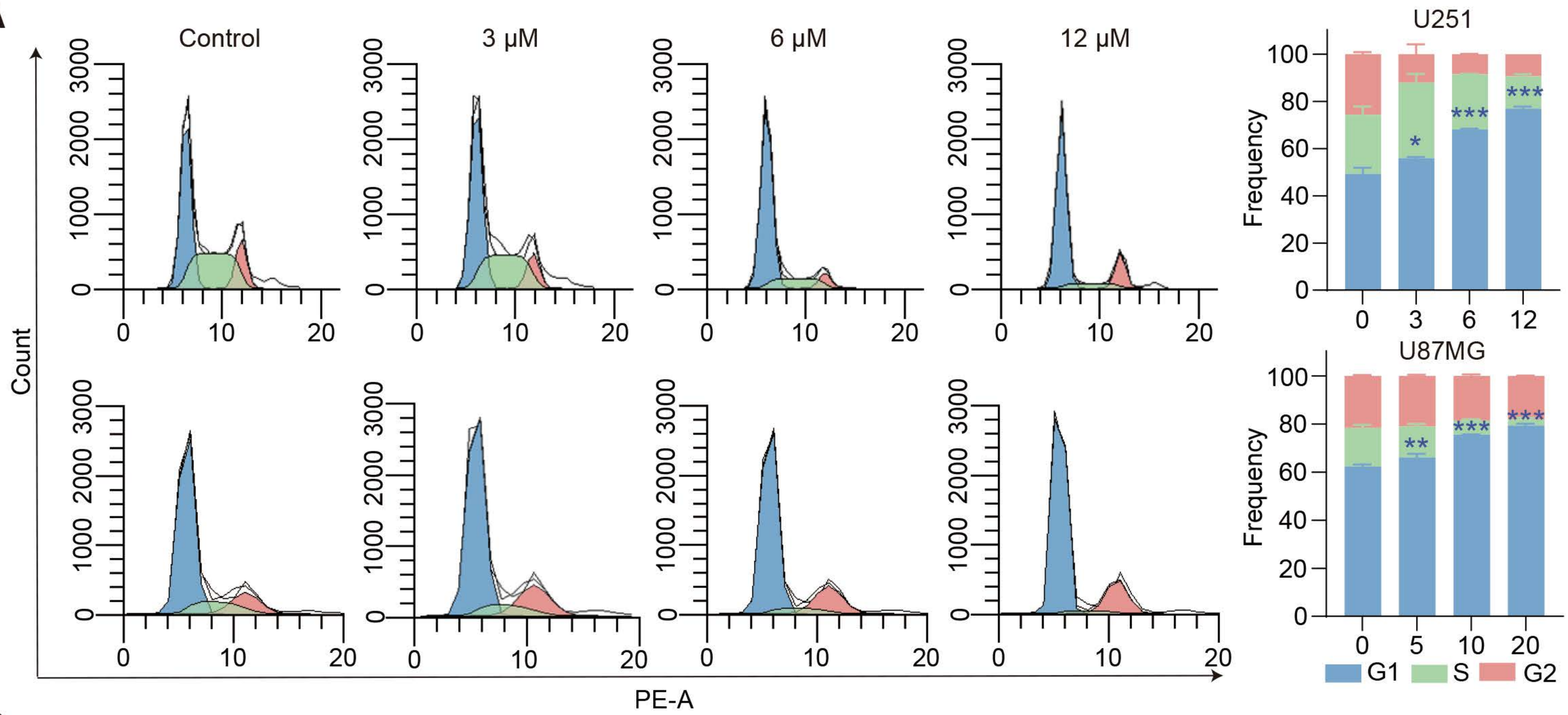

D
Calcein-AM
PI
Merge
U251
U87MG
GDPPH1
Control


E
EdU positive cells (%)
Control
GDPPH1
70
60
50
40
30
20
10
0
***
U251
U87MG

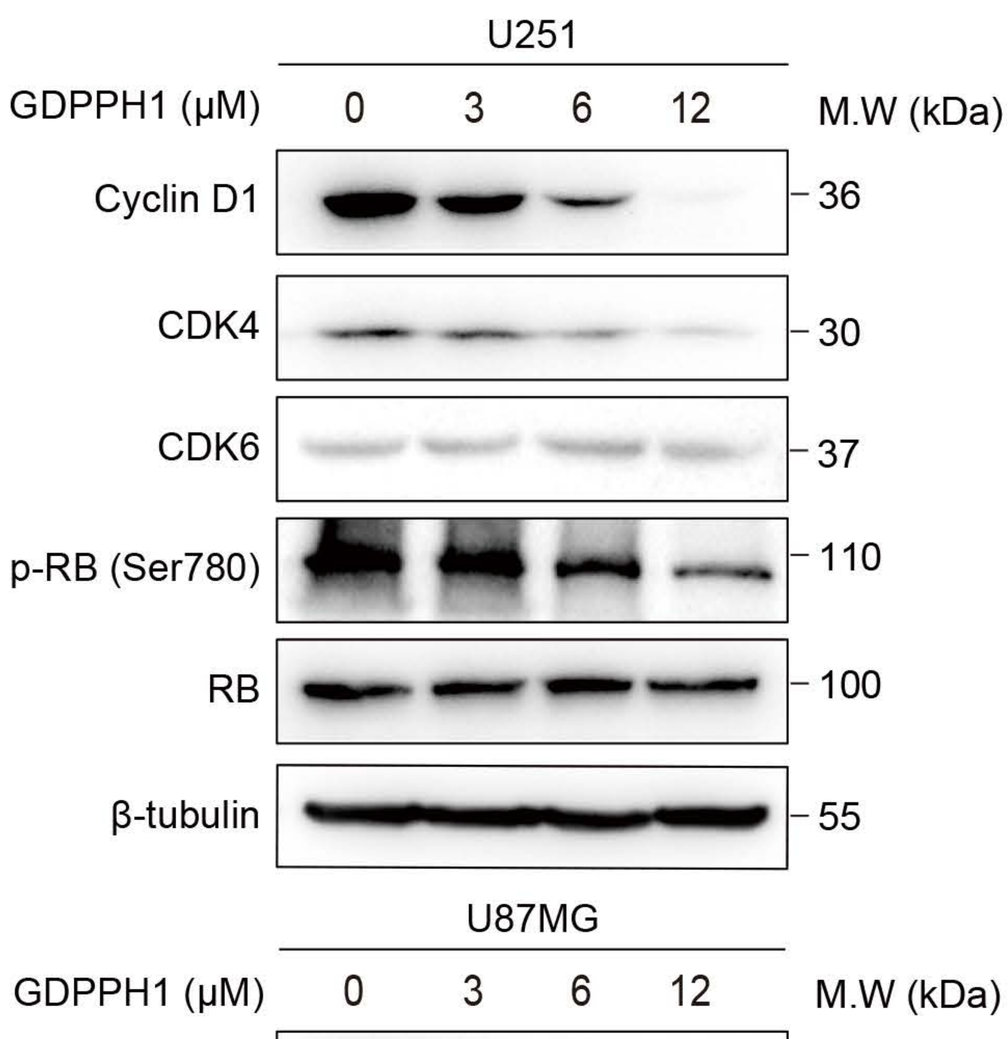

F
Cell viability (%)
Control
GDPPH1
120
100
80
60
40
20
0
***
U251
U87MG

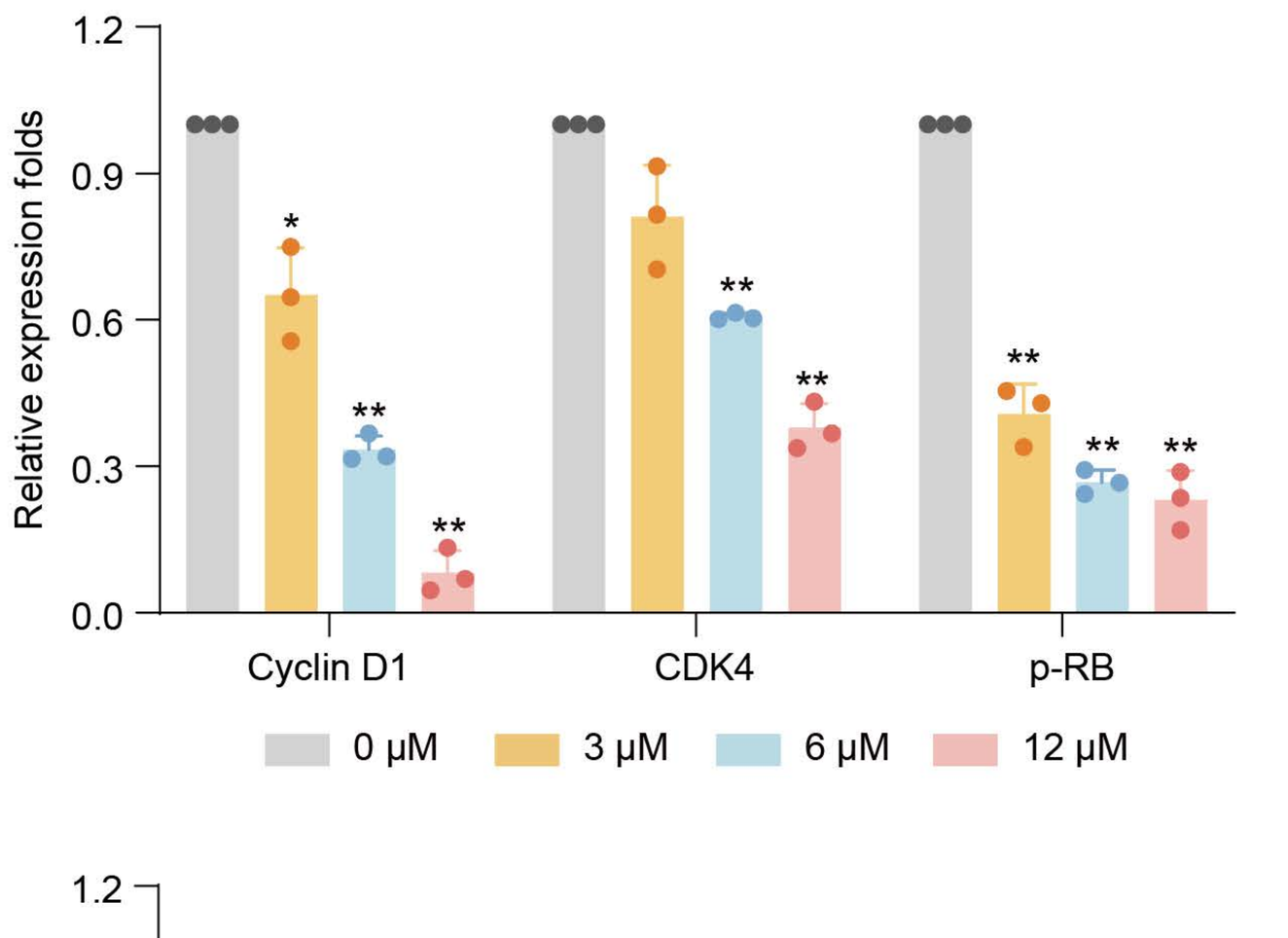

G
Control
Low
High
PI-PE
Annexin V-FITC
0.41
2.62
94.7
2.28
3.46
6.97
88.0
1.56
2.24
30.9
55.0
11.9
0.31
0.50
98.5
0.67
1.32
2.37
95.3
0.95
2.72
14.2
78.9
4.16
U251
U87MG
Apoptosis Rate (%)
Control Low High
*
***

A

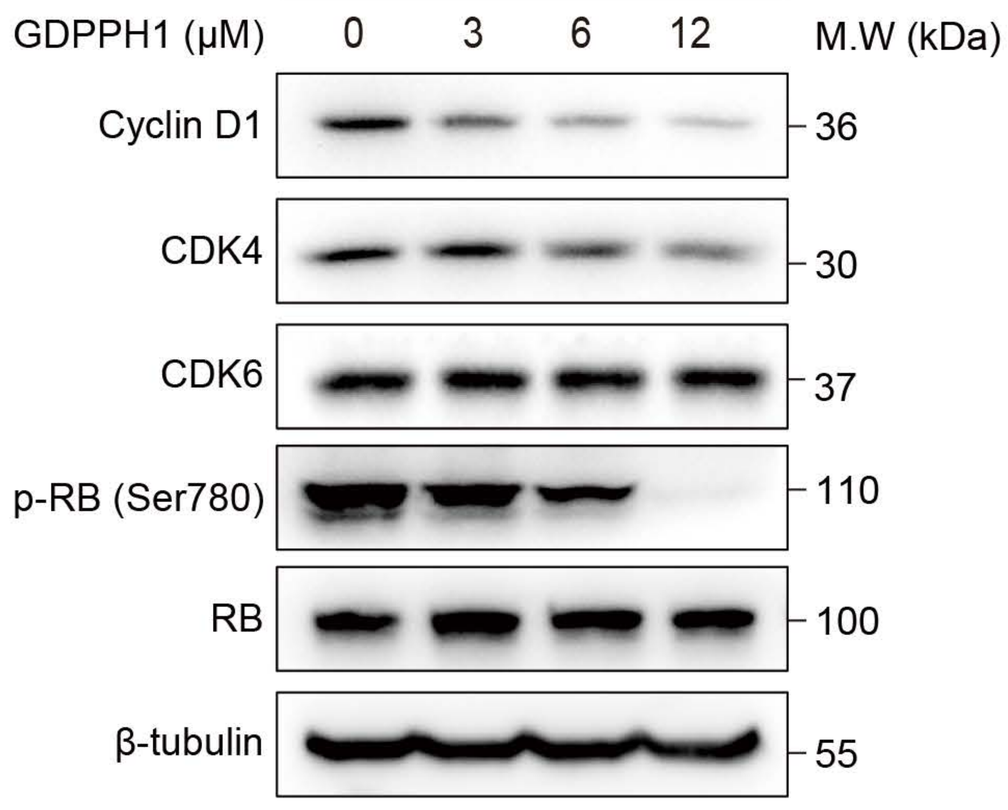

Control
3 μM
6 μM
12 μM
Count
PE-A
U251
U87MG
Frequency
G1
S
G2

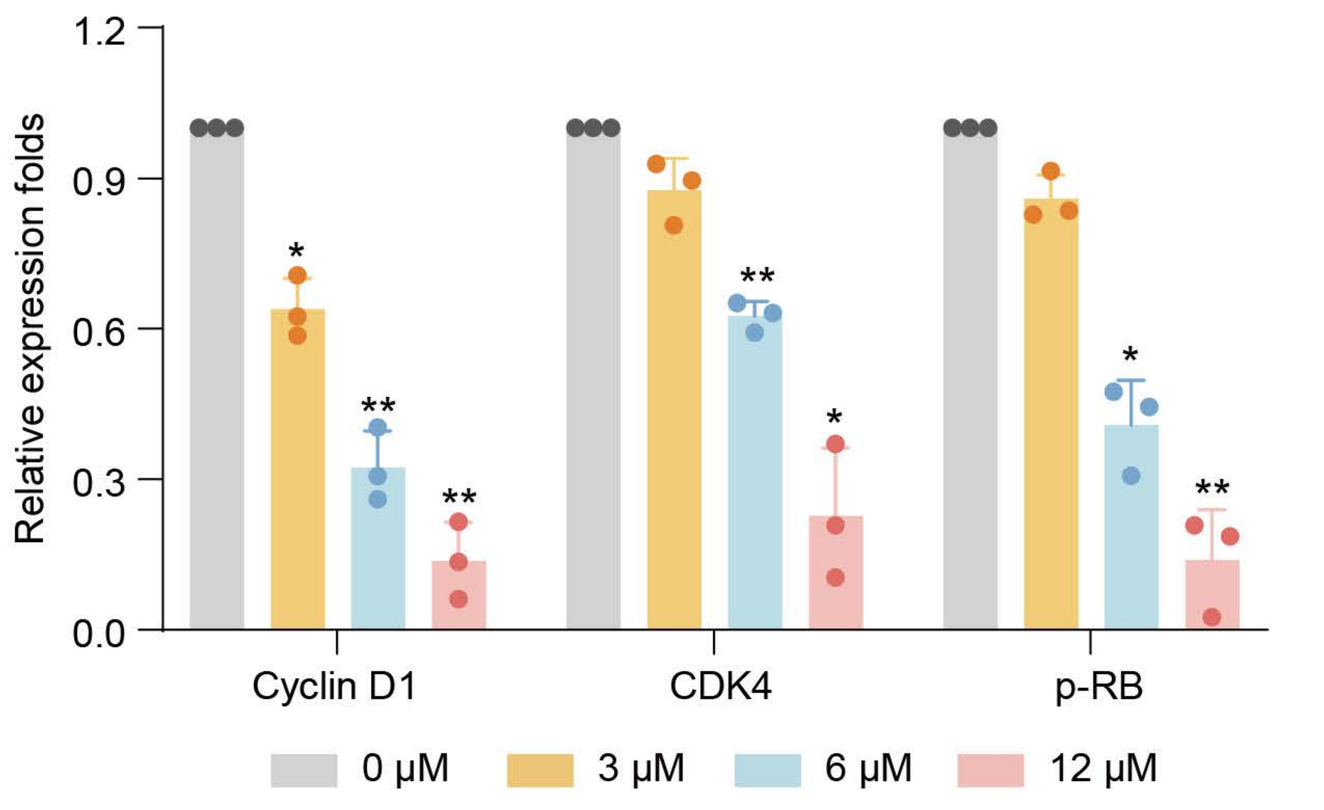
B


U251
GDPPH1 (μM)
0
3
6
12
M.W (kDa)
Cyclin D1
CDK4
CDK6
p-RB (Ser780)
RB
β-tubulin
36
30
37
110
100
55

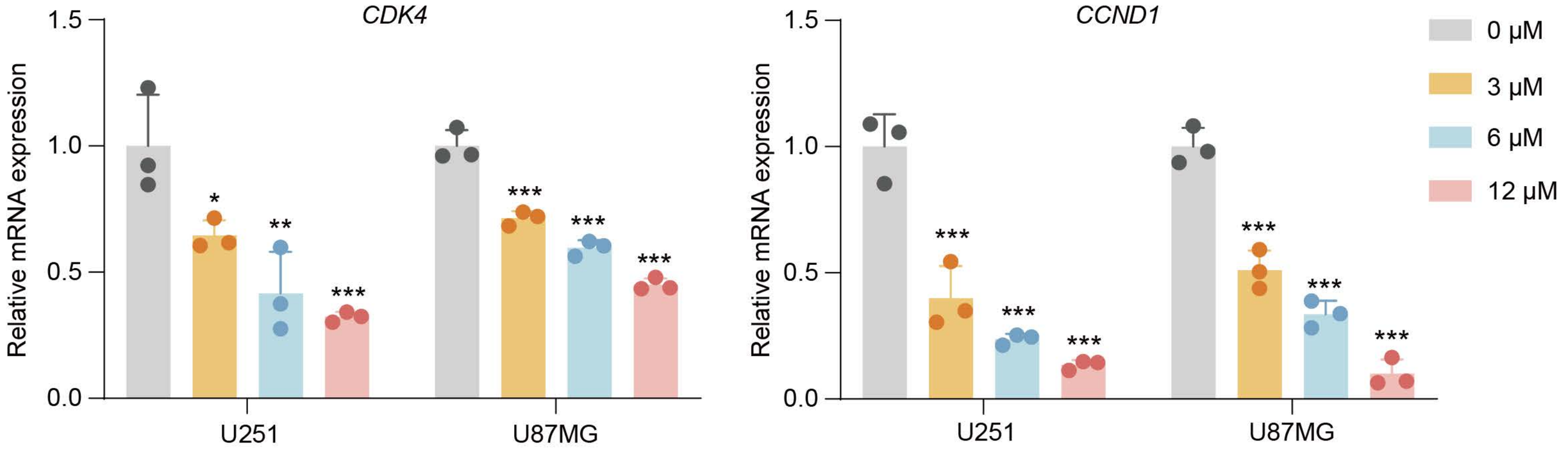

Relative expression folds
Cyclin D1
CDK4
p-RB
0 μM
3 μM
6 μM
12 μM

C

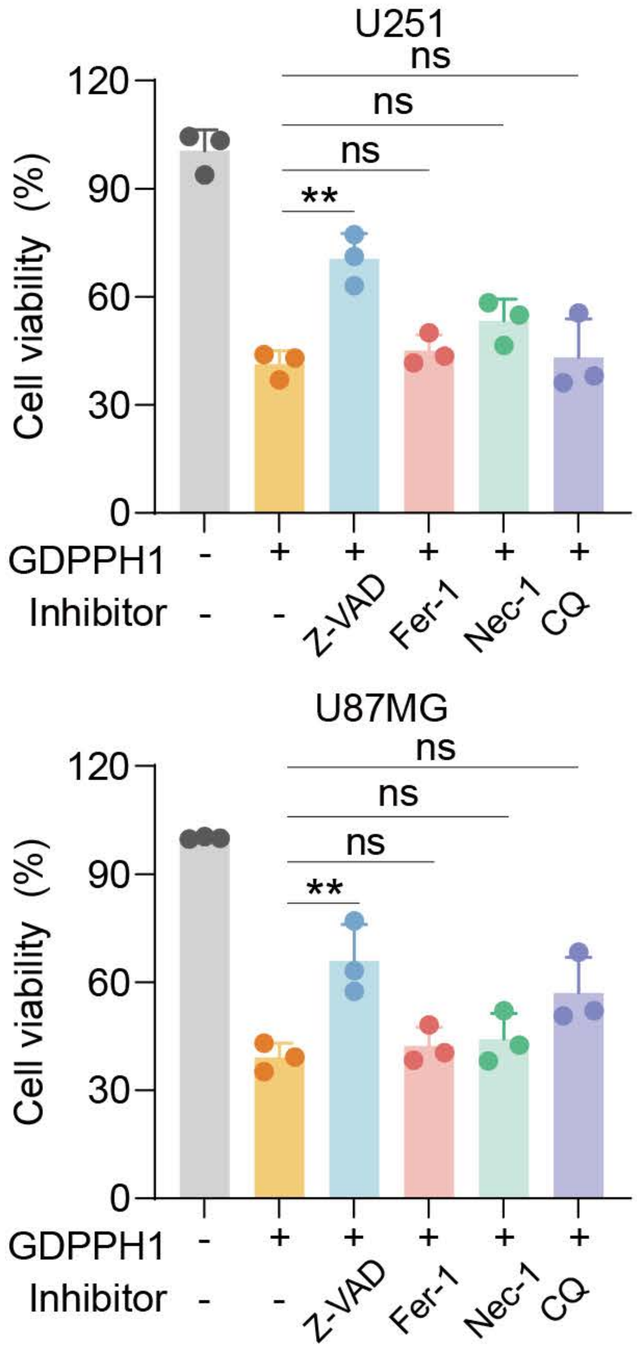

U87MG
GDPPH1 (μM)
0
3
6
12
M.W (kDa)
Cyclin D1
CDK4
CDK6
p-RB (Ser780)
RB
β-tubulin
36
30
37
110
100
55


Relative expression folds
Cyclin D1
CDK4
p-RB
0 μM
3 μM
6 μM
12 μM

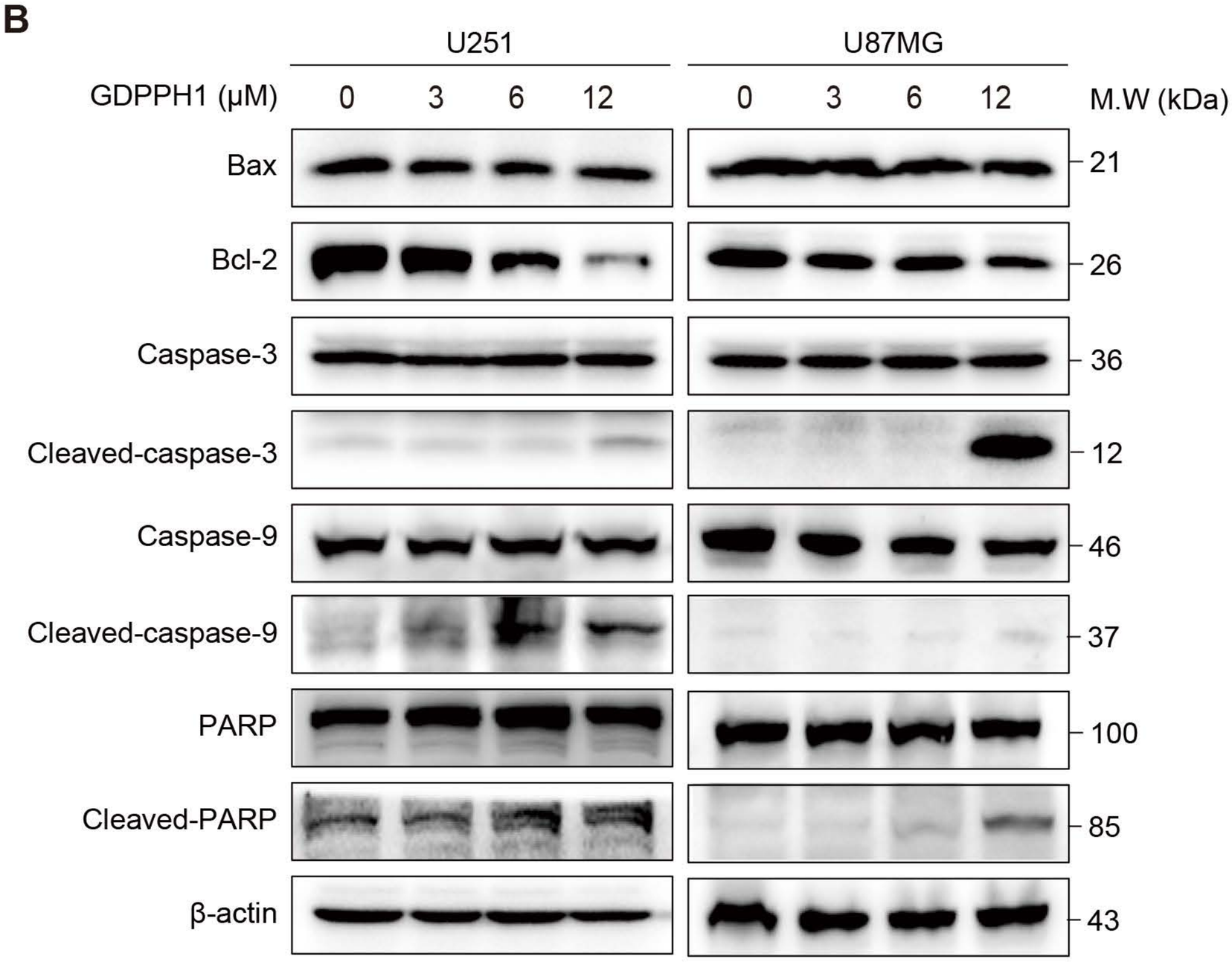
D


CDK4
CCND1
Relative mRNA expression
U251
U87MG
0 μM
3 μM
6 μM
12 μM

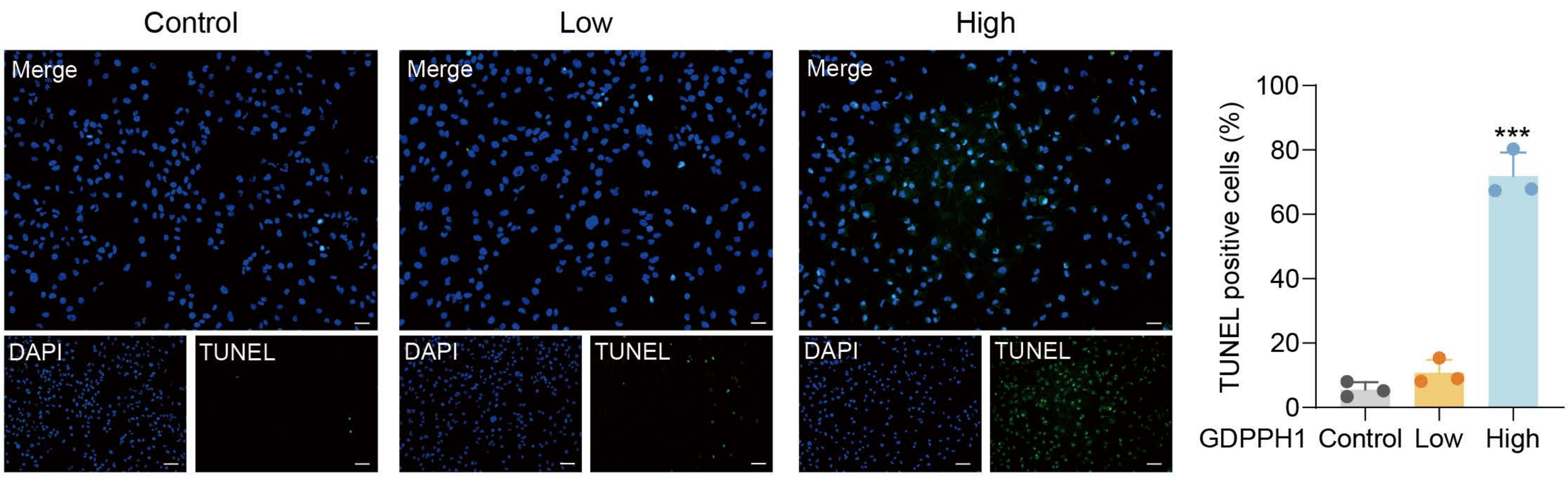
A


U251
U87MG
Cell viability (%)
120
90
60
30
0
ns
ns
ns
**
GDPPH1 - + + + + +
Inhibitor - - Z-VAD Fer-1 Nec-1 CQ

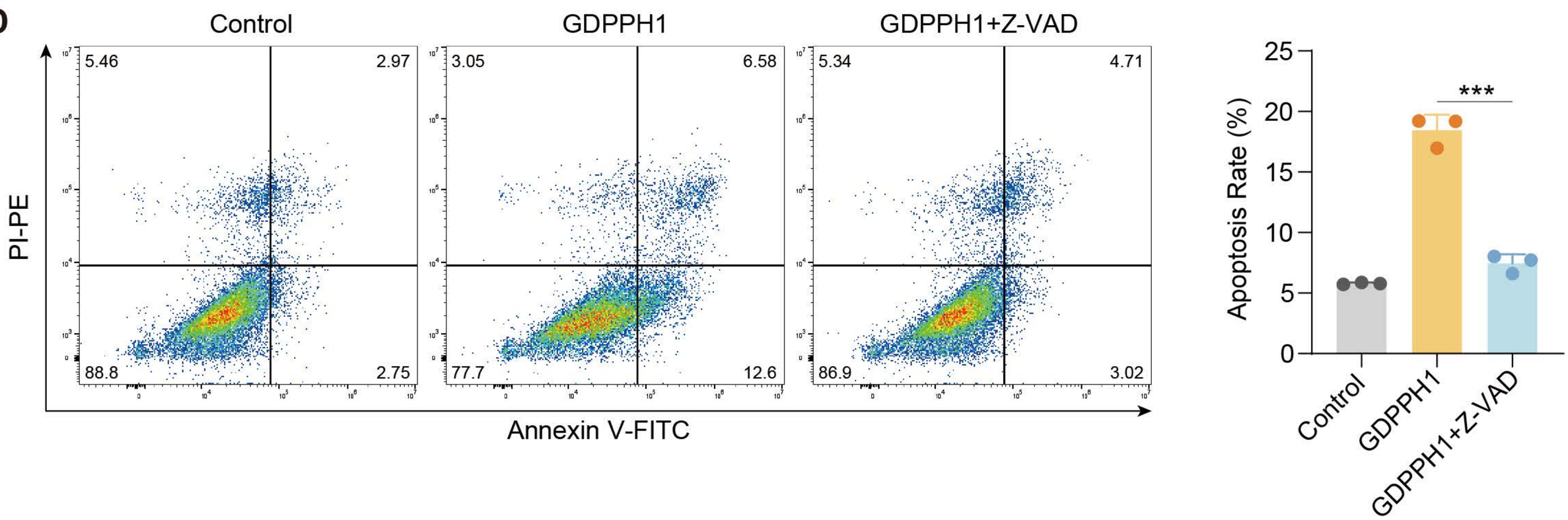
B

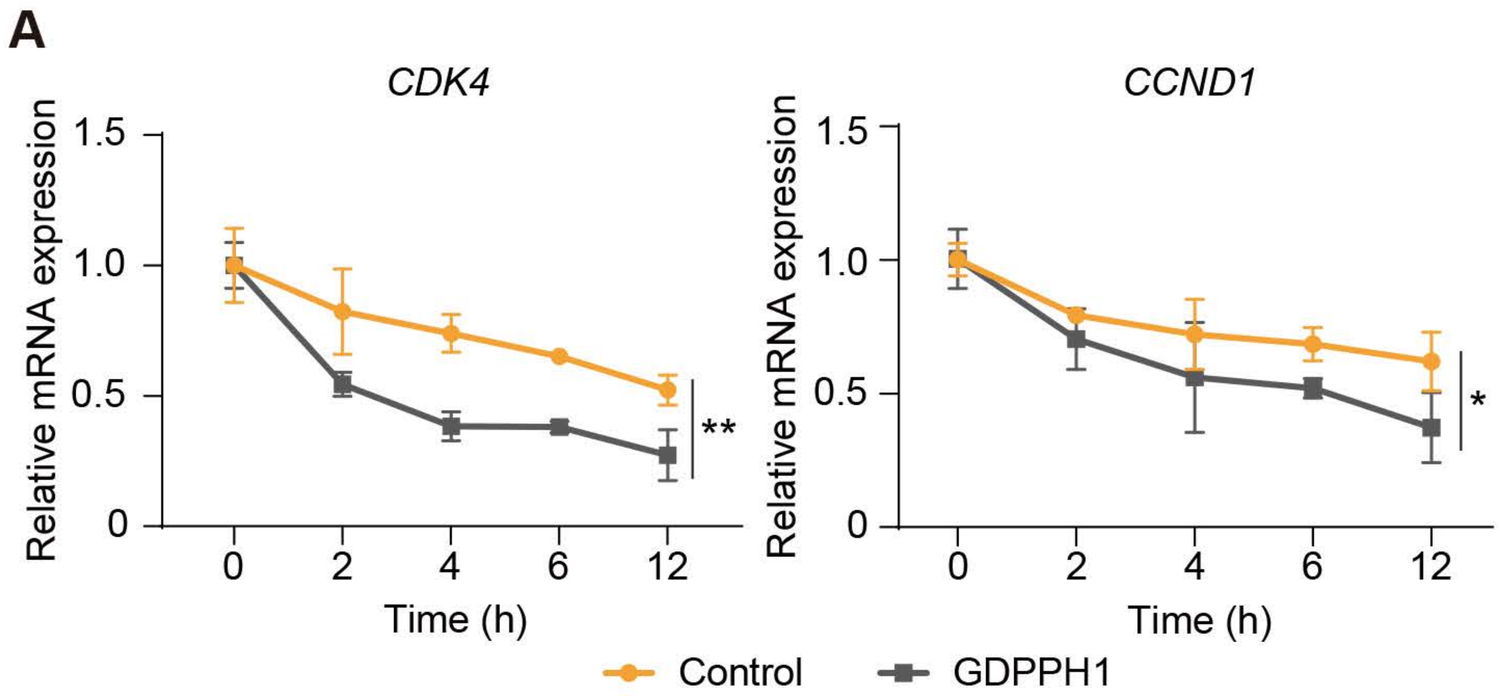

U251
U87MG
GDPPH1 (μM) 0 3 6 12 0 3 6 12
M.W (kDa)
Bax
Bcl-2
Caspase-3
Cleaved-caspase-3
Caspase-9
Cleaved-caspase-9
PARP
Cleaved-PARP
β-actin
21
26
36
12
46
37
100
85
43

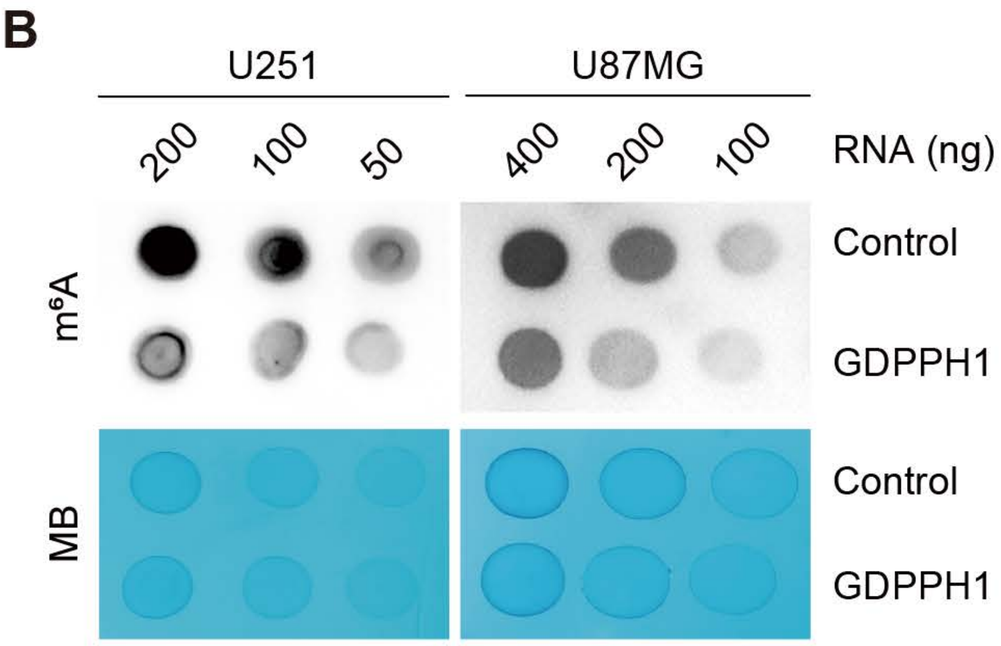
C

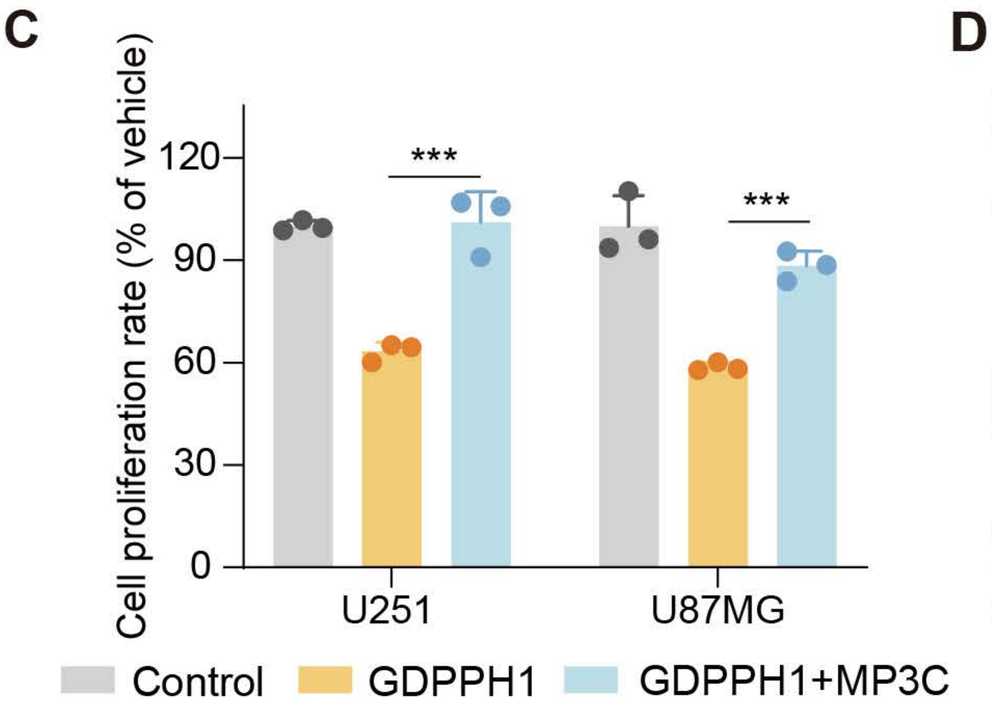

Control
Low
High
Merge
DAPI
TUNEL
TUNEL positive cells (%)
100
80
60
40
20
0
***
GDPPH1 Control Low High

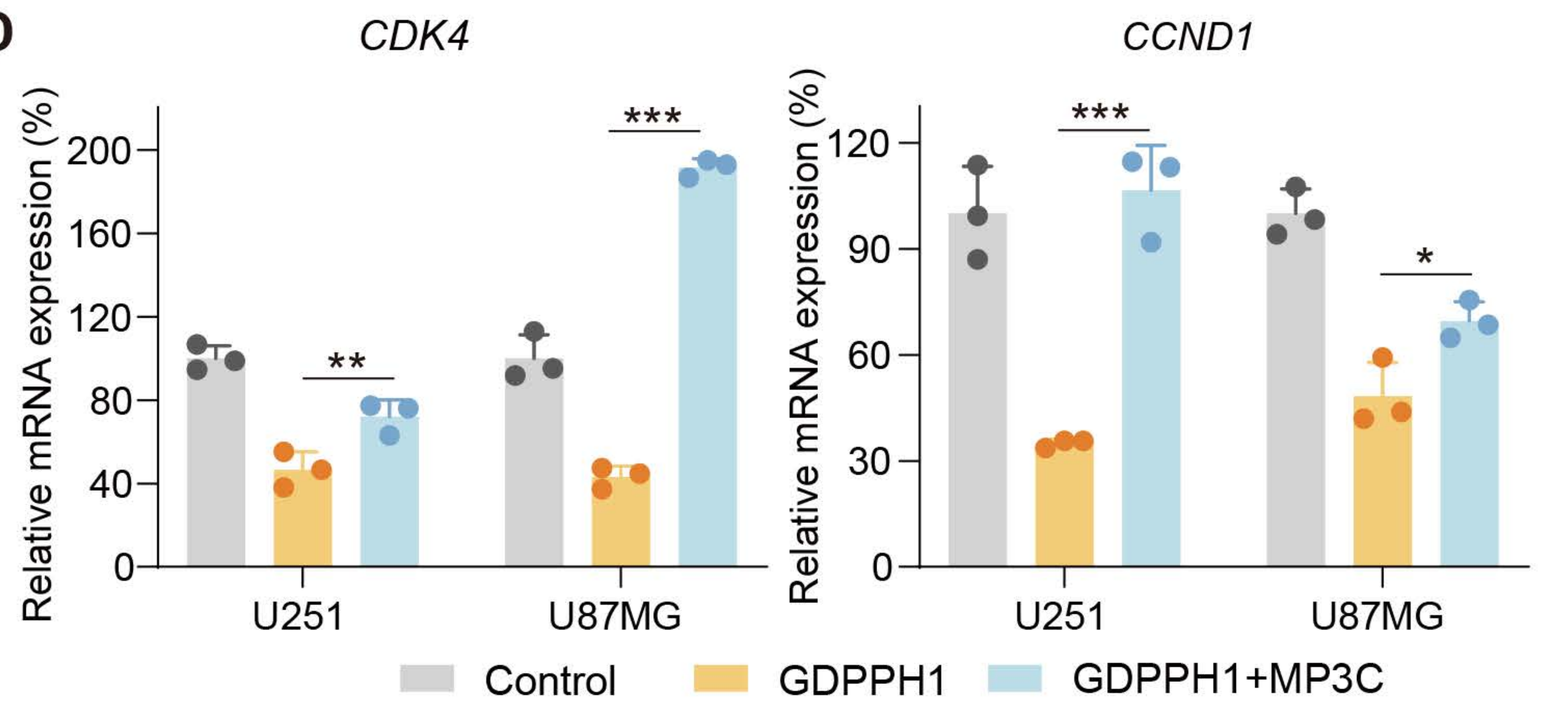
D

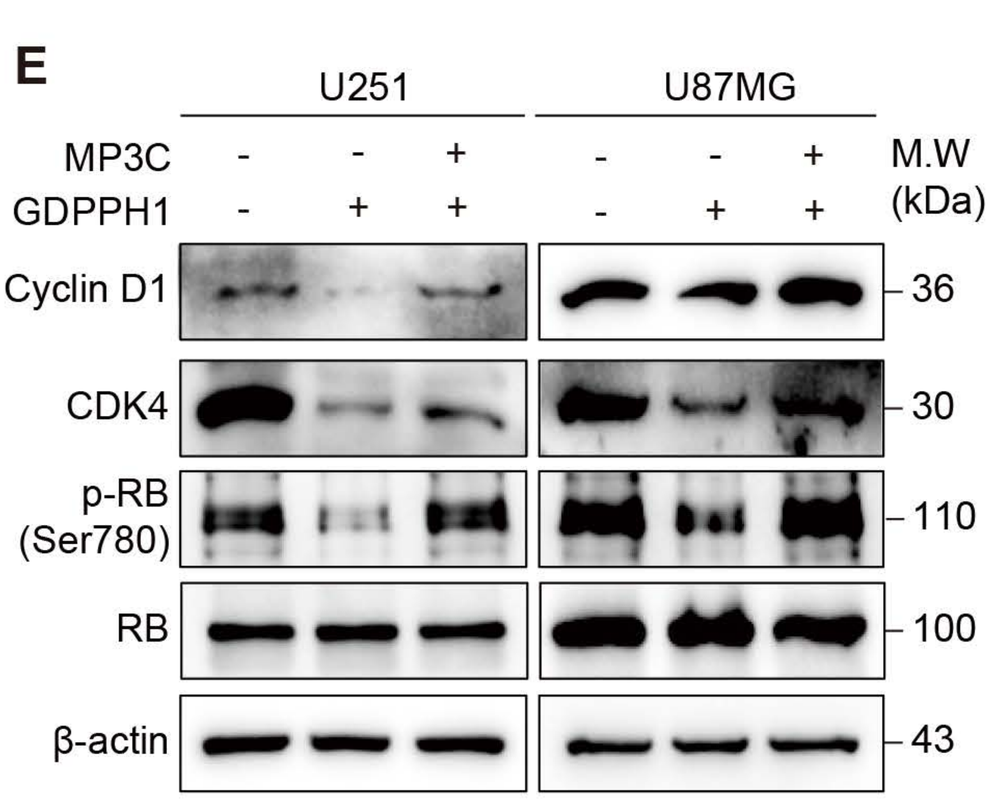

Control
GDPPH1
GDPPH1+Z-VAD
5.46
2.97
88.8
2.75
3.05
6.58
77.7
12.6
5.34
4.71
86.9
3.02
PI-PE
Annexin V-FITC
Apoptosis Rate (%)
25
20
15
10
5
0
***
Control
GDPPH1
GDPPH1+Z-VAD

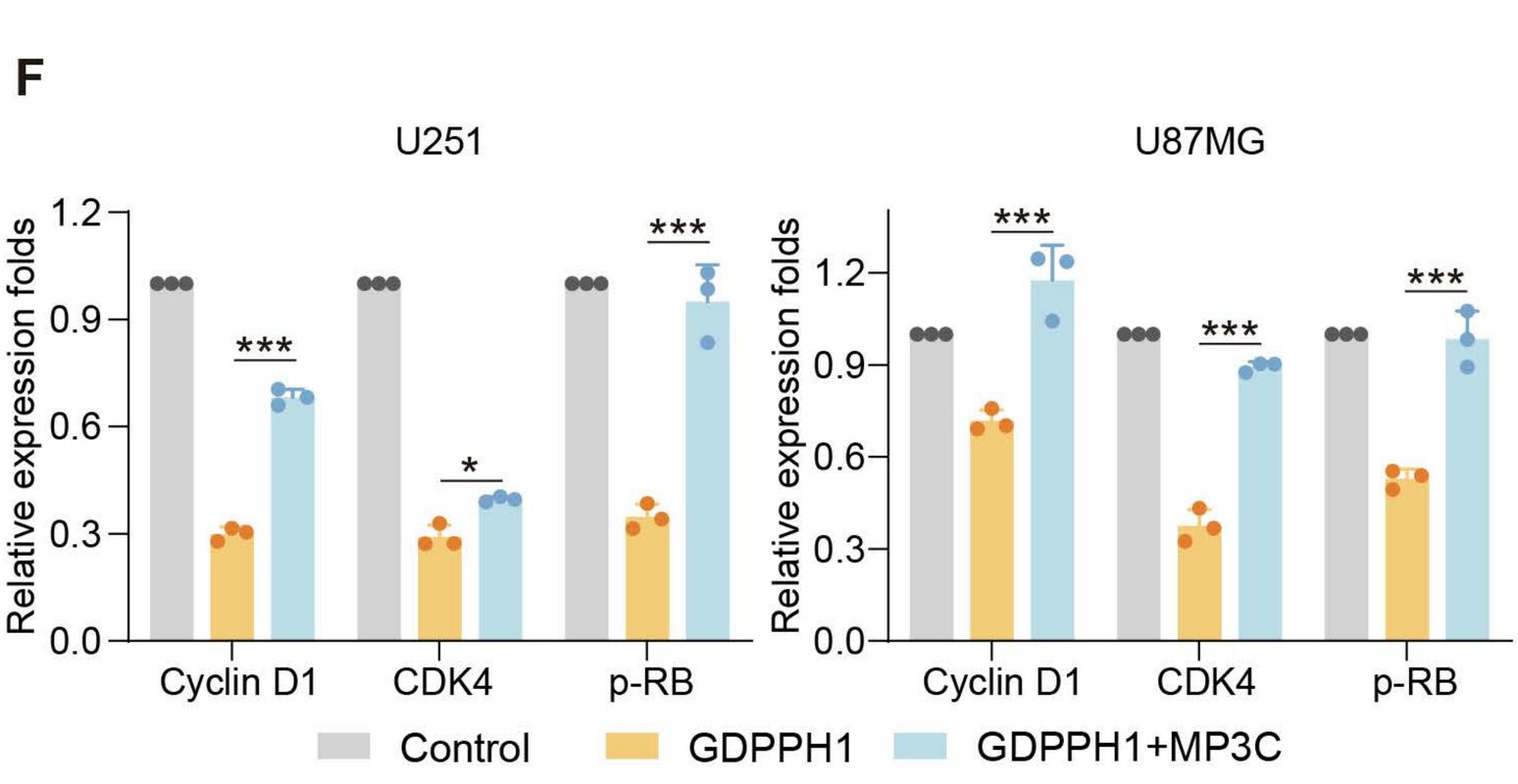

A
CDK4
CCND1
Relative mRNA expression
1.5
1.0
0.5
0
0
2
4
6
12
Time (h)
**
*
Control
GDPPH1

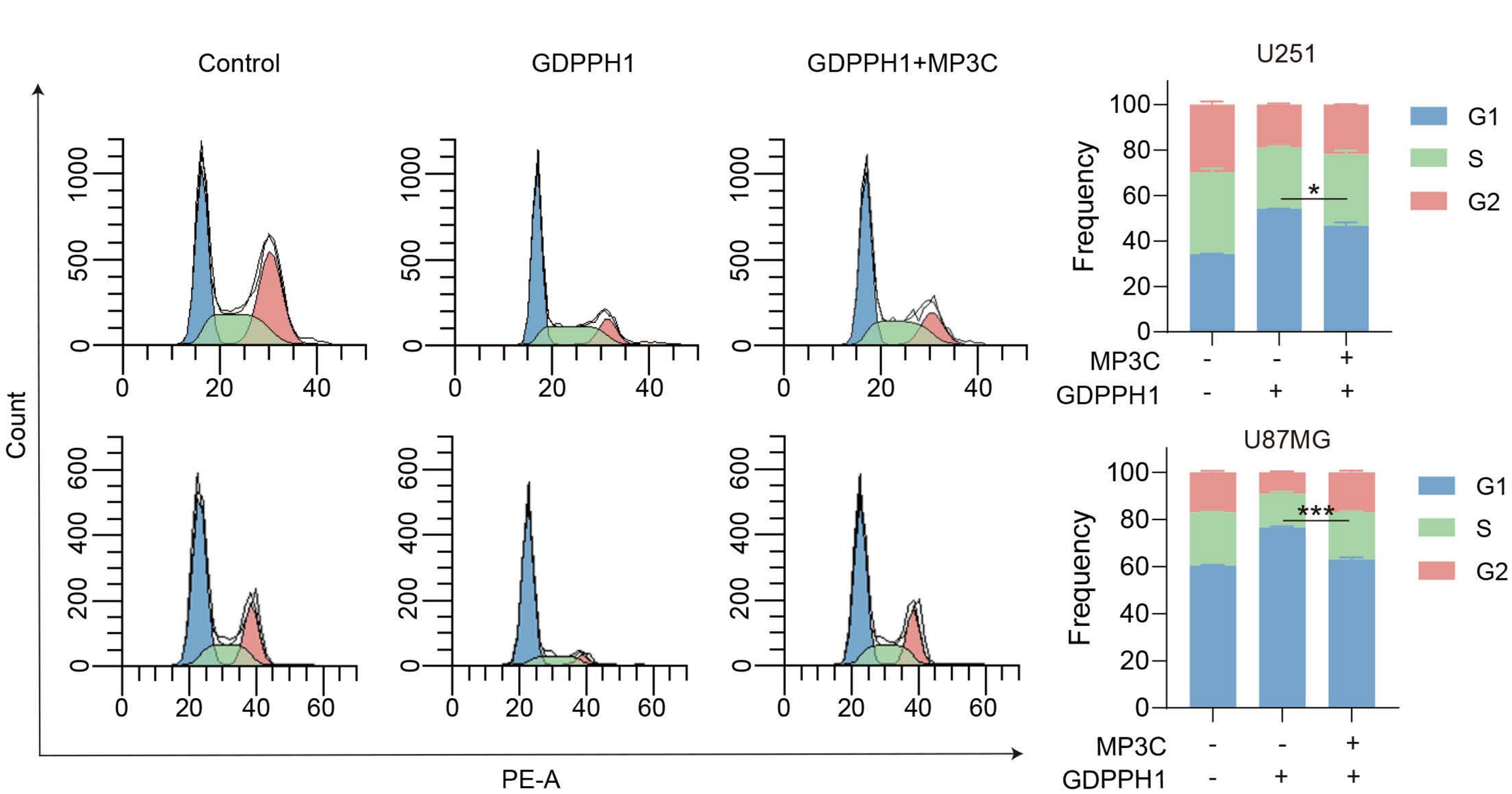

B
U251
U87MG
200
100
50
400
200
100
RNA (ng)
m⁶A
MB
Control
GDPPH1
Control
GDPPH1

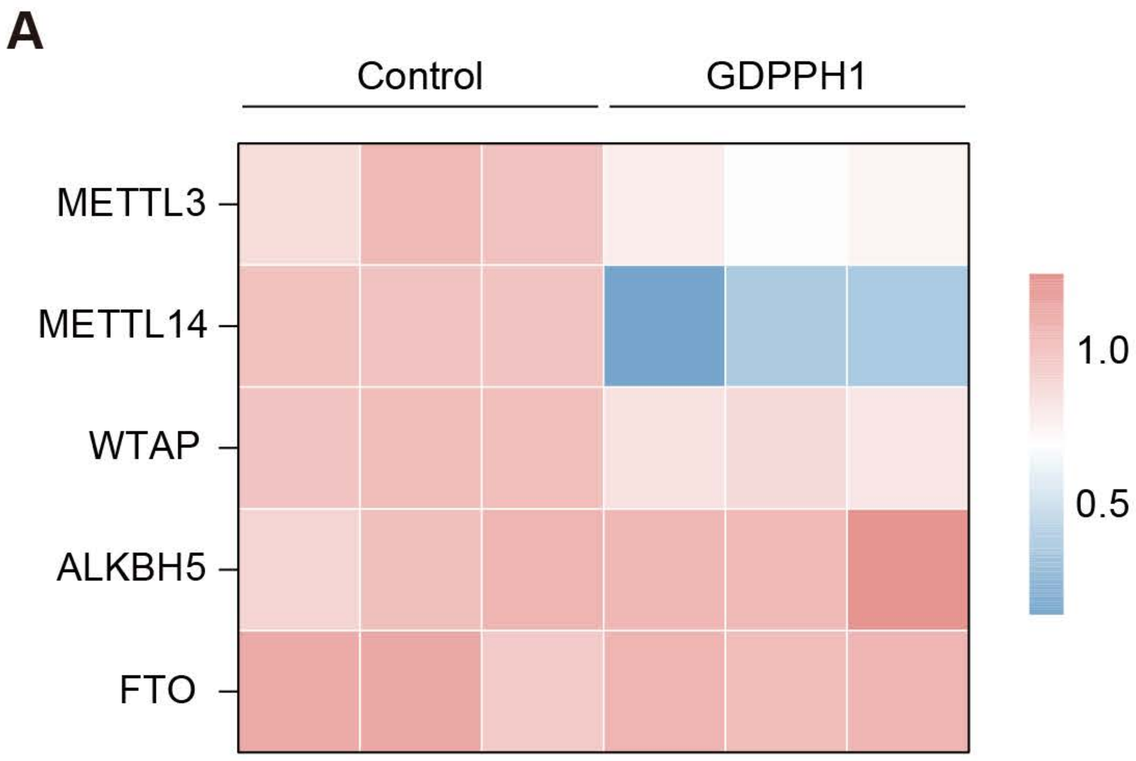

C
Cell proliferation rate (% of vehicle)
120
90
60
30
0
***
***
U251
U87MG
Control
GDPPH1
GDPPH1+MP3C

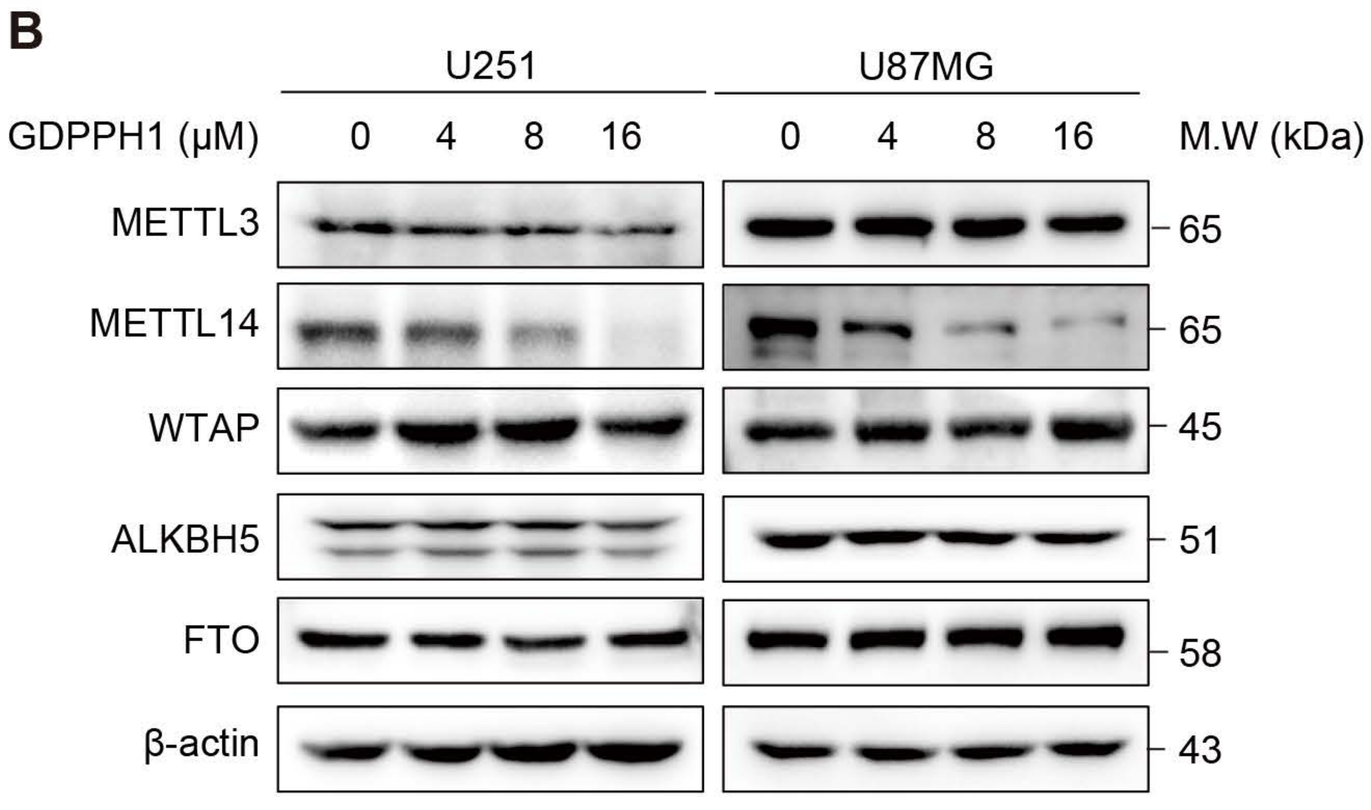

D
CDK4
CCND1
Relative mRNA expression (%)
200
160
120
80
40
0
**
***
***
*
U251
U87MG
Control
GDPPH1
GDPPH1+MP3C

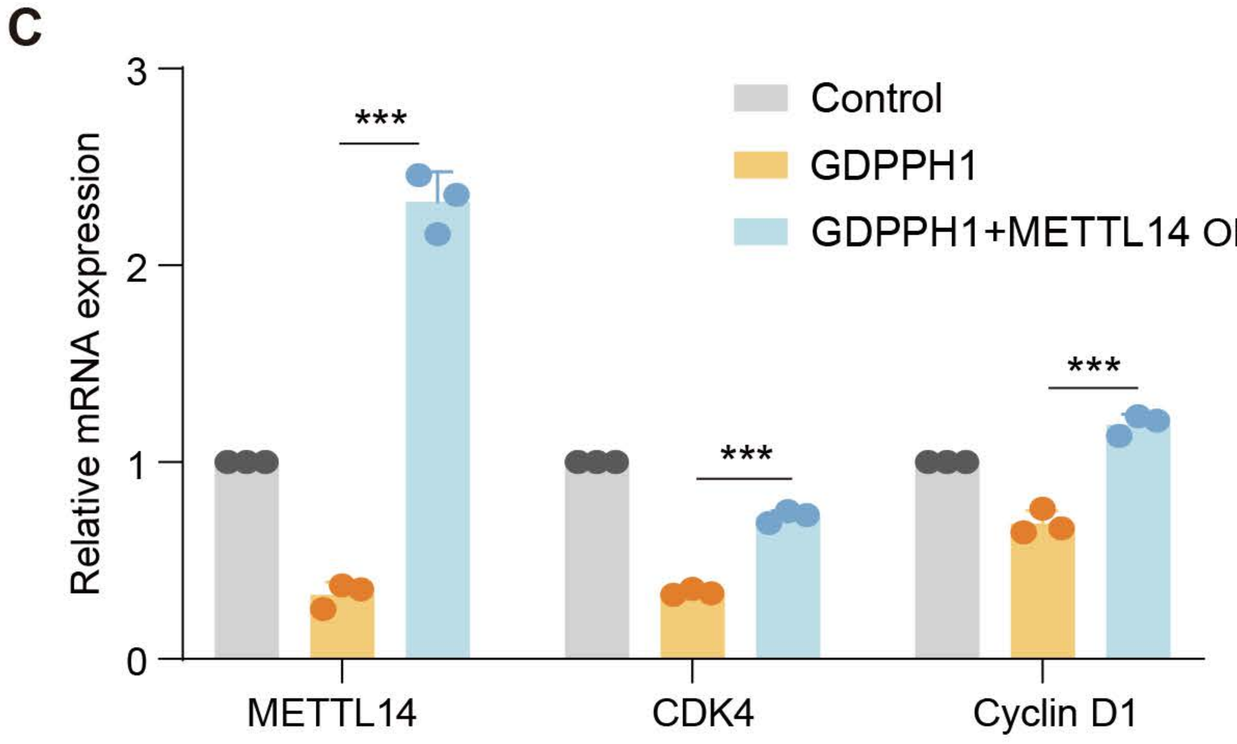

E
U251
U87MG
MP3C - - + - - + M.W
GDPPH1 - + + - + +
(kDa)
Cyclin D1
CDK4
p-RB (Ser780)
RB
β-actin
36
30
110
100
43

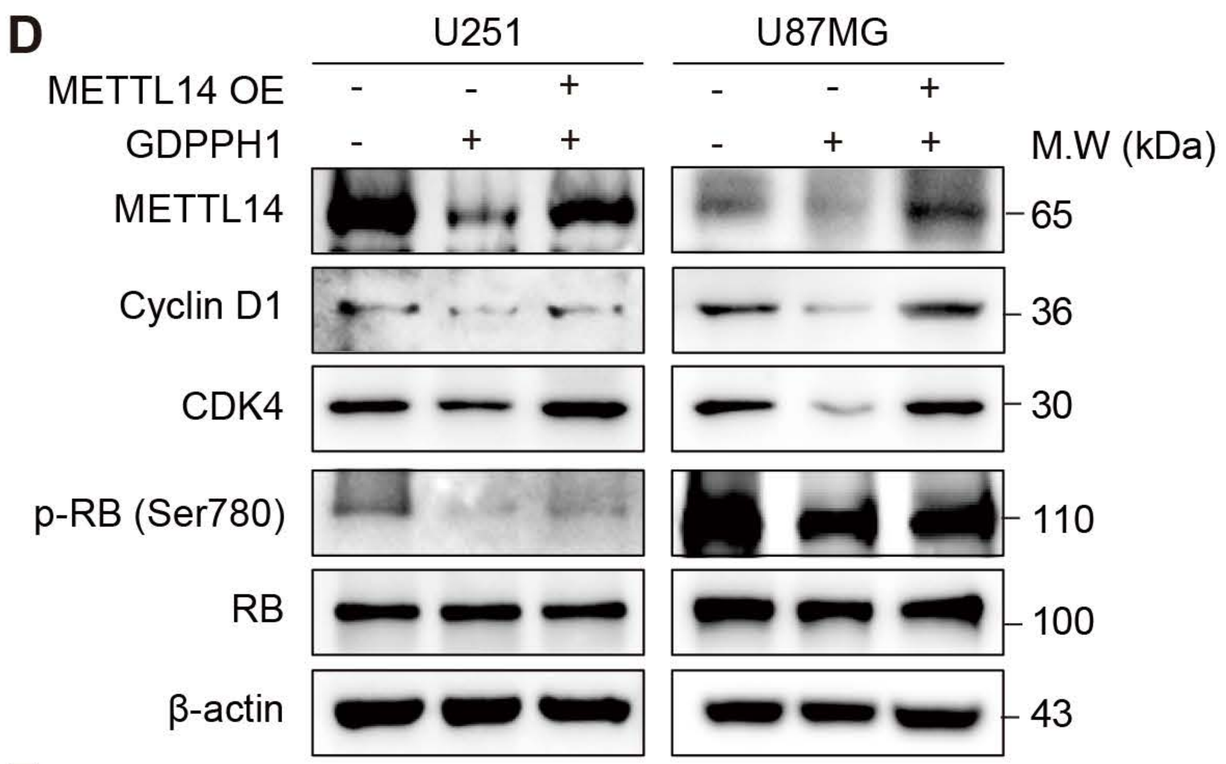

F
U251
U87MG
Relative expression folds
1.2
0.9
0.6
0.3
0.0
***
*
***
***
***
***
Cyclin D1
CDK4
p-RB
Control
GDPPH1
GDPPH1+MP3C

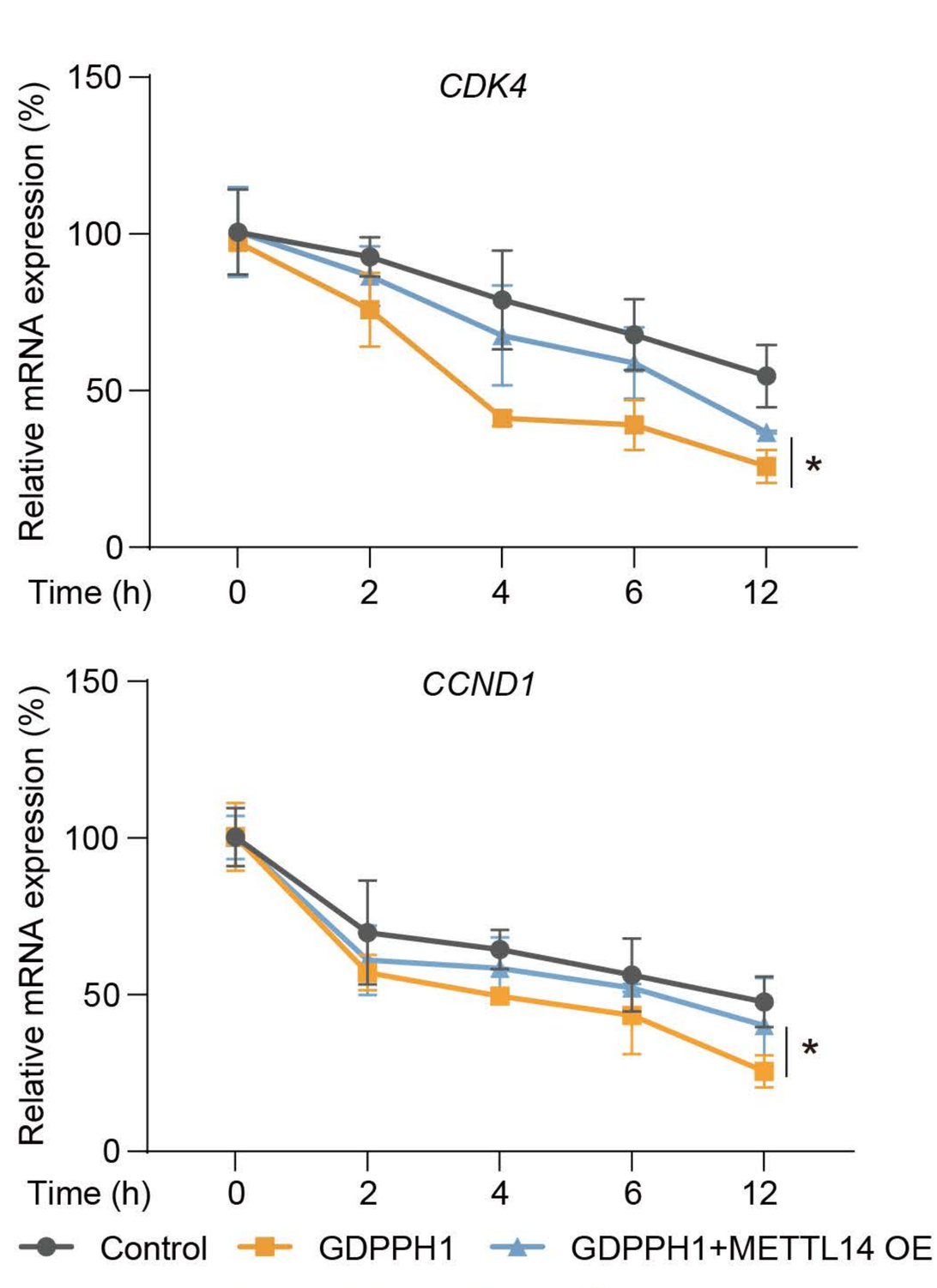

G
Control
GDPPH1
GDPPH1+MP3C
Count
PE-A
U251
U87MG
Frequency
G1
S
G2
*
***
MP3C
GDPPH1

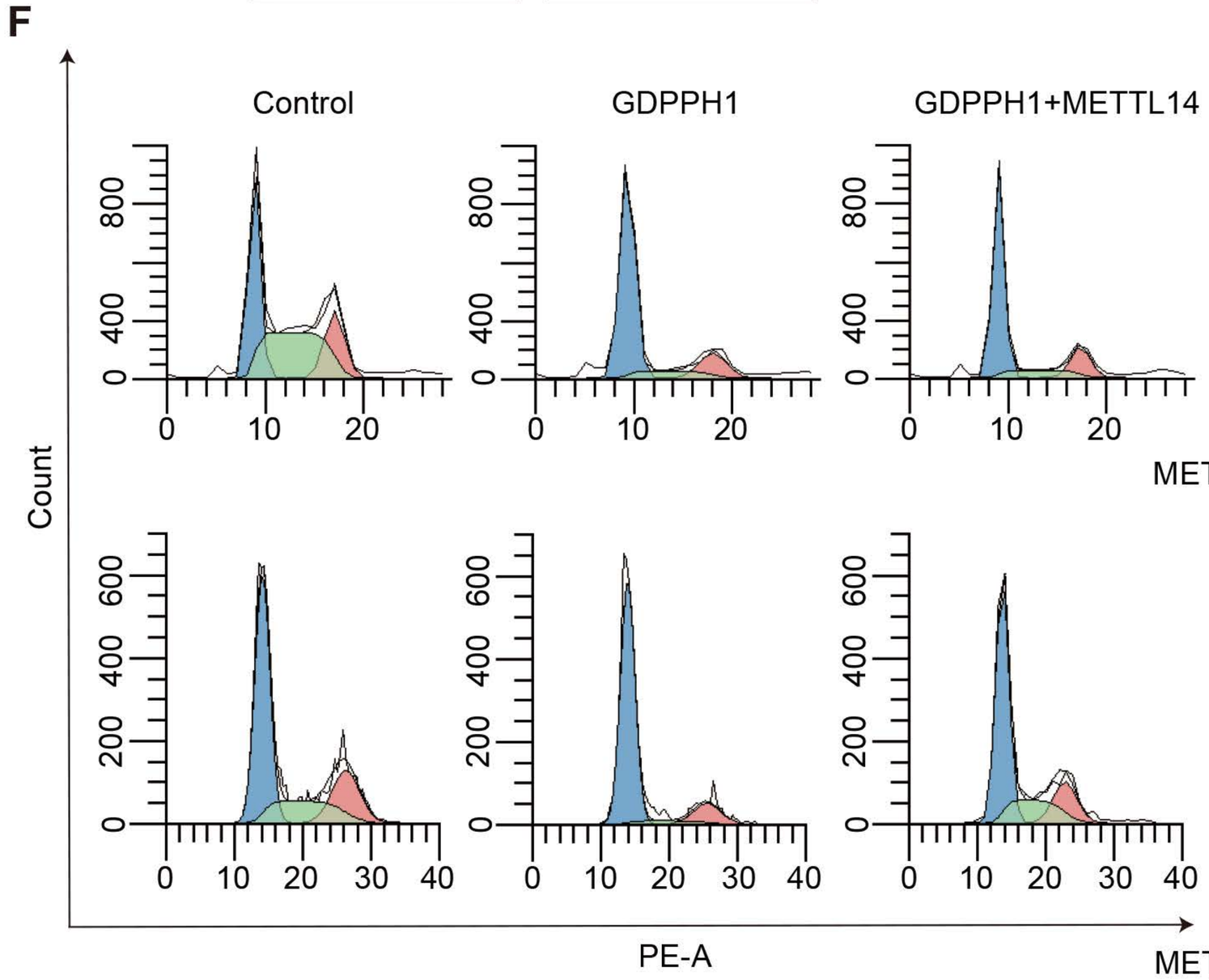

A
Control
GDPPH1
METTL3
METTL14
WTAP
ALKBH5
FTO
1.0
0.5

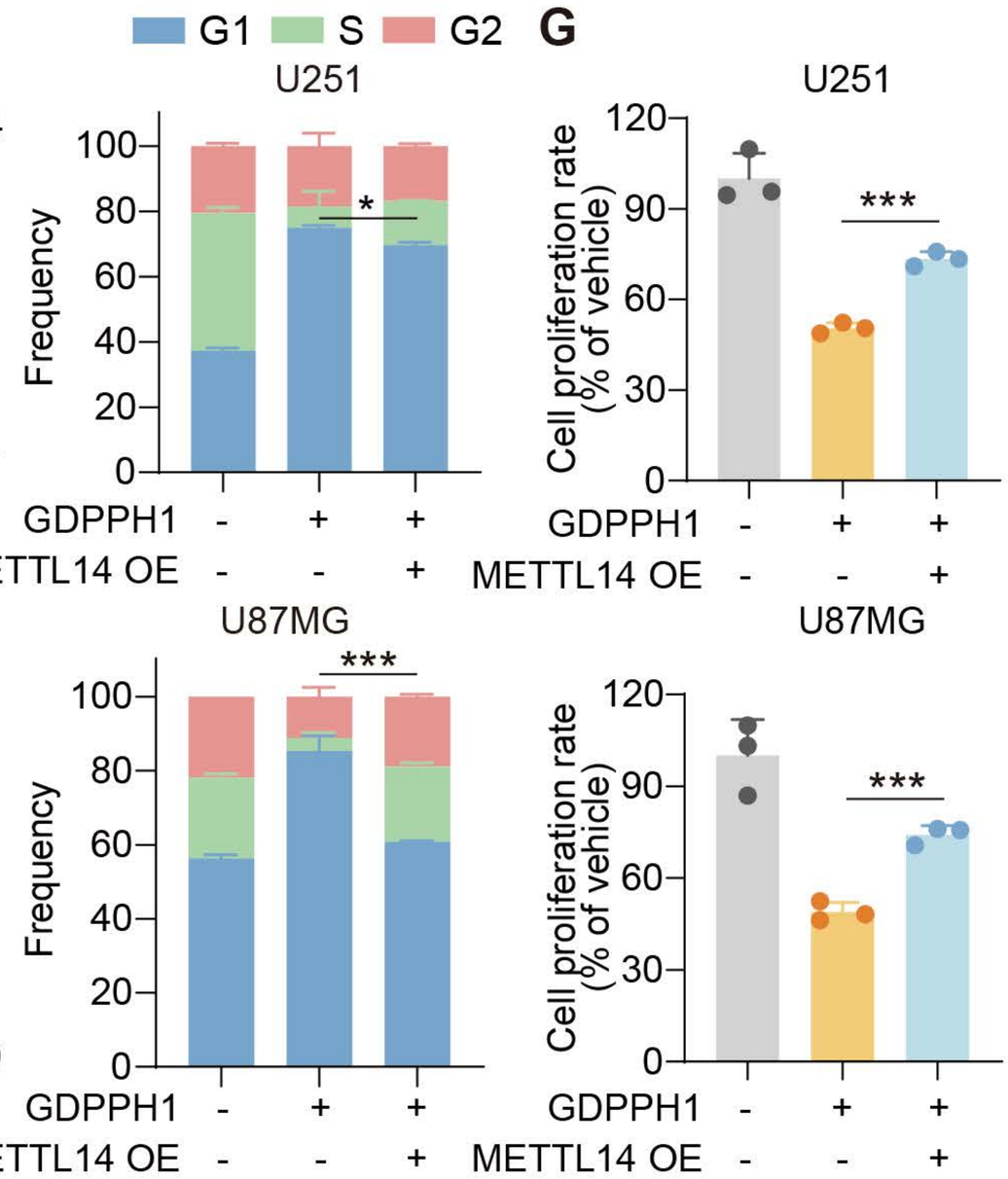

B
U251
U87MG
GDPPH1 (μM)
0
4
8
16
M.W (kDa)
METTL3
METTL14
WTAP
ALKBH5
FTO
β-actin
65
65
45
51
58
43

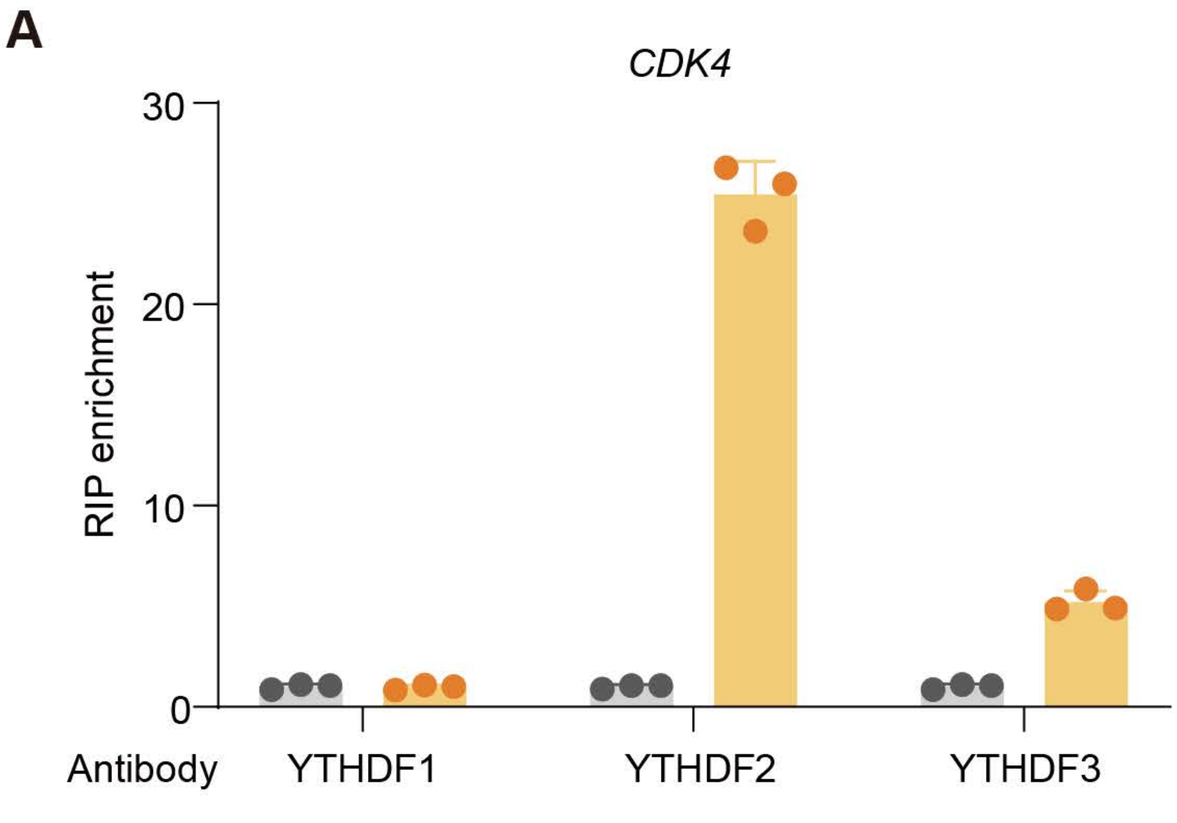

C
Relative mRNA expression
Control
GDPPH1
GDPPH1+METTL14 OE
***
***
***
METTL14
CDK4
Cyclin D1

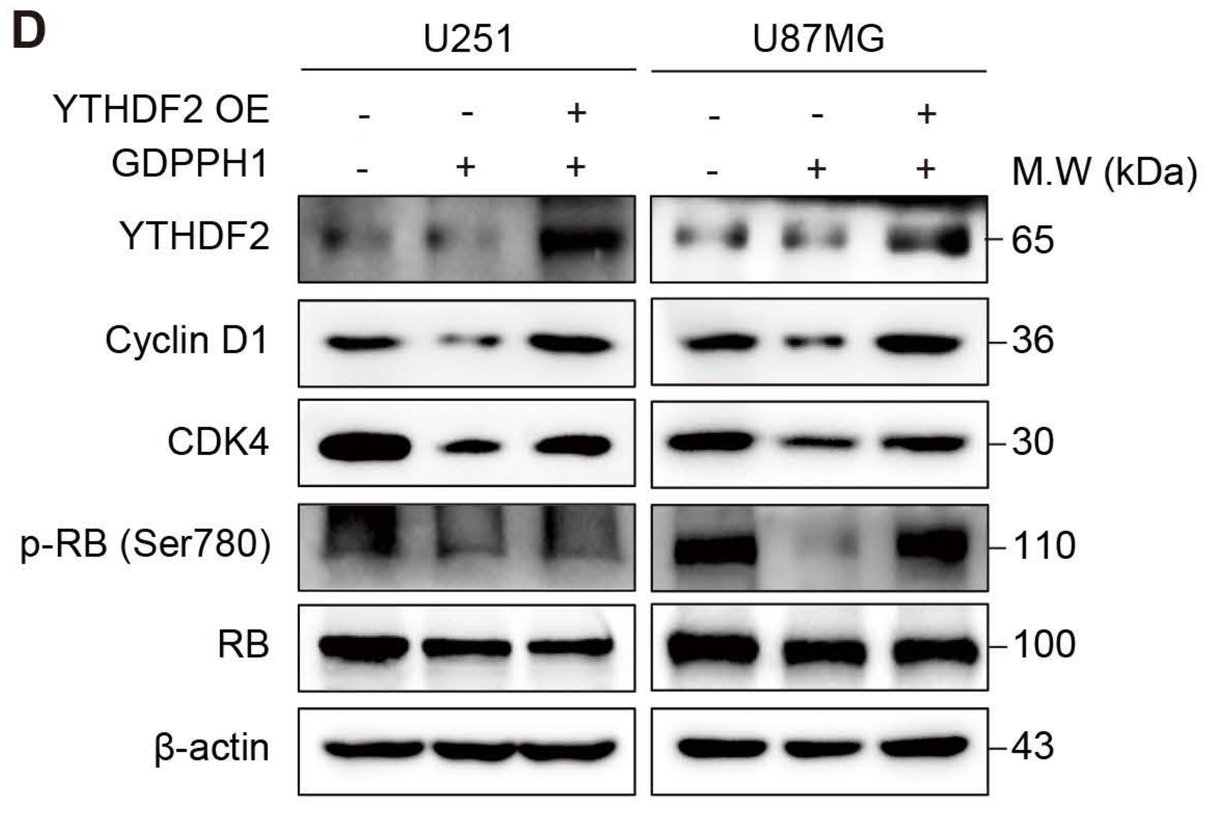

D
U251
U87MG
METTL14 OE
GDPPH1
M.W (kDa)
METTL14
Cyclin D1
CDK4
p-RB (Ser780)
RB
β-actin
65
36
30
110
100
43

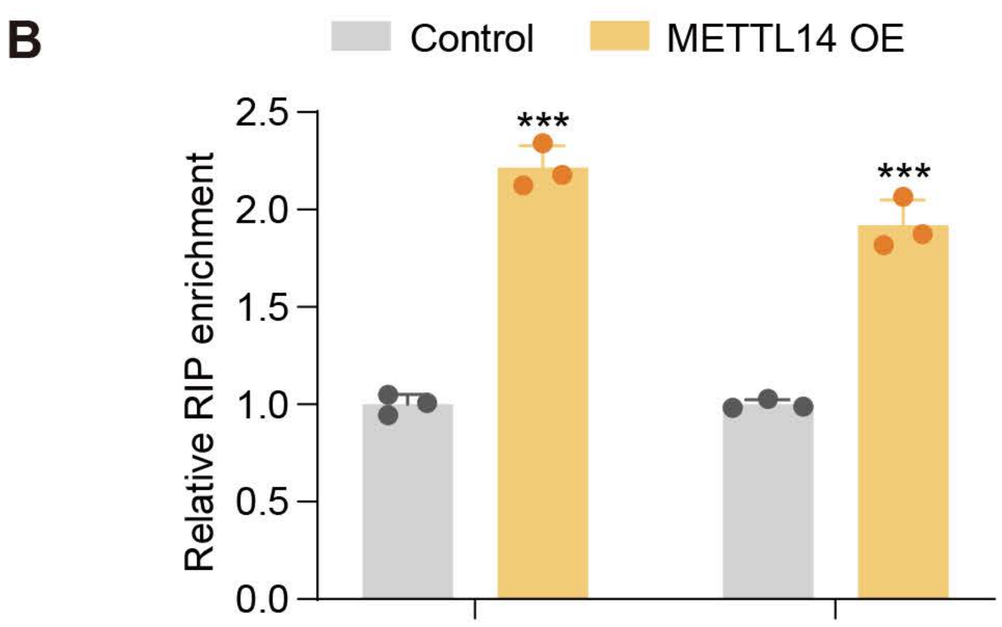

E
CDK4
CCND1
Relative mRNA expression (%)
Time (h)
0
2
4
6
12
*
Control
GDPPH1
GDPPH1+METTL14 OE

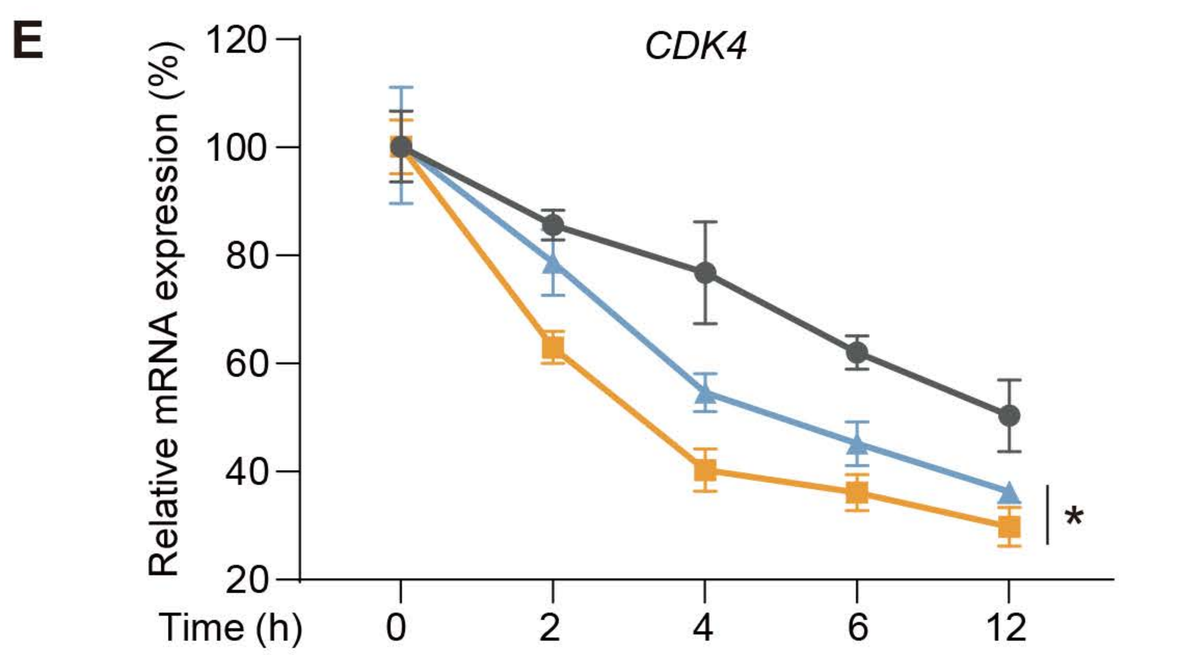

F
Control
GDPPH1
GDPPH1+METTL14
Count
PE-A
G1
S
G2

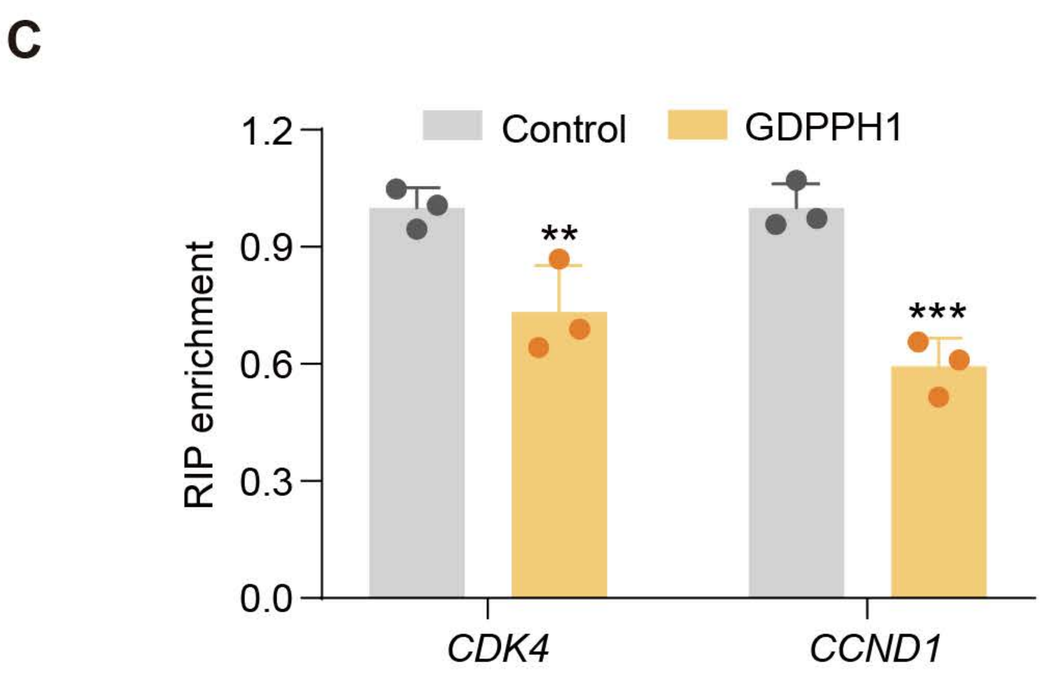

G
U251
U87MG
Frequency
Cell proliferation rate (% of vehicle)
GDPPH1
METTL14 OE
*
***

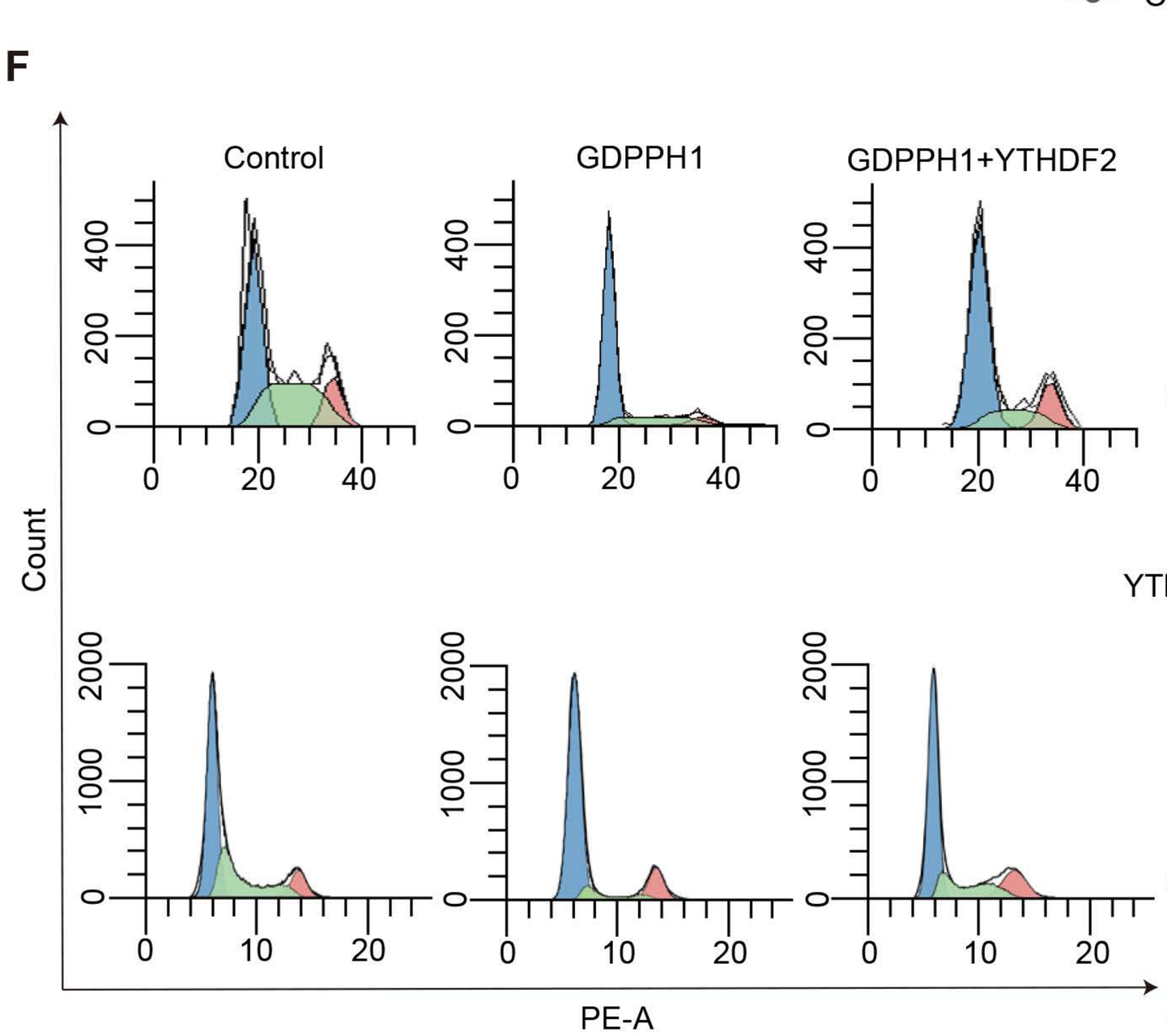

A
CDK4
RIP enrichment
30
20
10
0
Antibody
YTHDF1
YTHDF2
YTHDF3

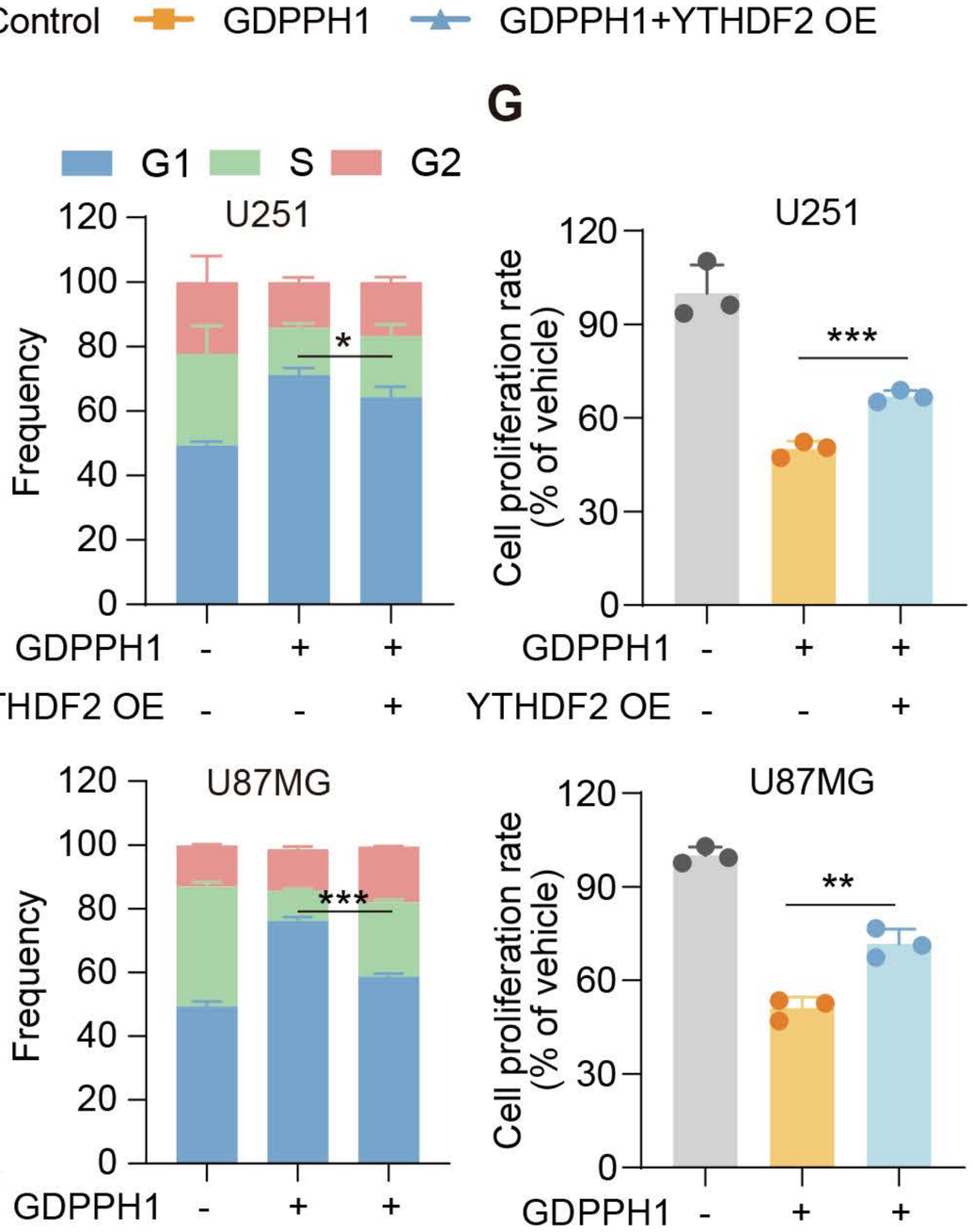

D
U251
U87MG
YTHDF2 OE
GDPPH1
M.W (kDa)
YTHDF2
65
Cyclin D1
36
CDK4
30
p-RB (Ser780)
110
RB
100
β-actin
43

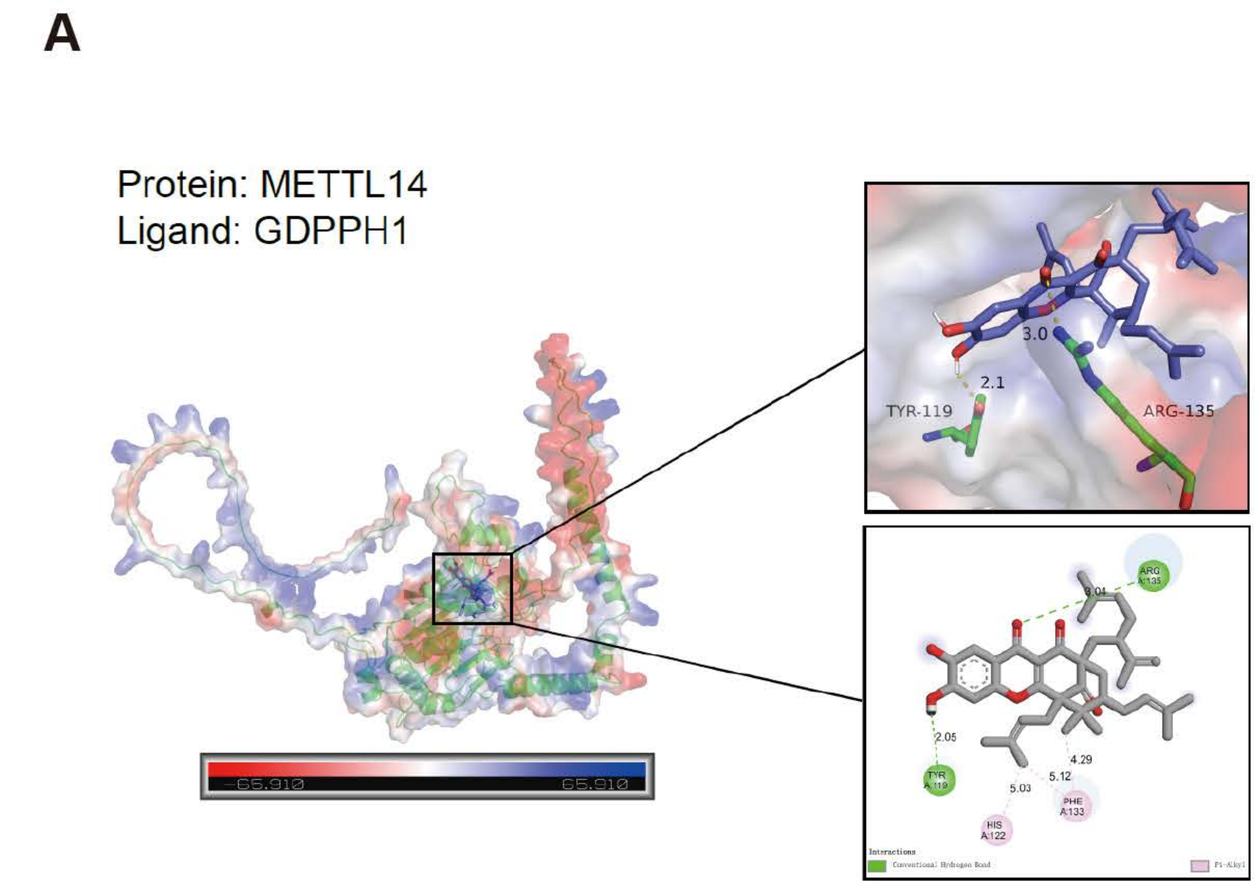

B
Control
METTL14 OE
Relative RIP enrichment
2.5
2.0
1.5
1.0
0.5
0.0
***
***
CDK4
CCND1

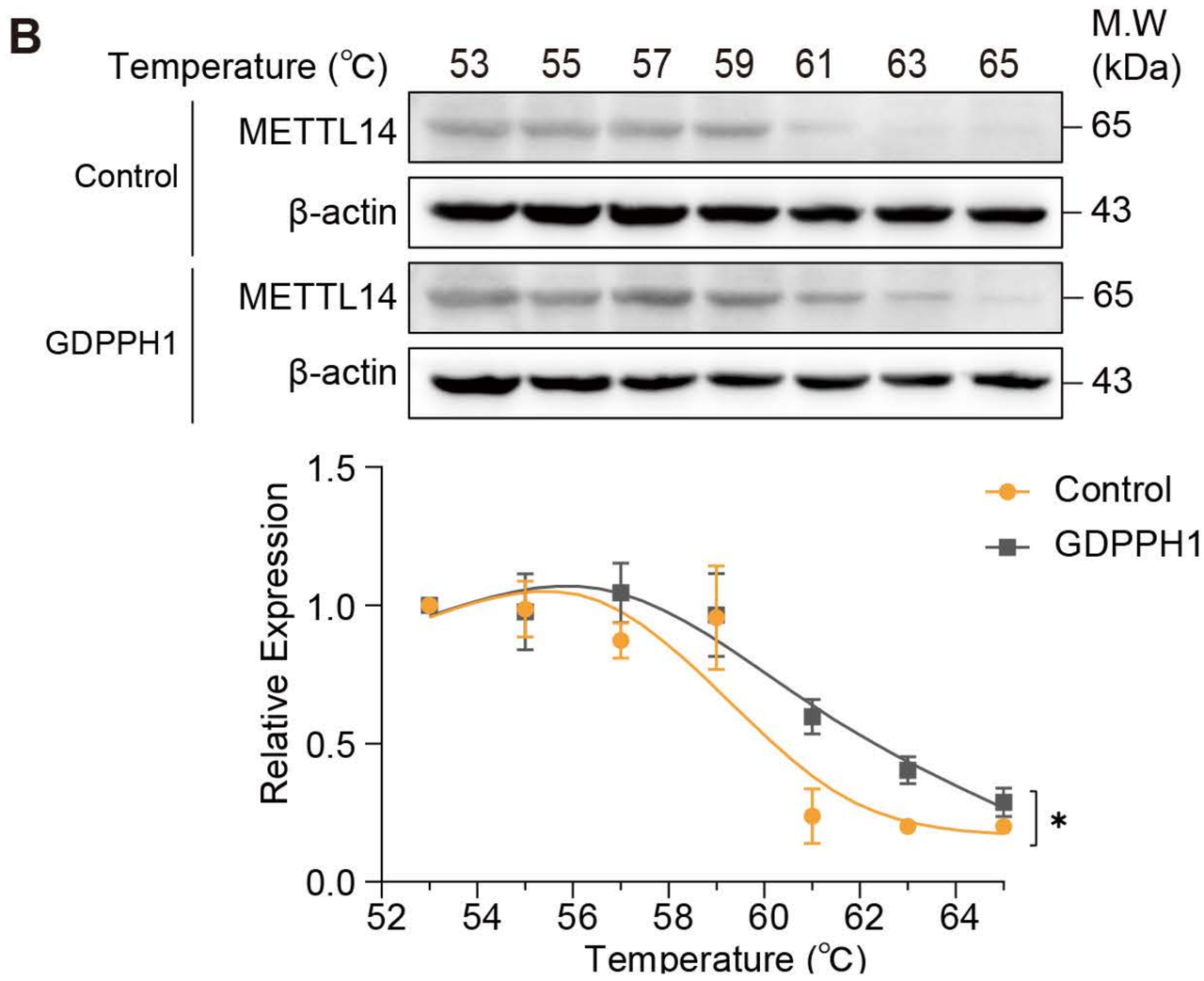

E
CDK4
Relative mRNA expression (%)
120
100
80
60
40
20
Time (h)
0
2
4
6
12
*
CCND1
150
100
50
0
*
Control
GDPPH1
GDPPH1+YTHDF2 OE

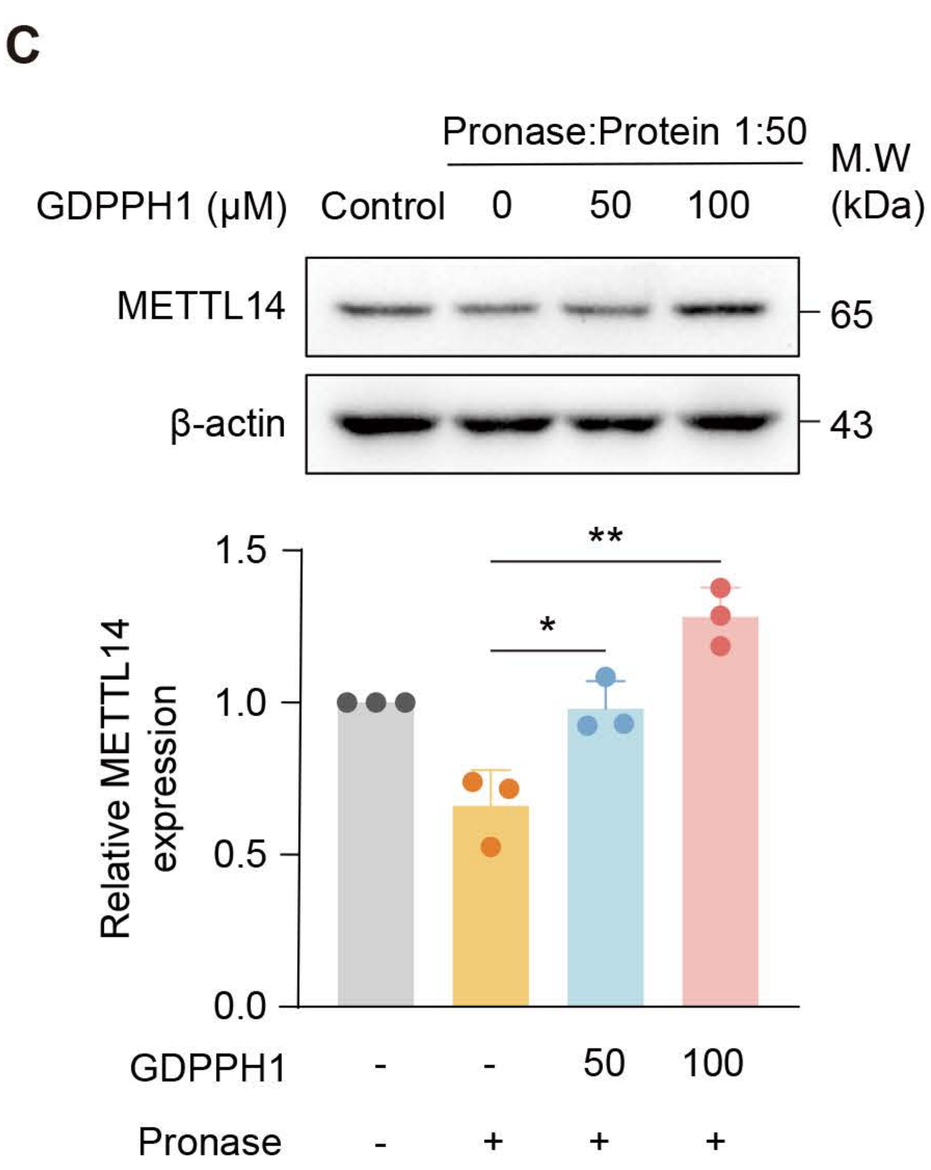

C
Control
GDPPH1
RIP enrichment
1.2
0.9
0.6
0.3
0.0
**
***
CDK4
CCND1

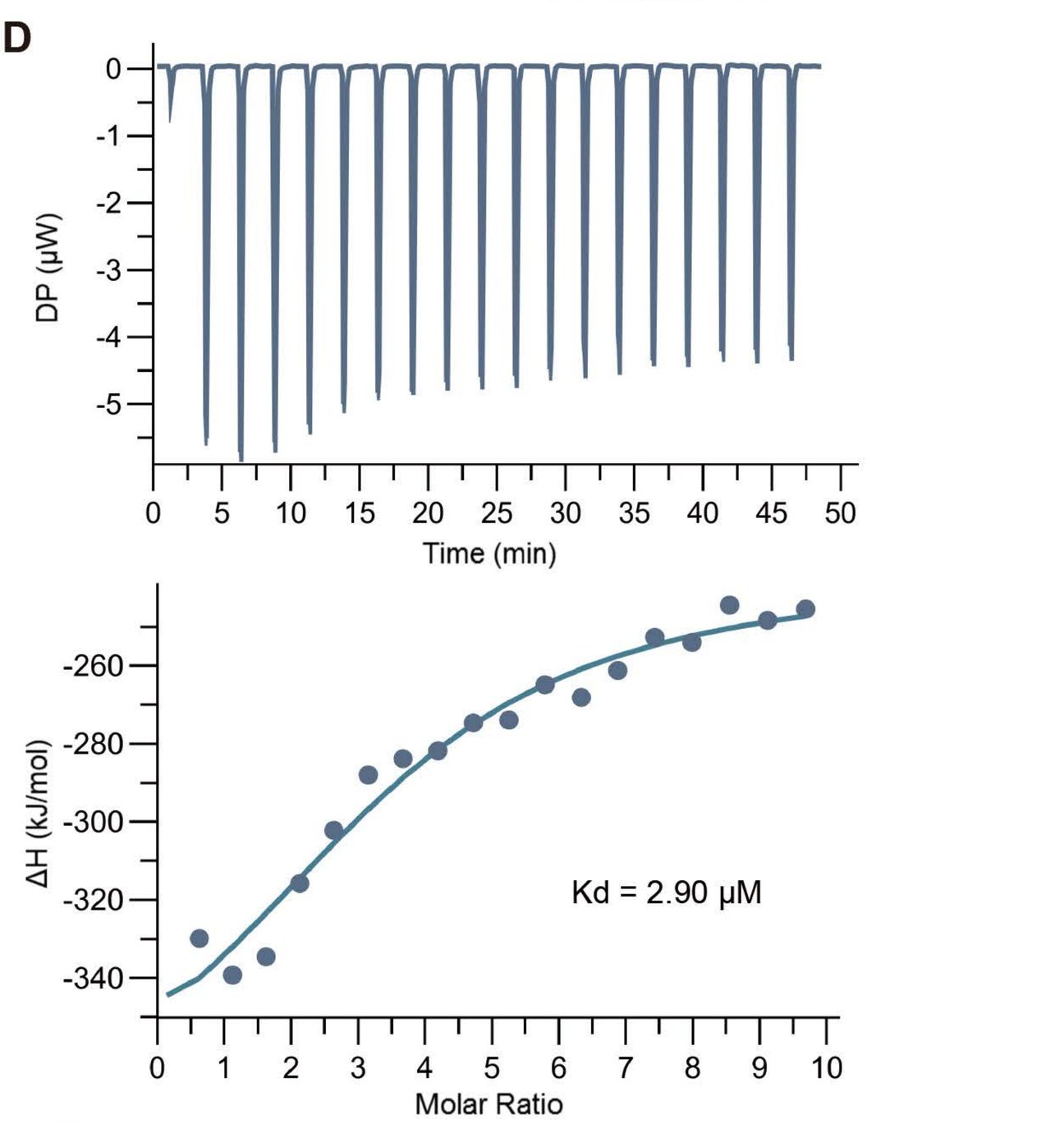

F
Control
GDPPH1
GDPPH1+YTHDF2
Count
PE-A

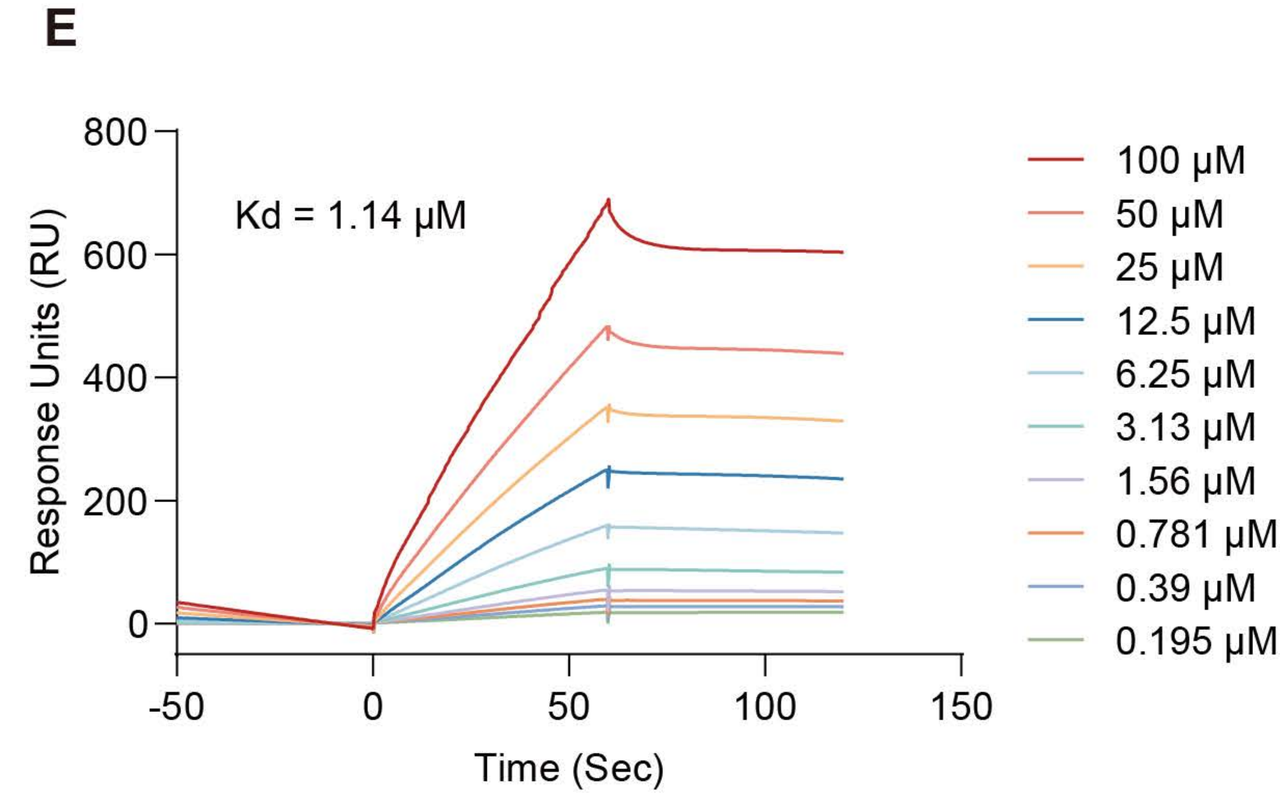

G
G1
S
G2
U251
Frequency
*
GDPPH1
YTHDF2 OE
U251
Cell proliferation rate (% of vehicle)
***
U87MG
***
U87MG
**

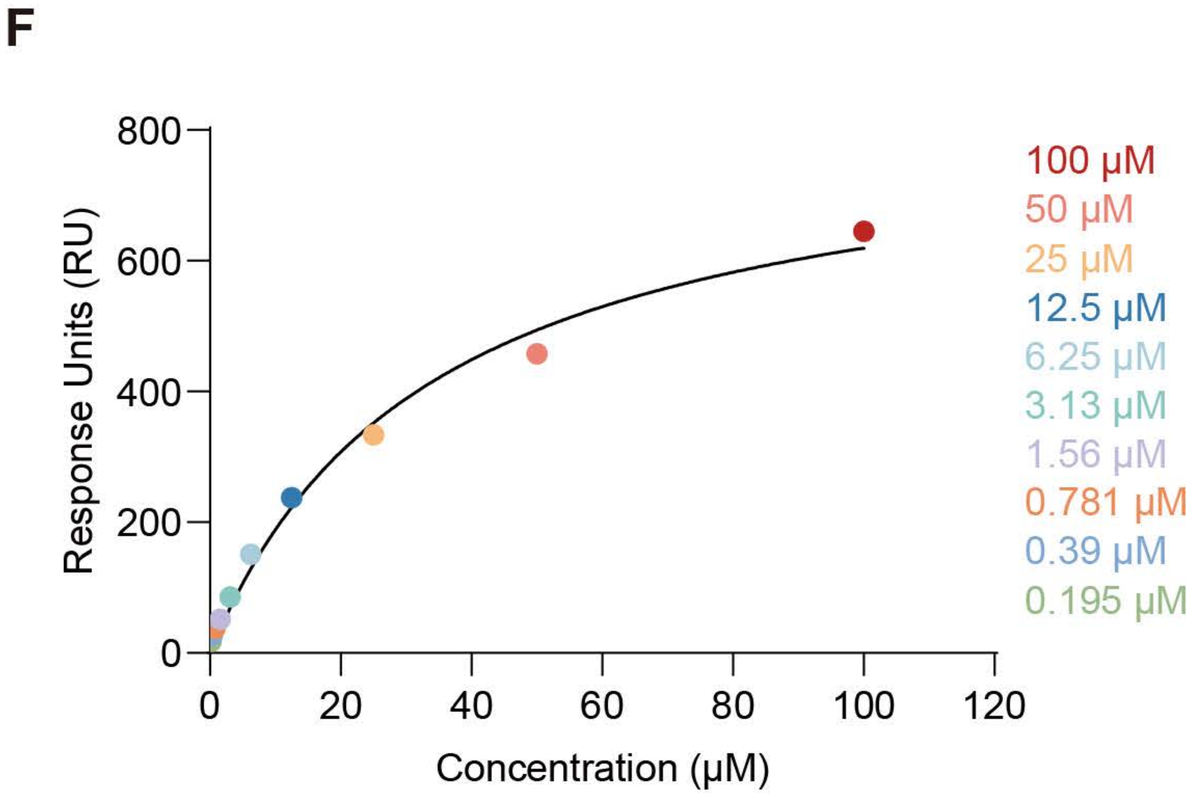

A
Protein: METTL14
Ligand: GDPPH1
-65.910
65.910
3.0
2.1
TYR-119
ARG-135
3.01
2.05
4.29
5.12
5.03
TYR A:119
PHE A:133
HIS A:122
Interactions
Conventional Hydrogen Bond
Pi-Alkyl

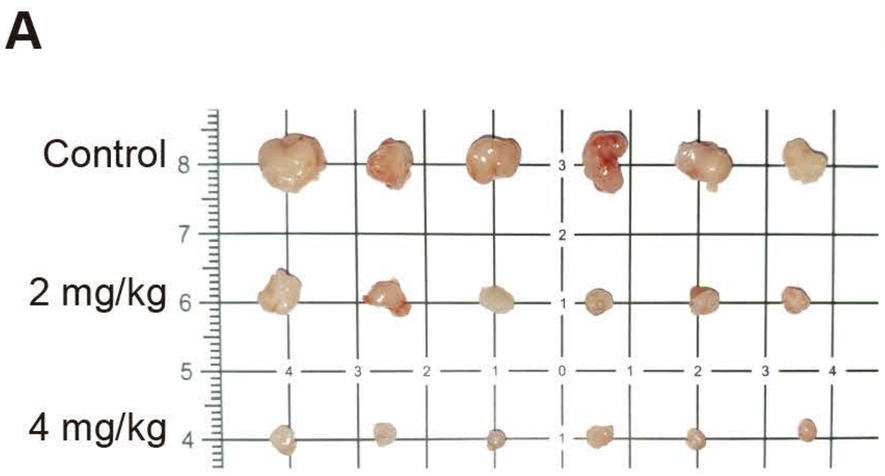

B
Temperature (℃) 53 55 57 59 61 63 65
M.W (kDa)
Control
METTL14
65
β-actin
43
GDPPH1
METTL14
65
β-actin
43
Relative Expression
1.5
1.0
0.5
0.0
52 54 56 58 60 62 64
Temperature (℃)
Control
GDPPH1
*

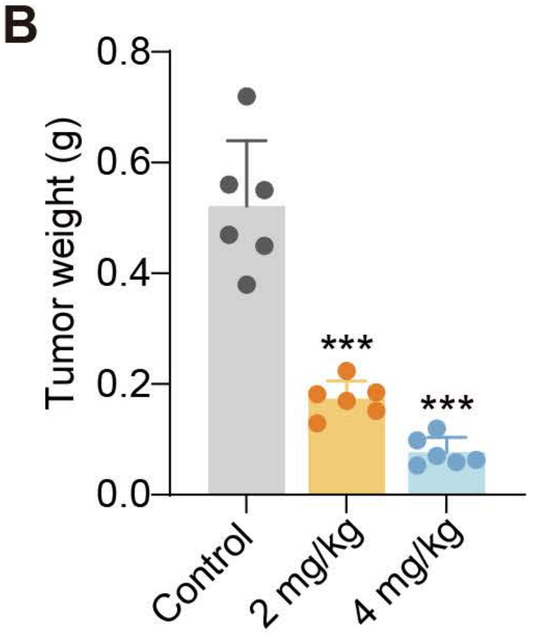

C
Pronase:Protein 1:50
GDPPH1 (μM) Control 0 50 100
M.W (kDa)
METTL14
65
β-actin
43
Relative METTL14 expression
1.5
1.0
0.5
0.0
**
*
GDPPH1 - - 50 100
Pronase - + + +

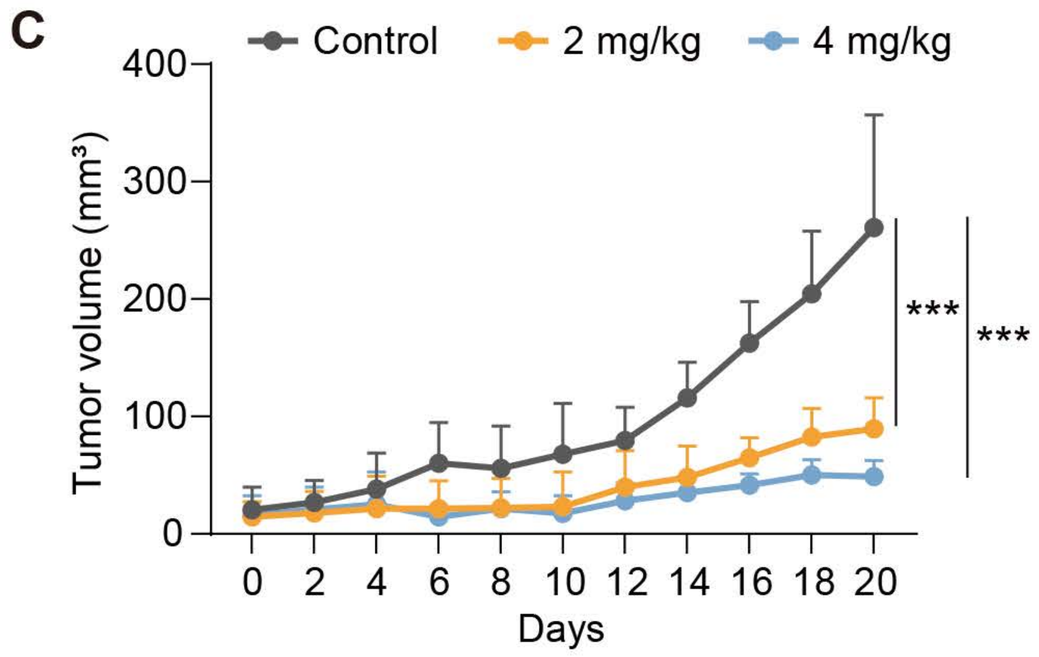

D
DP (μW)
0
-1
-2
-3
-4
-5
0 5 10 15 20 25 30 35 40 45 50
Time (min)
ΔH (kJ/mol)
-260
-280
-300
-320
-340
Kd = 2.90 μM
0 1 2 3 4 5 6 7 8 9 10
Molar Ratio

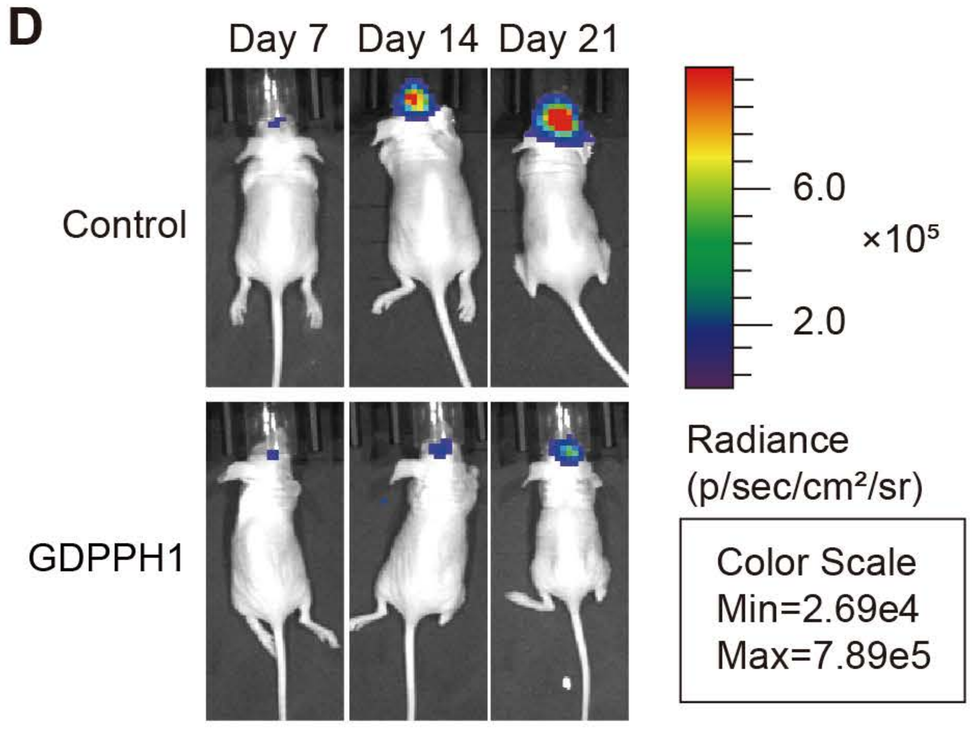

E
Kd = 1.14 μM
Response Units (RU)
800
600
400
200
0
-50 0 50 100 150
Time (Sec)
100 μM
50 μM
25 μM
12.5 μM
6.25 μM
3.13 μM
1.56 μM
0.781 μM
0.39 μM
0.195 μM

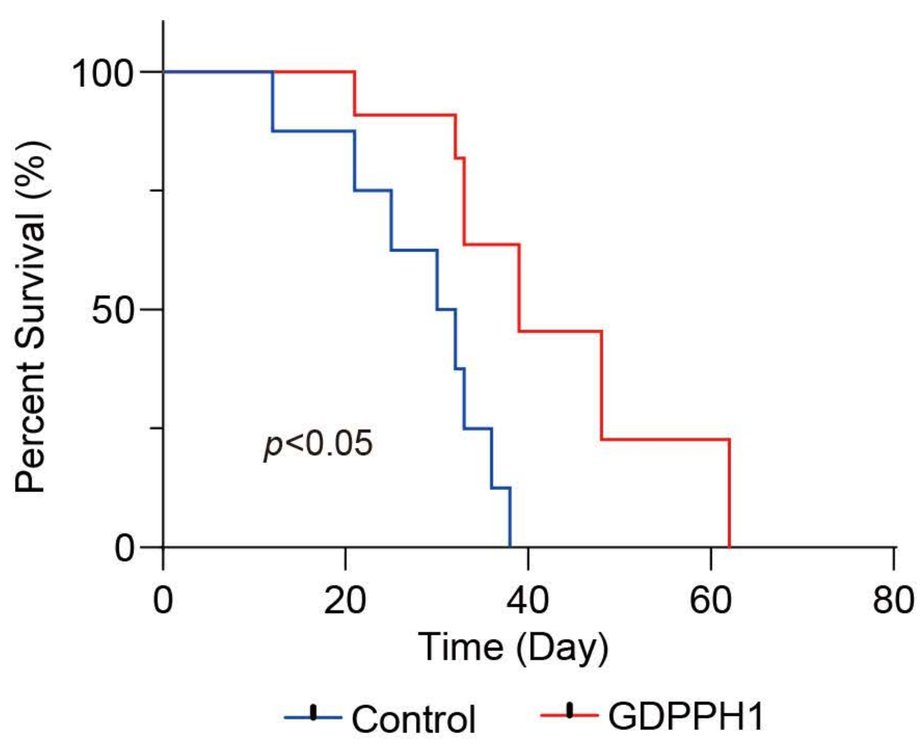

F
Response Units (RU)
800
600
400
200
0
0 20 40 60 80 100 120
Concentration (μM)
100 μM
50 μM
25 μM
12.5 μM
6.25 μM
3.13 μM
1.56 μM
0.781 μM
0.39 μM
0.195 μM

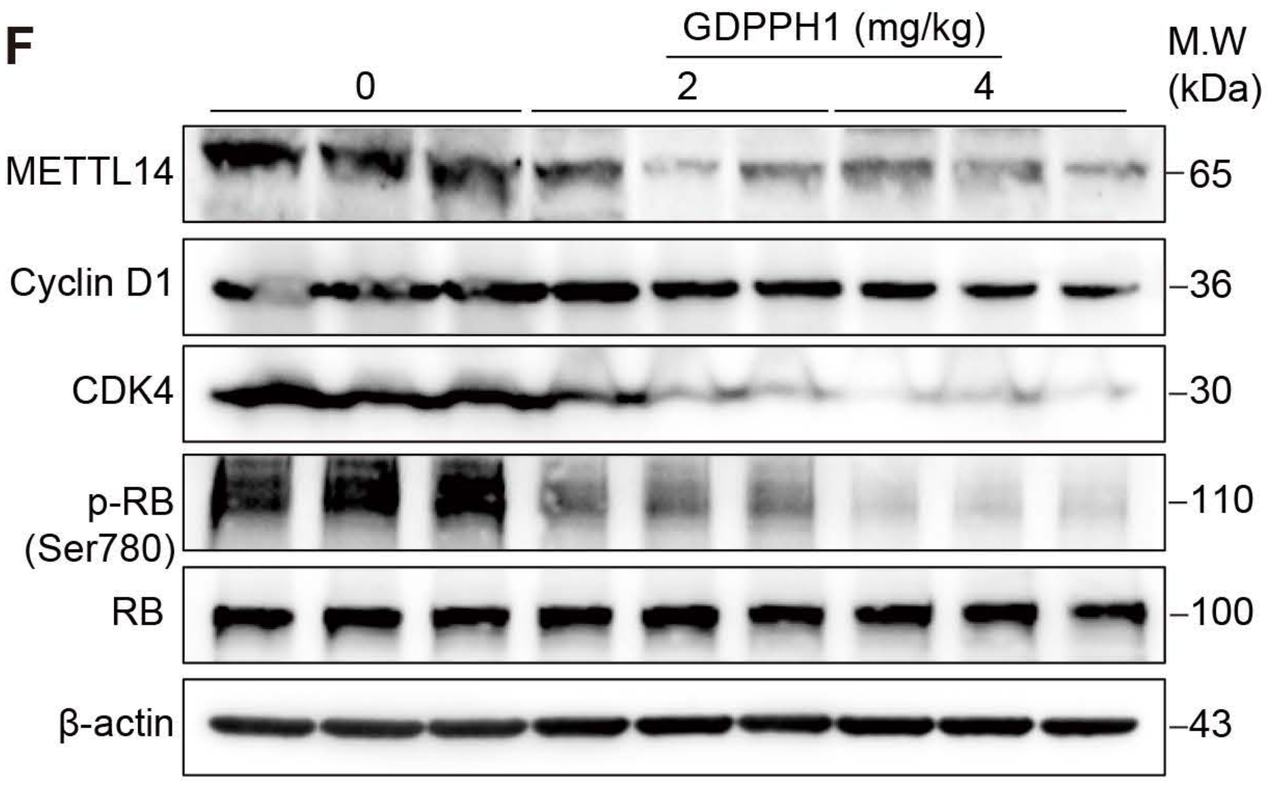

A
Control
2 mg/kg
4 mg/kg

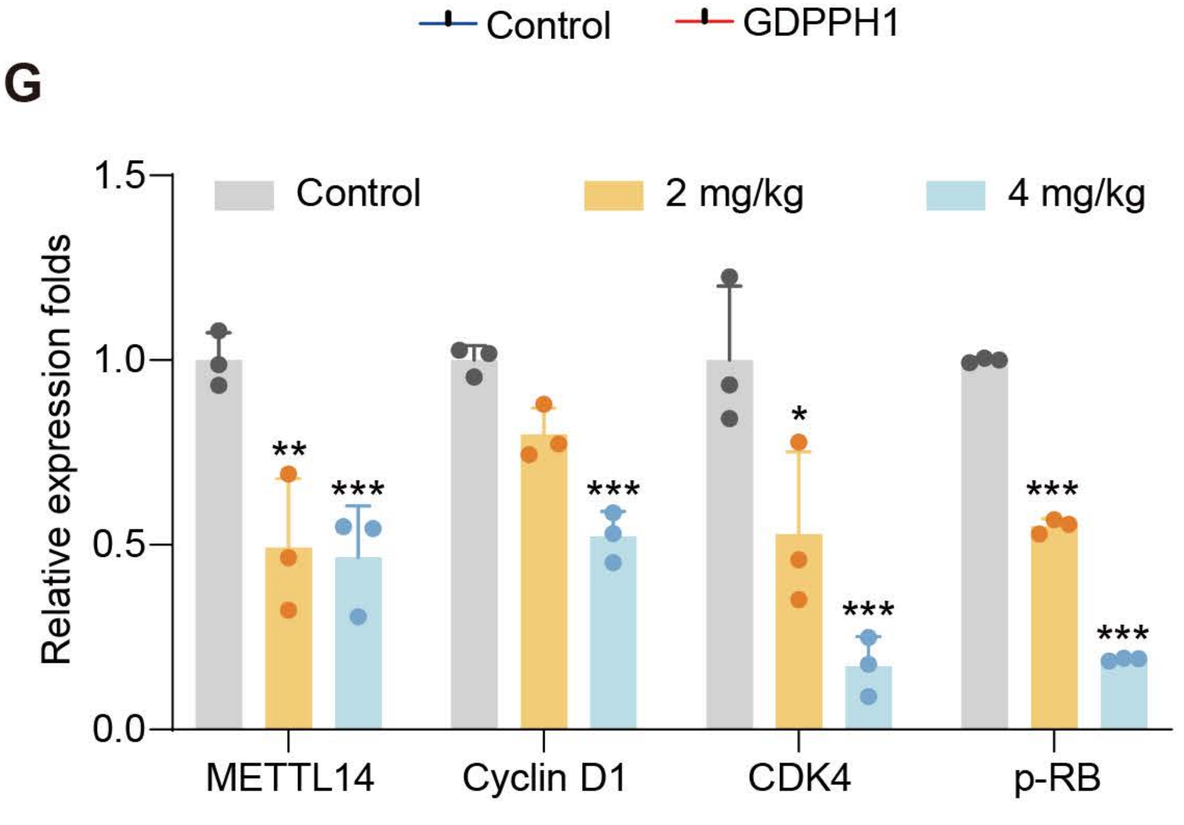

B
Tumor weight (g)
0.8
0.6
0.4
0.2
0.0
***
***
Control
2 mg/kg
4 mg/kg

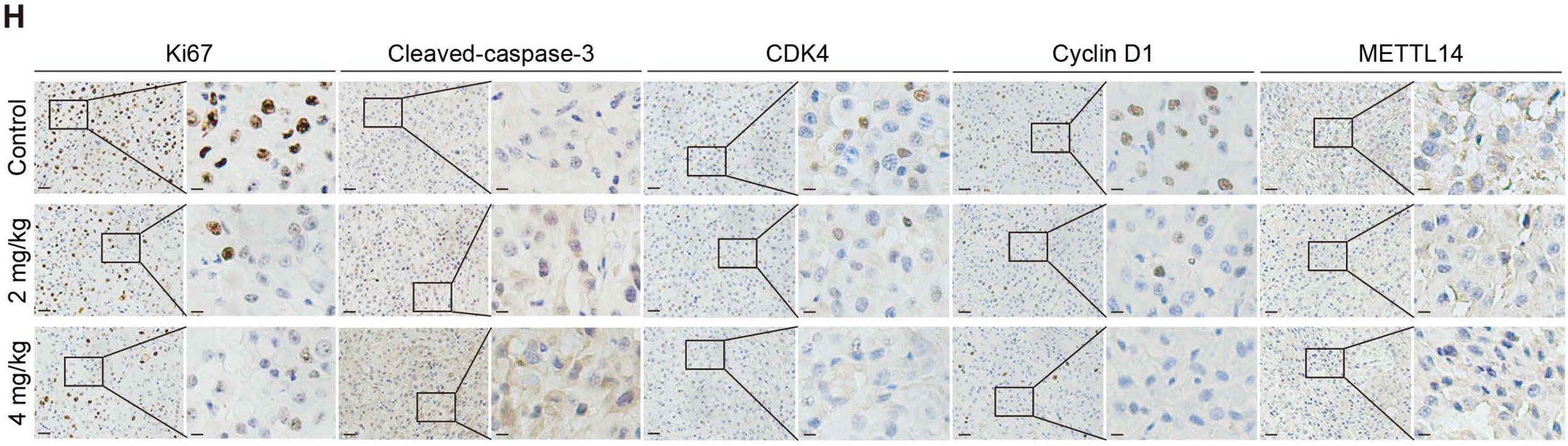

C
Control
2 mg/kg
4 mg/kg
Tumor volume (mm³)
400
300
200
100
0
***
***
0 2 4 6 8 10 12 14 16 18 20
Days

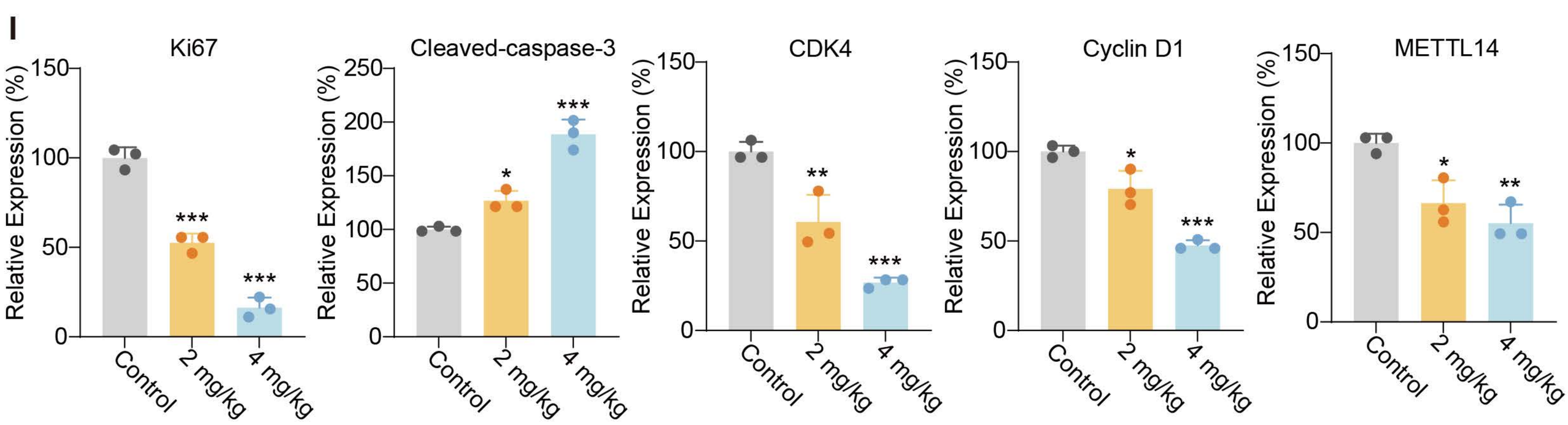

D
Day 7
Day 14
Day 21
Control
GDPPH1
6.0
×10⁵
2.0
Radiance
(p/sec/cm²/sr)
Color Scale
Min=2.69e4
Max=7.89e5

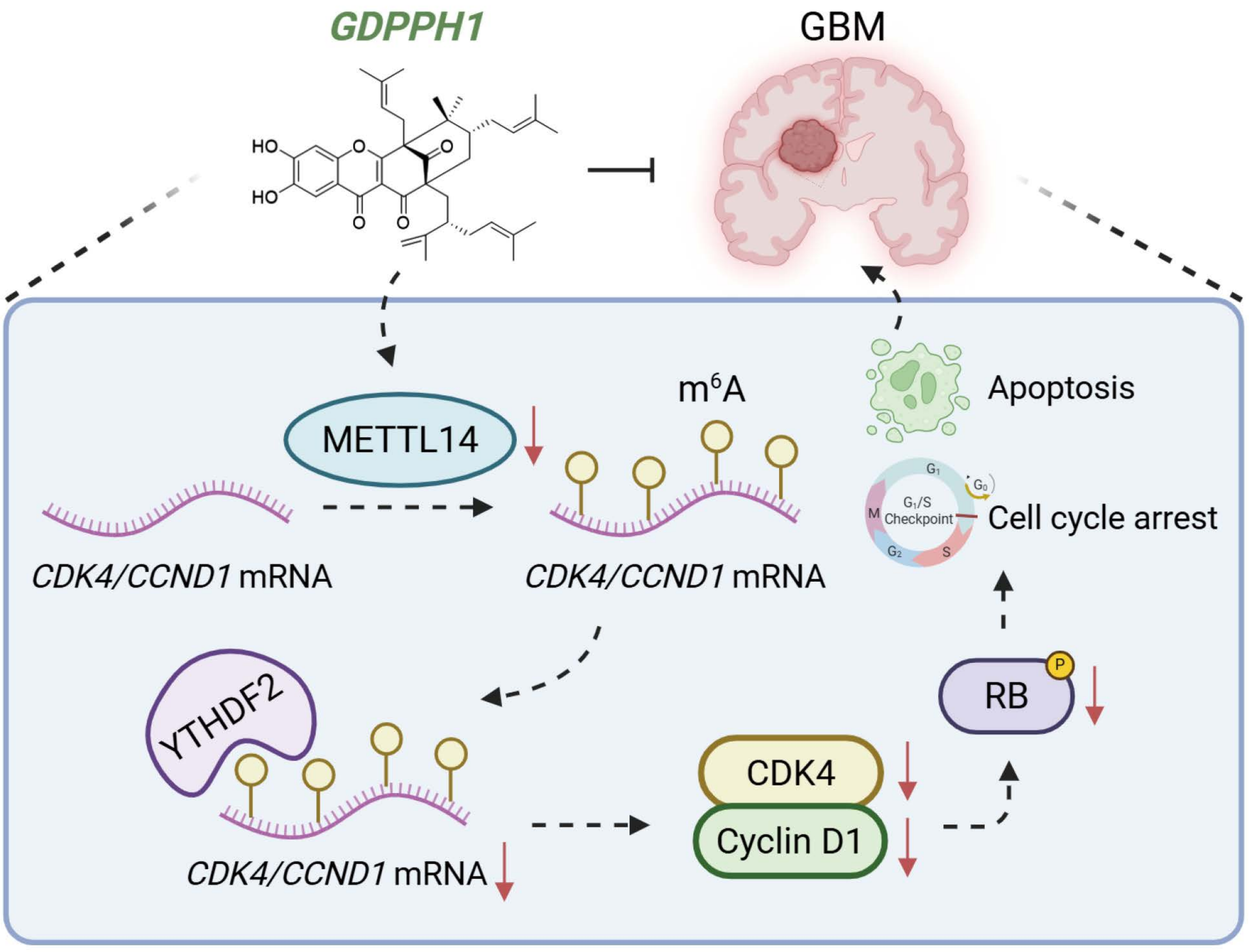

E
100
50
0
Percent Survival (%)
p<0.05
0
20
40
60
80
Time (Day)
Control
GDPPH1


F
GDPPH1 (mg/kg)
0
2
4
M.W
(kDa)
METTL14
65
Cyclin D1
36
CDK4
30
p-RB
(Ser780)
110
RB
100
β-actin
43


G
Control
2 mg/kg
4 mg/kg
Relative expression folds
1.5
1.0
0.5
0.0
**
***
***
*
***
***
METTL14
Cyclin D1
CDK4
p-RB


H
Ki67
Cleaved-caspase-3
CDK4
Cyclin D1
METTL14
Control
2 mg/kg
4 mg/kg


I
Ki67
Cleaved-caspase-3
CDK4
Cyclin D1
METTL14
Relative Expression (%)
Control
2 mg/kg
4 mg/kg


GDPPH1
GBM
HO
HO
O
O
O
O
m⁶A
METTL14
Apoptosis
G1
G0
G1/S
Checkpoint
M
G2
S
Cell cycle arrest
CDK4/CCND1 mRNA
CDK4/CCND1 mRNA
YTHDF2
RB
P
CDK4
Cyclin D1
CDK4/CCND1 mRNA